MANCHESTER 1824

The University of Manchester

Colloidosomes and stretchable hydrogels prepared from pH-responsive microgels and nanogels

A thesis submitted to the University of Manchester for the degree of Doctor of Philosophy in the Faculty of Science & Engineering

Submitted 2018

Wenkai Wang

Student ID: 8366313

School of Materials

Faculty of Science & Engineering

University of Manchester

Content

List of Schemes

List of Table

List of Figures

List of Abbreviations

APS	Ammonium persulfate
BDDA	1,4-Butanediol diacrylate
CLSM	Confocal laser scanning microscopy
CMC	Critical micelle concentration
COOH	Carboxylic acid group
CV	Coefficients of variation
DDD	Degenerative disc disease
DLS	Dynamic light scattering
DLVO	Derjaguin-Landau-Verwey-Overbeek
DX MG	Doubly crosslinked microgel
EA	Ethyl acrylate
E-BDDA	Poly(EA/MAA/BDDA) microgel
EGDMA	Ethylene glycol dimethacrylate
FTIR	Fourier-transform infrared spectroscopy
GMA	Glycidyl methacrylate
HEA	2-Hydroxyethyl acrylate
HEMA	2-Hydroxyethyl methacrylate
IVD	Intervertebral disc
IVDD	Intervertebral disc disease
K_2HPO_4	Potassium phosphate dibasic
MAA	Methacrylic acid
MG	Microgel
MMA	Methyl methacrylate
mol%	Mole percent

N_2	Nitrogen
NaCl	Sodium chloride
NaOH	Sodium hydroxide
NIPAM	N-isopropylacrylamide
PAAM	polyacrylamide
PBS	Phosphate-buffered solution
PCS	Photon correlation spectroscopy
PD	Poly dispersity
PMMA	Poly methyl methacrylate
PNIPAM	Poly(N-isopropylacrylamide)
SDS	Sodium dodecyl sulfate
SEM	Scanning electron microscopy
SXM	Singly crosslinked microgel
TEM	Transmission electron microscopy
TEMED	N,N,N',N'-tetramethylethane-1,2-diamine

List of Symbols

α	Degree of neutralisation
A_{eff}	Hamaker constant
c_0	Polymer concentration inside the particles at collapsed state,
C_{in}	Concentration of the ions inside the particles.
C_{out}	Concentration of the ions outside the particles.
D	Rotor diameter
E	Modulus
f	Number of effective chains formed per crosslinking monomer
$g^{(1)}(\tau)$	Light field autocorrelation function
$G^2(\tau)$	Light intensity autocorrelation function
I	Scattered light intensity
M_A	Molar mass of monomer A
n	Rotational speed
ρ_A	Density of monomer A
R_α	Hydrodynamic radius
S	Shear rate
V_u	Molar volume of the structural unit
V_A	Molar volume of the structural monomer
V_{att}	Van Der Waals attractive force
V_E	Emulsion volume

V_{rep}	Energy contributed by electrostatic repulsion and opposes aggregation
V_{str}	Steric repulsive energy
V_t	Total energy of interaction
x_B	Mole fraction of crosslinking monomer
X_i	Mole fraction of the ionic comonomer
χ	Flory Huggins interaction parameter
ε	Dielectric constant of the solution
ψ_d	Surface potential energy at the Stern layer
ζ	Zeta potential
γ	Molar fraction of acidic units
Π_{in}	Osmotic pressures of mobile ions inside the nanogels
Π_{out}	Osmotic pressures of mobile ions in the bulk solution
Π_{el}	Elastic pressure of the polymeric network
Γ	Characteristic decay rate,
τ	Delay time
η	Viscosity
θ	Angle of the incident beam
κ	Inverse thickness of the diffuse layer
λ	Wavelength
σ_b	Stress-at-break

ε_b	Strain-at-break
λ_b	Extension ratio-at-break

Thesis abstract

This thesis presents a study towards a new concept which would use inter-crosslinked microgels to prepare double crosslinked hydrogels with high internal porosity. In the initial research a convenient method to form the doubly crosslinked pH-responsive colloidosomes was demonstrated. The colloidosomes were made by functionalised microgels of particles poly(ethylacrylate-co-methacrylic acid-co-1,4-butanediol diacrylate)-glycidyl methacrylate (GMA-MG). First of all, the non-functionalised microgels particles poly(ethylacrylate-co-methacrylic acid-co-1,4-butanediol diacrylate) (MGs) and GMA-MGs were prepared used emulsion polymerisation. The latter were then used to stabilise emulsions particles preparing the colloidosomes. The oil/water interface promoted sufficient microgel deformation and interpenetration to enable covalent inter-linking of peripheral vinyl groups on the microgel particles via free-radical coupling using UV light. Uniquely, our method for DX MG-colloidosome preparation used only one type of (colloidal) building block for shell assembly. It also showed that the doubly crosslinked pH-responsive colloidosomes had similar pH-responsive swelling properties as the GMA- MGs.

The initially established method for pH-responsive colloidosomes preparation was not compatible with scale up, which limits its potential for use. Therefore, in the next research, we established the best conditions to prepare the stable Pickering emulsion which used an ethylacrylate based microgels (EA-MGs) system. Furthermore, we demonstrated a general, gram scale method, which used high shear rate and thermal reaction to form the smallest pH-responsive microgel colloidosomes yet reported. It also showed that the doubly crosslinked pH-responsive colloidosomes had a selective pore size, which could be varied with pH. The properties of these microgel

colloidosomes dispersions imply that they have good potential for future application as injectable gels for release and delivery applications.

After the research of colloidosomes, because of the limitation of the mechanical and release property of the colloidosomes, we required more stretchable particles while the gels used above in the colloidosmes were brittle. Accordingly, new particles were synthesised by emulsion polymerisation of methyl methacrylate, methacrylic acid and without any crosslinking monomer. This is a new nanogel-based approach for preparing highly stretchable -COOH-rich hydrogels. The NGs had very high MAA content (84 mol. %). And the latter were vinyl functionalised and gave dispersions that could be crosslinked to form highly stretchable gels. The gels could form any shape and could be tied in knots and stretched considerably without damage. The DX NG gel prepared at pH 10 could be stretched to more than 250% of its original length. The maximum compressive strain for the covalent interlinking of these NGs prepared at pH 10 was 93 % without breaking. This is the highest value reported for a DX NG system to date. It also gave highly-stretchable pH-responsive DX NGs with a stretchability of up to 520%. The results of this study provide design tools for improving DX NG ductility and hence increasing the range of potential applications for this new class of hydrogel and DX pH-responsive NG-colloidosomes in future.

Declaration

I declare that no portion of the work referred to in the thesis has been submitted in support of an application for another degree or qualification of this or any other university or other institute of learning.

Wenkai Wang

25.01.2018

Copyright statement

Acknowledgements

Four years of PhD study and life has been on hold. But it is worth it as I look forward to the start of a new journey. This research and thesis is done under the cordial care and patience of my supervisor Prof. Brian Saunders. Brian created a good academic atmosphere for me and constantly motivates me to work harder and harder. It is the kind of indefatigable spirit from Brian that teaches me how to study hard and never give up. Maybe I'm not your best student, but you are my most respected teacher. Also, I would like to extend my gratitude to my co-supervisor Dr. Christopher Blanford who supports my academic life.

I would like to thanks to each one of our team members who have accompanied me over the past four/five years. Dr. Jane Bramhill, Dr. Jennifer Saunders, Dr. Junfeng Yan, Dr. Zhengxing Cui, Dr. Mu Chen, Dr. Kyriaki Pafiti, Dr. Amirhossein Milani, Dr. Nur Nabilah Shahidan, Dr. Sineenat Thaiboonrod, Dr. Judith McCann, Dr. Robert Farley, Dr. Melody Obeng, Dr. Nam Nguyen, Qing Lian, Shanglin Wu, Mingning Zhu, Dongdong Lu, Muhamad Sharan Musa, Aloïs Mispelon, Muhamad Zulhasif Mokhtar, Syazwani Mohd Zaki, Hannah Shanks, Chotiros Dokkhan. You are all respected partners in my study. At the same time, I would like to thank Dr. Louise Carney for helping me in the CLSM. Dr Christopher Wilkins taught me how to master the use of SEM patiently and kindly. Furthermore, I would like to thank Polly Greensmith for her best care and training for the past five years to ensure our clean and safe experimental environment.

Thanks to all the friends who accompanied me all the way, especially, my roommates--Yucong Zhao and Fang Wang. You two have always encouraged me and supported me, no matter how frustrating times were.

I would like to express my sincere thanks to all my family members. My Mom and Dad give me the most selfless support and concern both physically and spiritually, so that I could pay all my attention to finishing my studies successfully. In particular, Danlin Zhao, who has helped me find the right direction in my life. Thank you for coming into my life at the right time.

Chapter 1: Introduction

1.1 Motivation

According to the previous studies of our group, it has been investigating many different types of microgel based materials, especially it also has been shown that the pH-responsive doubly crosslinked microgel (DX MG) system can be applied as an injectable gel to restore the mechanical properties of the degenerated intervertebral disc (IVD). However, the increasing modulus leads to the DX MG becoming brittle. An idea overcomes to how to increase the ductility of these high modulus DX MGs. Furthermore, the DX MGs are not internally porous and are not well designed for release in vivo. In this project we aimed to demonstrate a new concept in preparing DX MGs with high internal porosity and aim to prepare covalent hydrogels with improved mechanical performance. The plan was to construct DX MG colloidosmes and then interlink them to obtain highly porous gel. However, due to lack of time and concerns about brittleness, the focus was on the colloidosomes and in proving gel ductility.

1.2 Survey of thesis

The research conducted in this project is demonstrated in three experimental chapters. The literature review was performed and presented in Chapter 2. In the literature review the fundamentals and theories, which were related to different aspects of this project, were considered.

In Chapter 3, The colloidosomes were made by functionalised microgels particles poly(ethylacrylate-*co*-methacrylic acid-*co*-1,4-butanediol diacrylate)-glycidyl methacrylate (GMA-MGs). First of all, the non-functionalized microgels particles poly(ethylacrylate-*co*-methacrylic acid-*co*-1,4-butanediol diacrylate) (MGs) and functionalized microgels particles (GMA-MGs) were prepared. The uniform spherical pH-sensitive DX MG-colloidosomes were constructed by a simple, one-component method and had a good morphology with high yield (see Scheme 1.1). The pH-triggered swelling properties of DX MG-colloidosome were also investigated.

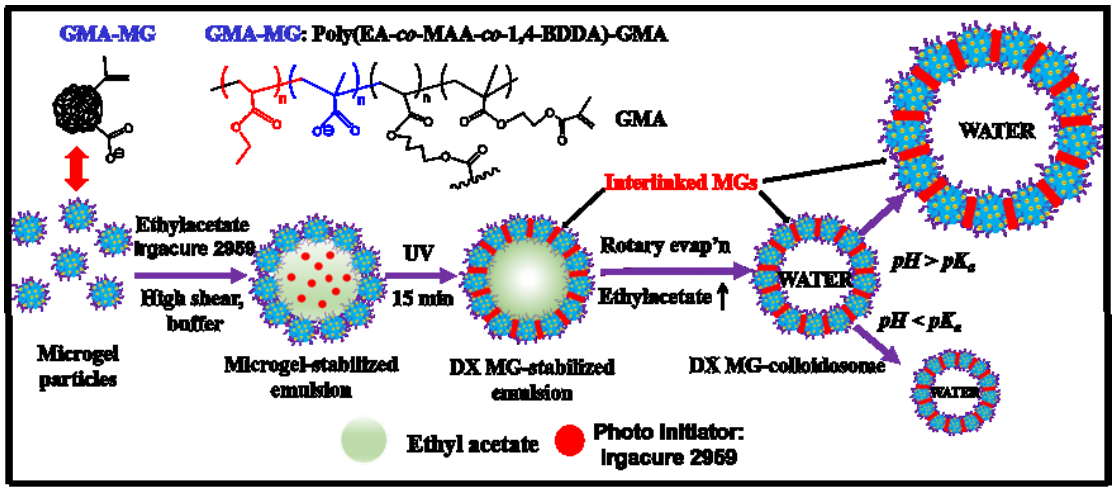

Scheme 1.1 Illustration of DX MG colloidosome preparation using pH-responsive MG particles.

In Chapter 4, firstly, we optimised microgel-stabilisation of oil-in-water emulsions. Secondly, we studied a new method to prepare DX MG colloidosomes with high

shear and very high shear (see Scheme 1.2). The DX MG-colloidosomes have been scaled up to the gram scale. Thirdly, the pH triggered swelling and permeability properties of the DX MG-colloidosomes were investigated.

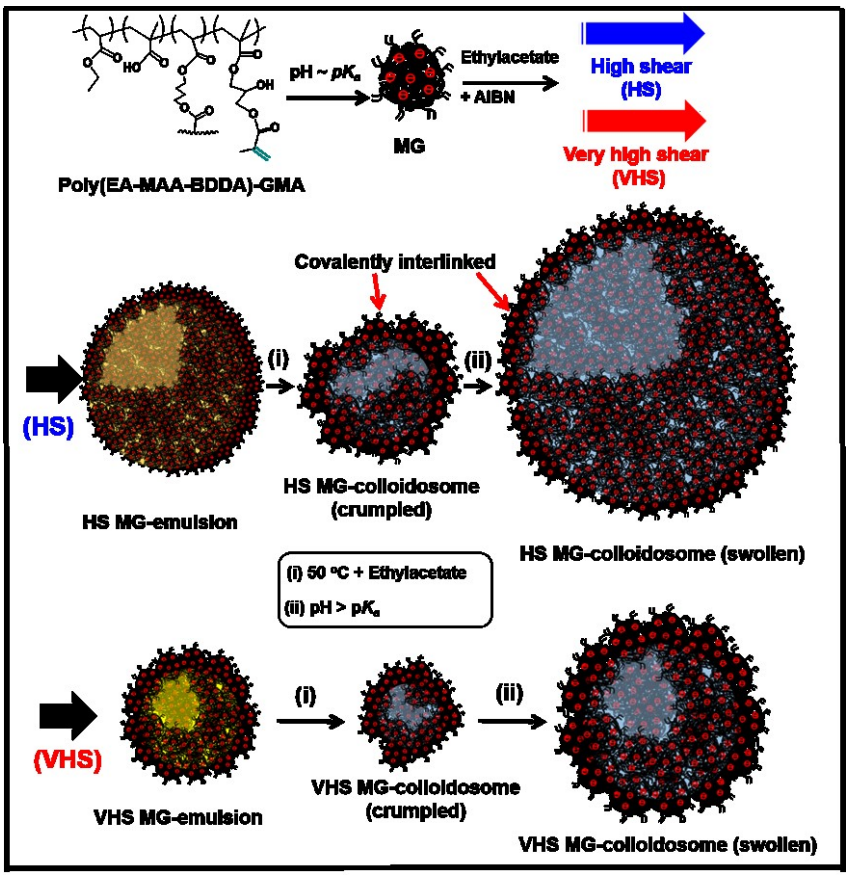

Scheme 1.2 Preparation of pH-responsive colloidosomes using microgels. Poly (EA-MAA-BDDA)-GMA MGs stabilized ethylacetate-in-water emulsions containing 2,2′-azobis(2-methylpropionitrile) (AIBN) and were heated to covalently interlink the MGs via free-radical coupling of surface vinyl groups. High shear (HS) or very high shear (VHS) mixing was used to control the emulsion and colloidosome size. The removal of ethylacetate formed crumpled colloidsomes that subsequently swelled when the pH was increased to above the pK_a.

In chapter 5, a new nanogel-based approach for preparing highly stretchable -COOH rich hydrogels has been established. This work aimed to reduce the brittleness of DX

MGs. The new type of nanogels was made using methyl methacrylate and methacrylic acid without adding crosslinker via emulsion polymerisation. They were subsequently vinyl functionalised by reaction with glycidyl methacrylate (GMA) (see Scheme 1.3). In this chapter, we first characterise the NGs and show that they were only weakly self-crosslinked. The morphology and mechanical properties of the new DX NGs are then investigated.

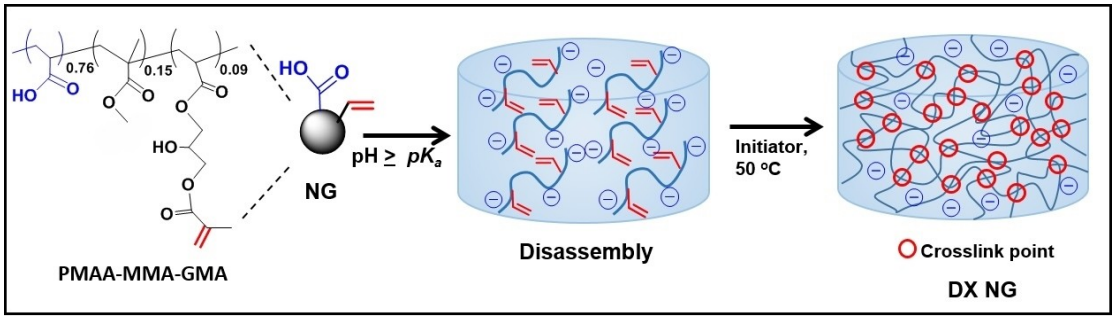

Scheme 1.3 Depiction of lightly self-crosslinked pH-triggered nanogel particle disassembly and DX NG formation.

1.2 Aim and objective of the thesis

First of all, the goal is to establish a new type of colloidosomes (hollow particles) which is constituted by microgel particles as the sole unit of its shell. This colloidosome has good cargo and release properties, which can carry tissues, cells, drugs into designated locations for release, treatment and repair of intervertebral disc disease (IVDD). Secondly, we expect to improve the mechanical properties of the microlgel/nanogel and develop a new generation of biodegradable, highly stretchable microlgel/nanogel as the treatment and repair of IDDD. Finally, we hope to combine the colloidosome and microlgel/nanogel together to form an injectable multifunctional new material for the treatment of IVDD.

Chapter 2. Literature review

2.1 Hydrogels

A hydrogel is a network of polymer chains that are swollen in water. It could be found as a colloidal gel. In 1960, Wichterle and Lim[1] were the first to make a crosslinked 2-hydroxyethyl methacrylate (HEMA) hydrogel[1]. Hydrogels have been of an interest as a biocompatible material for a long time. Researchers have achieved a lot of success in using hydrogels in cell encapsulation[2-4]. Most recently, hydrogels have been used in the field of 'tissue engineering', and were used as the matrices for regenerating and repairing a wide variety of tissues and organs[5]. The properties of hydrogels can be changed by pH, light, solution, temperature, and other methods[6]. The objective of research was to use simpler chemistry to control complex biological processes and synthesize the hydrogels. Hydrogel should be cheap and biocompatible materials for use in humans.

2.2 Microgel

A microgel particle is a crosslinked polymer particle which could be swelled in a suitable solvent[7](see Fig. 2.1.). The microgels could be made as a colloidal material, with a size of between 100 – 1000 nm[7, 8]. The term microgel has also been used to describe crosslinked polymer particles with sizes in the range of 10s of micrometres[9]. Dispersions of microgel particles with sufficiently high concentrations have the ability to swell to a point where they can form a physical gel. This swelling can occur due to stimulation by an external 'trigger'. The most common triggers used in microgel systems are temperature[10] and pH[11]. Microgels have been investigated as colloidal hydrogels[12] and used widely in different areas. Recently, research has begun to use these materials as biomaterials[13].

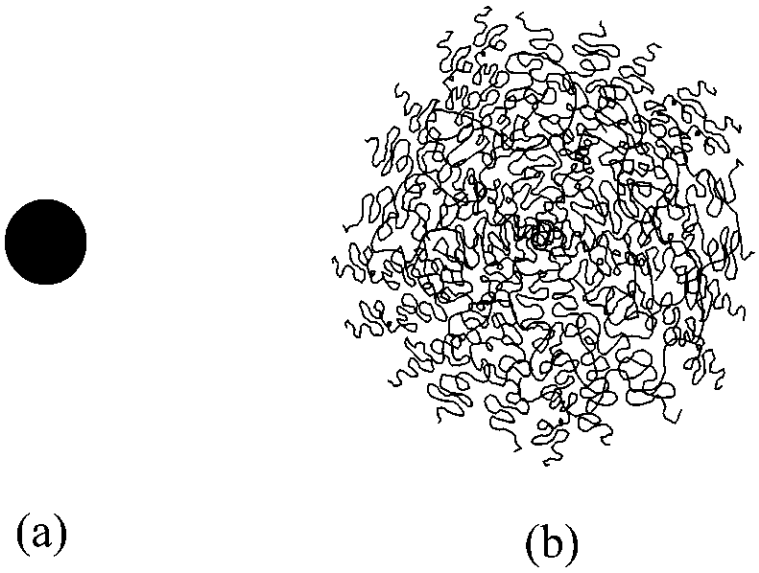

Figure 2.1 Depiction of a microgel particle at (a) collapsed state and (b) swollen state.[7]

2.2.1 Core-shell model of microgel particle structure

The preparation techniques used have been shown to result in a microgel structure, which can be designed by the 'core - shell model'. Poly(N-isopropylacrylamide) (PNIPAM) microgels have been shown to fit this model by Varga, et. al.[14] and poly(ethylacrylate-*co*-methacrylic acid-*co*-1,4-butanediol diacrylate) (EA/MAA/BDDA) microgels were shown to be core-shell by Rodriguez, et al.[15]. The later particles were prepared by seed-feed emulsion polymerization. This model is shown diagrammatically in Fig. 2.2 and indicates a central region (the core) of densely packed polymer chains of uniform structure and mesh size. They are surrounded by a less dense region of polymer chains (the shell), again of uniform structure and mesh size, but different to those at the core[10].

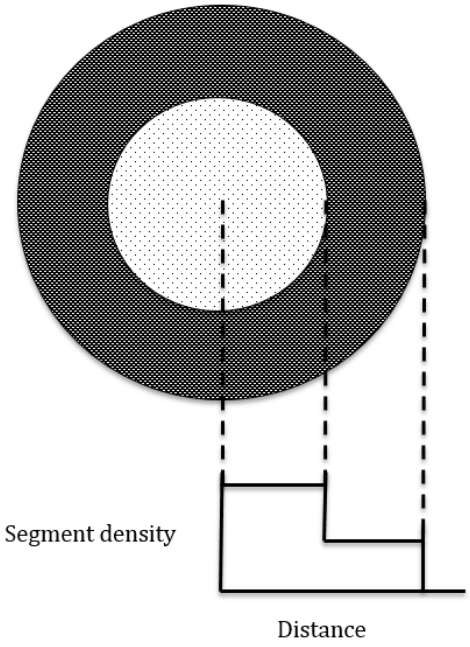

Figure 2.2 Diagrammatical representation of the core - shell structural model for a microgel particle. [12]

2.2.2 pH-responsiveness in microgels

The pH-responsive microgel particles used in this study contained three main monomers: a crosslinking monomer (e.g. BDDA), structural monomer (e.g. EA), and ionic monomer (e.g. MAA). Researchers have investigated that pH-responsive microgels could be swollen when the pH reached the pKa of the ionic monomer incorporated within the particles[8]. It is the presence of the ionic comonomer which dictates the swelling behaviour of the microgel, with the behaviour being determined by whether the monomer is anionic or cationic, and also by the extent of neutralization. The microgels used in this study contained COOH groups. As the pH approaches the pKa, the COOH groups will deprotonate, forming COO^- within the microgel particle. This leads to electrostatic repulsion between the neighbouring polymer chains and particle swelling[12]. At pH values greater than the pKa (i.e. as approaches 1.0), the particles become fully swollen[16].

The interactions between particles in microgel dispersions are functions of the polymer volume fraction (ϕ_2),and therefore the interactions are also a function of the swelling ratio, Q (as $Q = 1/\phi_2$)[12]. The Q volume can be controlled by design of the microgels by considering the below equation, derived by Flory[17].

$$Q \approx \left[\left(\frac{M_A}{f\rho_A x_B}\right)\frac{\alpha}{v_u}\right]^{3/2} \qquad (2.1)$$

Where: M_A is the molar mass of monomer A, which is the monomer of highest weight fraction in the microgel (i.e. the structural monomer); f is the number of effective chains formed per crosslinking monomer (i.e. the functionality of the crosslinking monomer); ρ_A is the density of monomer A; x_B is the mole fraction of crosslinking monomer; V_u is the molar volume of the structural unit and equal to V_A/X_i, where V_A is

the molar volume of the structural monomer, and X_i is the mole fraction of the ionic comonomer. This term is therefore a measure of the ionic group concentration[8].

α= degree of neutralisation (i.e. the fraction of the original COOH groups that exist in the anionic COO^- form) [12].

$$\alpha = \frac{1}{1+10^{(pK_a - pH)}} \qquad (2.2)$$

Equations (1) and (2) show that Q increases with decreasing of x_B, and that the pKa also plays a major role in particle swelling. These are important factors to be considered during designing of a microgel. The equations are only an approximation, useful for simple estimations of the difference in swelling ratio likely to arise from a change in formulation of the microgel, or from the extents of swelling that can be expected at different pHs for one formulation. It is an approximation because it requires the assumptions that the Flory Huggins interaction parameter, $\chi \geq 0.3$ and that the electrolyte concentration of the external phase is much lower compared to the concentration of fixed ions in the microgel[8].

2.2.3 Microgel synthesis techniques

Accordingly, to make a stable microgles dispersion needs colloidal stability by steric stabilization, electrostatic stabilization, or a combination of both of them, which is the – electrostatic stabilization[8].

In this study microgels were synthesised using emulsion polymerisation which can be considered as a homogenous nucleation mechanism. Rodriguez had investigated a type of pH-responsive microgel--poly(EA/MAA/BDDA)[15]. This method requires the mixing of monomers, surfactant and initiator in water. The water-soluble initiator would initiate the polymerization once the surfactant led to the formation of the emulsion of monomer. The growing microgels particles without a surfactant would coagulate and then the interfacial area would be reduced. Therefore, the most important factor in this method is to ensure the presence of a surfactant to prevent coagulation.

2.2.4 Emulsion polymerisation

Goodyear Tyre and Rubber Company was developed the emulsion polymerisation in the 1920's.[18] Emulsion polymerisation is used widely in the plastics, paints and construction materials. A produce a huge range of products[19] are developed using them. Emulsion polymerization is in the emulsion of water or other liquids as medium, and the isolated latex particles are produced by the micelle mechanism or the oligomer mechanism. In addition, free radical polymerization or ionic polymerization is used to produce polymers during the emulsion polymerization. The emulsion polymerization system has low viscosity, easy heat dissipation and high reaction rate and high molecular weight. In the process of emulsion polymerization, although the viscosity of the latex particles is very high, the viscosity of the whole system is not high due to the continuous period of being in water. The water as medium is low in cost and less in environmental pollution. In emulsion polymerization, the average life span of the free radical chain is longer, and the free radical has sufficient time to increase to a high molecular weight. Importantly, the equipment used for emulsion polymerization is simple and easy to operate.

There are two types of emulsion polymerisation mechanism. The type of mechanism usually depends on the concentration of surfactant currently in the system[20]. When the concentration of surfactant is lower than its critical micelle concentration (CMC), free radicals from the initiator react with the monomer in aqueous phase and create oligomeric nuclei. During propagation of these nuclei the surfactant molecules adsorb to the surface and causes colloidal stabilization. During this route, larger particles usually with narrow size distribution are achievable[20]. When the concentration of surfactant is higher than its CMC, the micellar nucleation will be occurred. In this case monomers diffuse into the micelles first and then polymerisation begins once

free radical initiators are absorbed into the micelles (see Figure 2.3). The particles formed via this method are usually smaller than those produced by the surfactant free emulsion polymerisaion but may have a broader size distribution[21].

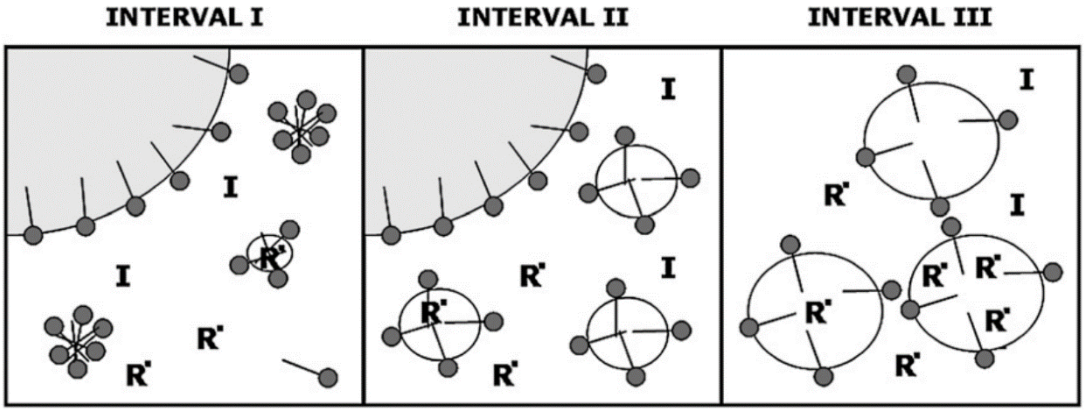

Figure 2.3 The three intervals of a typical emulsion polymerization reaction, showing surfactant molecules (), large monomer droplets, micelles (indicated by clusters of surfactant molecules within Interval I), radicals ($R^{\cdot}$), initiator (I) and surfactant-stabilized latex particles[21]

In this work emulsion polymerisation was conducted using a seed-feed method. In this method, very small particles are formed (called seed) at the first step of the reaction by addition of small portion of total monomer; hence the number of particles increases during this step. The rest of the monomer is then added as a feed with a certain rate to the reaction, gradually. By utilising this method, ideally, the particle nucleation occurs only in the seed step and particle growth occurs during the feed step. This means that particles grow at a constant rate and also there will be a uniform distribution of polymer segments within the particles.

2.3 Colloidal stability: DLVO theory

The DLVO theory is named after Derjaguin, Landau, Verwey and Overbeek[23-25], which is a theory to explain the stability of aqueous colloidal dispersion. The DLVO theory involves attractive van der Waals forces and repulsive double layer interactions, which will be discussed in the following segments.

2.3.1 Van der Waals force

Van der Waals forces include permanent and induced dipoles which are the attractive forces between molecules. London dispersion forces describe the effects of the outer electrons of two molecules, which have the result of causing fluctuating dipoles to form. The forces discussed are addiction and are modelled considering two particles of similar radius, a, and separated by a distance H, as shown in Figure 2.4.

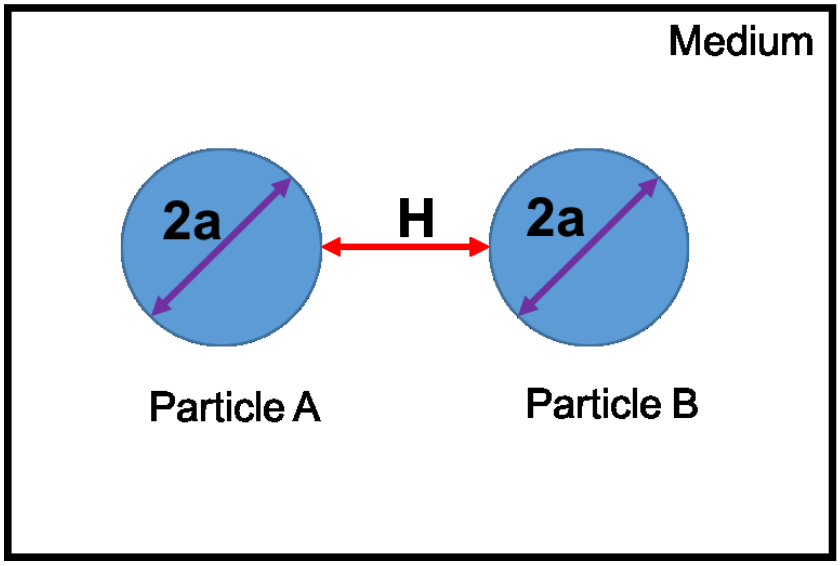

Figure 2.4 Schematic diagram of two particles in a medium.

The Van der Waals attractive force, V_{att}, can be calculated from equation 2.3[26].

$$V_{att} = -\frac{A_{eff}}{12}\left[\frac{1}{x(x+2)} + \frac{1}{(x+1)^2} + 2\ln\frac{x(x+2)}{(x+1)^2}\right] \qquad (2.3)$$

Where A_{eff} is the Hamaker constant, x is a function of the size and a is the separation distance of the particles as shown in Equation 2.4.

$$x = \frac{H}{2a} \tag{2.4}$$

These equations show that these forces are directly related to the distance between the particles. The attractive forces greatly increase when they are closer. When H is smaller than a, the equation can be simplified to equation 2.5[24].

$$V_{att} = -\frac{A_{eff}a}{12H} \tag{2.5}$$

2.3.2 Electrical double layer

The surfaces of colloids will have a net surface electric charge (either positive or negative). Changes affect the distribution of opposite (counter-ions) or similar charges (co-ions) near to the surface. The effect of the surface charge on the nearby ions leads to the formation of an electric double layer, a diagram of which is shown in Figure 2.3 for a negatively charged particles. Here it can be seen that the electric double layer is made up of two regions, the Stern layer and the diffuse layer. This model was proposed by Stern[27] in 1924, where the two regions are separated by the Stern plane, which is located approximately one hydrated ion radius from the surface[28].

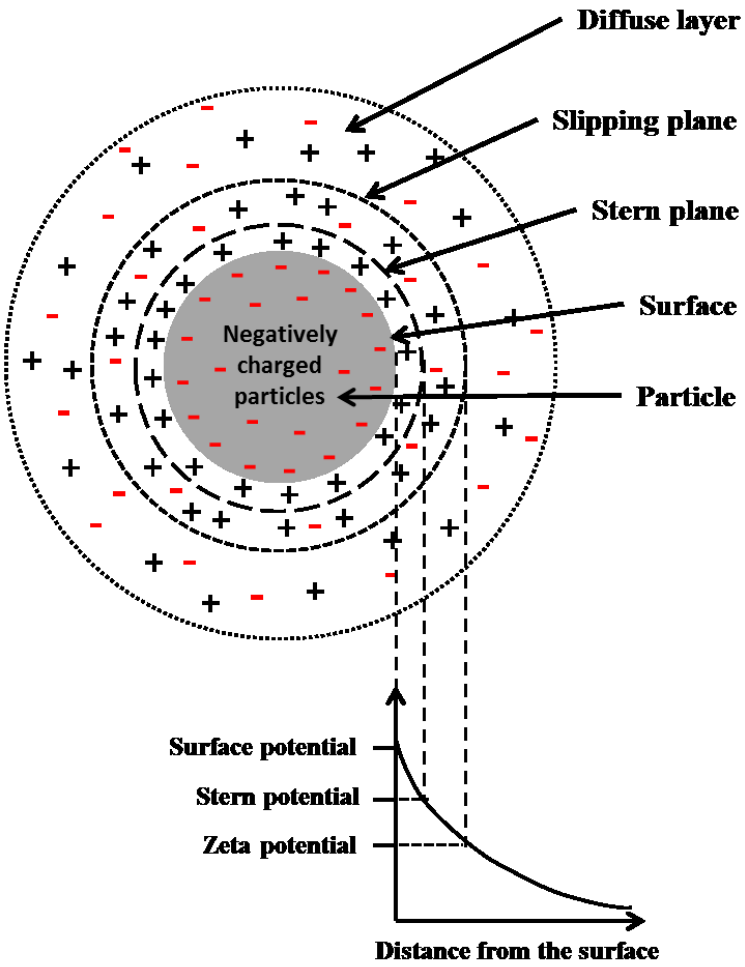

Figure 2.5 The different planes and potentials at the double layer[28]

The Stern layer, closest to the particle surface, is made up mainly of counter-ions, some of which are adsorbed to the surface. The diffuse layer contains ions which are affected by the electric forces of the particle as well as random thermal motion[28]. The thickness of the Stern layer is defined as 1/κ which is the distance away from the surface that the electrostatic interactions caused by the surface charges are significant[28]. V_{rep} represents the energy contributed by electrostatic repulsion and opposing aggregation. V_{rep} can be calculated from Equation 2.6 for spherical particles at 25 °C[30].

$$V_{rep} = \frac{\varepsilon a \psi_d^2}{2} \ln[1+exp(-\kappa H)] \quad (2.6)$$

Where ε is the dielectric constant of the solution and ψ_d is the surface potential energy at the Stern layer (shown in Figure 2.5). The ζ value, which is also shown in Figure 2.5, is the potential at the shear plane and is discussed later.

2.3.3 Combined interparticle Interactions

Figure 2.6 shows the potential energy curves for monodispersed spherical particles. The total energy of interaction (V_t) is given by:

$$V_t = V_{att} + V_{rep} \qquad (2.7)$$

Where V_{att} is originated from attractive van der Waals forces and V_{rep} results from electrical double layer forces. The potential energy profile can be obtained by calculating V_t as a function of interparticle distance (H).

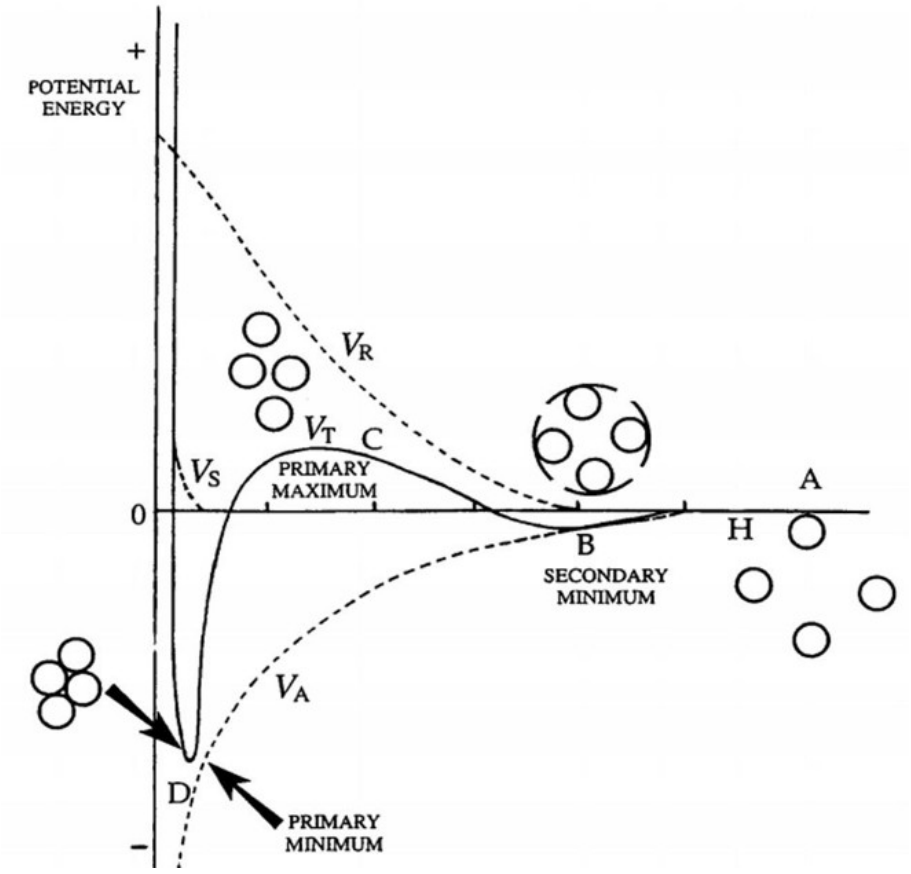

Figure 2.6 Schematic diagram of potential energies versus distance of two particles[30]

When there is a larger distance between particles, both V_{att} and Vrep are negligible (region A in Figure 2.6). At lower distance (region B), both V_{att} and V_{rep} will be

increased. The V_{att} term will increases at a higher rate than that of V_{rep}. Therefore, there is a slight domination of attractive forces which results in the appearance of a weak secondary minimum in V_t curve. The aggregation of the particles in this situation is reversible and is termed flocculation. When particles approach more closely (region C in Figure 2.6), the V_{rep} becomes the dominant term. This causes the appearance of a large energy barrier which prevents the further approach of particles. If the kinetic energy of the particles is high enough then they may pass a critical distance, where the attractive van der Waals forces increase substantially and dominate repulsive forces (D region in Fig. 2.6). This results in a strong and irreversible aggregation which is termed coagulation.

2.3.4 Steric stabilisation

When polymeric particles are at the stabilising polymer chain of the periphery and are in a good solvent, the chains extend outward. This situation results in a positive Gibbs free energy of polymer chain which prevents the approach of particles and therefore increases the stability of the colloid system[28]. This repulsive force should be added to the total energy of interaction as displayed in Equation (2.8)

$$V_t = V_{att} + V_{rep} + V_{str} \qquad (2.8)$$

For pH responsive microgels used in this study, the electrostatic stabilisation originates from surfactants or neutralised acid groups and the steric stabilisation occurs when particles are swollen and chains at the periphery of the particles are expanded.

Combinations of steric and electrostatic stabilizations are also possible which is termed electrostatic stabilization. Fig. 2.7 illustrates the three general mechanisms of stability imparted by polymers. The MG particles used in this thesis are surrounded by the negative charge and the particles swell and therefore the electrosteric stabilisation contributes to the stability of MG dispersion. Moreover, the value of V_{att} also approaches DLVO for stable MGs[32, 33].

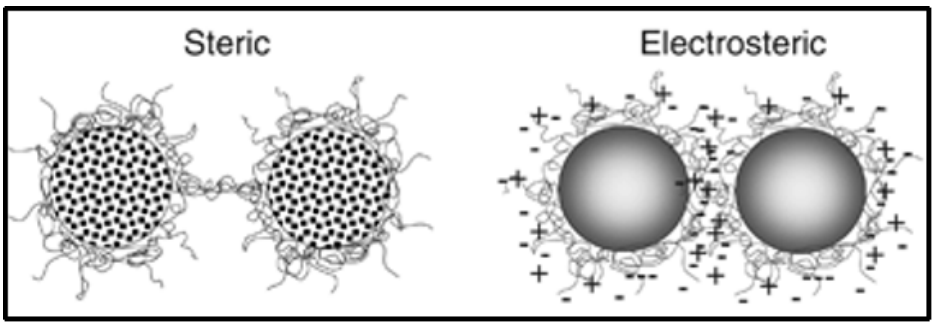

Figure 2.7 Mechanisms of polymeric stabilization[28]

2.4 The swelling of microgel particles

2.4.1 Theory of Swelling and Elasticity of pH-Responsive microgels

The equation of swelling of microgels is determined by the balance between the osmotic pressure inside and outside the microgels as described by Equation 2.9[34]:

$$\Pi_{in} + \Pi_{el} = \Pi_{out} \quad (2.9)$$

Where the Π_{in} and Π_{out} indicate the osmotic pressures of mobile ions inside the nanogels and in the bulk solution, respectively[35], Π_{el} is the elastic pressure of the polymeric network described by Equation 2.10[36]:

$$\Pi_{el} = -\frac{RTc_0}{2N_X Q^{1/3}} \quad (2.10)$$

where $Q = (R_\alpha / R_{\alpha=0})^3$ the swelling ratio of microgels, N_X is the crosslink density, and c_0 is the polymer concentration in the particles in a collapsed state. R_α represents the hydrodynamic radius of the particle at a particular α and $R_{\alpha=0}$ represents the hydrodynamic radius of the uncharged (α = 0) particle. Both are measured using the DLS technique. The terms Π_{in} and Π_{el}can be described by:

$$\Pi_{in(out)} = RTC_{in(out)} \quad (2.11)$$

where C_{in} and C_{out} are the concentrations of the ions inside and outside the nanogels. Recently, Cloitre and coworkers showed that the theoretical prediction of the relative swelling of polyelectrolyte nanogels agreed with experimental data [35]. In the absence of salt, that is, C_{out} = 0, all the counter-ions associated with the ionized units are trapped inside the polymeric network by electrostatic attraction exerted by fixed charges,

$$C_{in} = \alpha c_0 \gamma / Q \quad (2.12)$$

where c_0 is the polymer concentration inside the particles at collapsed state, γ is the molar fraction of acidic units, and α is the neutralization degree. By combining Equations 2.9 to 2.11, the swelling ratio Q of the nanogels relating to the degree of neutralization, α, and crosslinked density, N_X can be described by the scaling relation below:

$$Q \propto (\alpha N_x)^{3/2} \quad (2.13)$$

Which assumes that all the counter-ions are trapped inside the nanogels. They compared this prediction with the experimental data and showed that the data measured for different crosslinked densities collapsed onto a master curve, in good agreement with theoretical prediction in Figure 2.8.

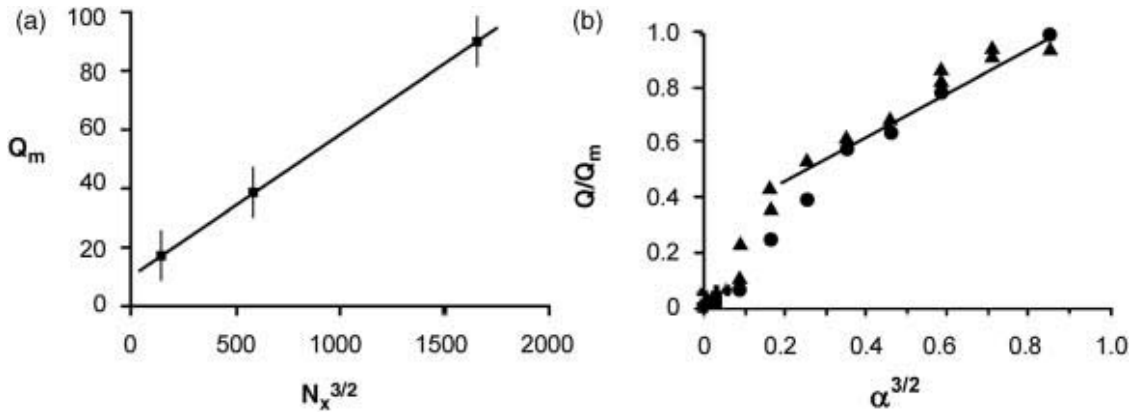

Figure 2.8 (a) Variation of the swelling ratio at maximum swelling versus the crosslinked density. (b) Variation of the swelling ratio with the neutralization degree for N_X=140 (filled circle), N_X=70 (filled diamond), N_X=28 (filled triangle)[34]

2.4.2 pH-responsive doubly crosslinked microgels as gels

The doubly crosslinked microgel (DX MG) hydrogels are of particularly of interest for biological tissue engineering or biomedicine applications because of their similarity to tissues[37]. Conventional hydrogels are normally prepared by crosslinked microgels to form the stable macroscopic gels. They are easy to make but are generally not suitable for formation in vivo. In this thesis, we used the doubly crosslinked (DX) MGs which were formed by the covalent interlinking of swollen crosslinked MG particles.

The first example of a DX microgel in this literature is from Hu et al[38]. Their DX microgel was made from hydroxypropyl cellulose nanoparticles and exhibited much faster swelling/de swelling rates than conventional homogeneous hydrogels. They developed another DX MG-temperature responsive gel, from temperature responsive MG particles of N-Isopropylacrylamide (NIPAM) copolymerized with 2-hydroxyethyl acrylate (HEA) [39]. Since this work, most DX microgels studied both by this group and others around the world have been temperature responsive[40]. However, the team in Manchester were the first to publish details about pH responsive DX microgels[41], and it is the continuation of this work which forms the experimental part of this project.

2.4.3 Construction of pH-responsive doubly crosslinked microgels.

Liu et al[41] first reported the double crosslinked pH responsive MGs. The term “double crosslinked” is used to describe and distinguish between two types of crosslinking: the intra-crosslinking of particles provide a spherical internal networks and particles here are termed as singly crosslinked particles. When adjacent particles close enough (i.e. swelling), inter-crosslinking can be achieved to form external covalent between

particles via a free-radical reaction between vinyl groups on particles surfaces. Thus, they are called DX MG particles. The construction of the DX MG is shown in Fig. 2.9.

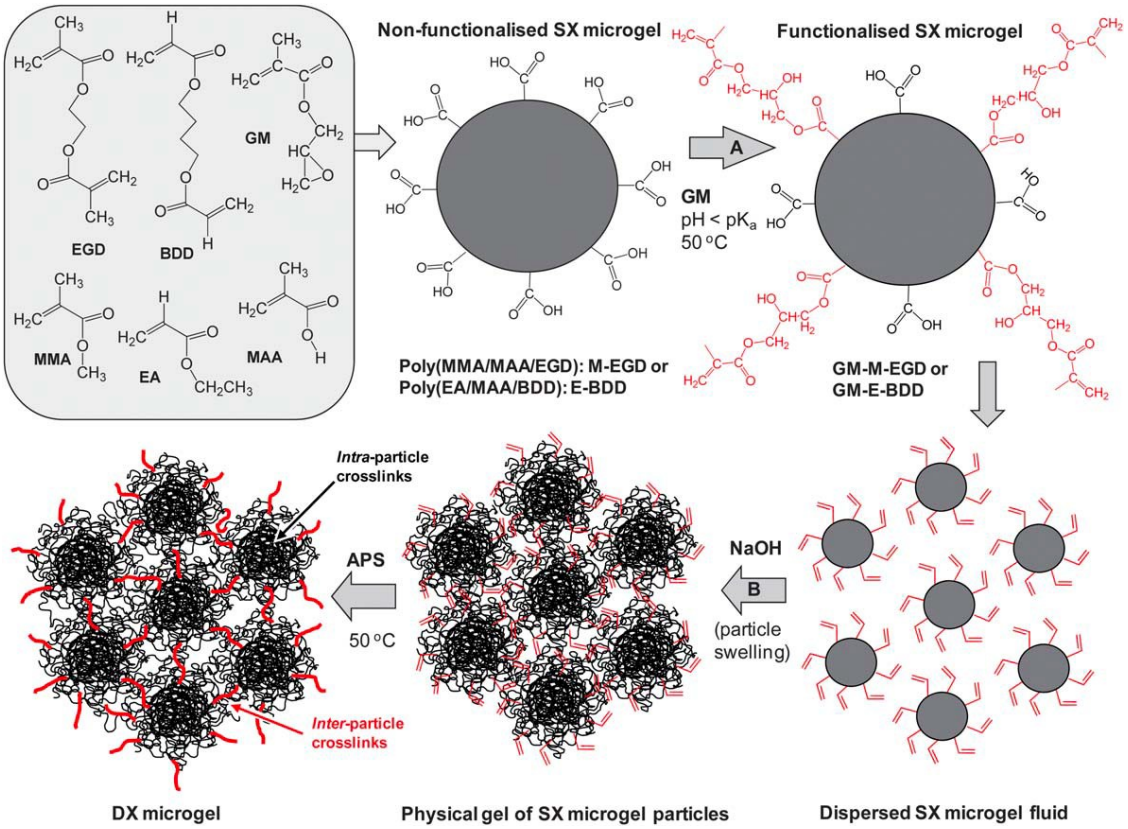

Figure 2.9 The schematic diagram of DX gels formation. In step A the surface of MG particles modified by vinyl groups. In step B the particles swell and make contact. The final step is the formation of DX MGs of covalent inter particles linking[40]

The main advantage of this DX gel system is that there is no extra small molecule (monomer or crosslinker) needed during covalent macroscopic gel formation. The irreversible DX process provide the possibility for an injectable dispersion to form a load bearing gel in vivo for dam aged soft tissues[36].

2.5 Colloidosomes

Colloidosomes are micrometer-sized hollow particles that have shells consisting of coagulated or fused colloid particles[31]. They were first reported by Velev et al[42]. Colloidosomes have been of great focus over the last decade[43, 44]. They have capsules comprising of polymer latex[45-47], and nanocomposite particles[48]. Fig. 2.10 shows different colloidosomes obtained with soft particles templates. Many examples of colloidosomes have been reported. Fig. 2.10 (a) and (b) show polystyrene/melamine-formaldehyde composite[50] and polystyrene particles[45] assembled on an oil-in-water droplet. Amine polystyrene particles were assembled on a water-in-sunflower oil droplet (Fig. 2.10c)[51]. Poly(DVB-55) porous particles were also assembled on a p-xylene-in-water droplet (Fig. 2.10d)[52]. Polymeric microrods were assembled on an agarose gel bead in tricaprylin (Fig. 2.10e)[53]. Polystyrene(PS) particles were assembled in a Janus arrangement (Fig. 2.10f)[54].

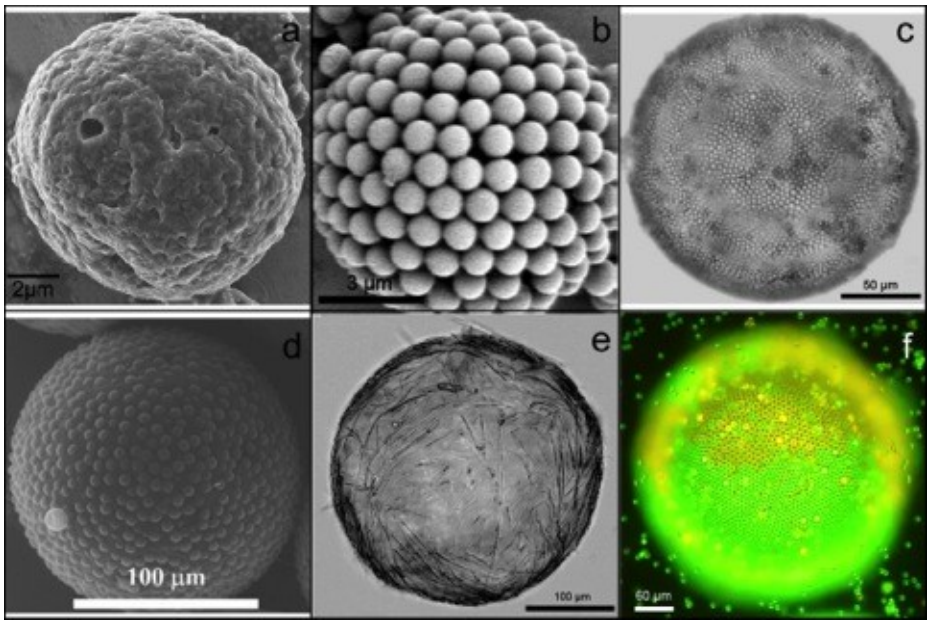

Figure 2.10 Different colloidosomes obtained with the soft template method step--adapted from Rossier-Miranda et al[48].

Depending on the different colloids particles on the shell of colloidosomes, they have potential applications in catalysis, electronic materials, lightweight fillers, artificial cells and vessels for confined reactions. Other uses may be in encapsulation of cosmetics and paints, coating manufacture. Particularly in biological system, the colloidosomes have the potential to help control the release of an encapsulated active drug species in pharmaceutical applications and may improve the handling and delivery of materials. They also have potential to aid the formation of highly porous scaffolds, which allow the ingrowth of tissue and aids nutrient transport in vivo[55-60]

2.5.1 Colloidosomes synthesis techniques

Colloidosomes can be prepared by a simple method. Fig. 2.11. shows a general methodology to produce colloidosomes. There are three main steps. Firstly, the colloidal particles adsorb on the surface of the emulsion droplets. Secondly, the colloidal particles which were adsorbed form an unstable shell that should be locked. The final step is to remove the fluid interface by exchanging the external fluid with the fluid inside the hollow particles.

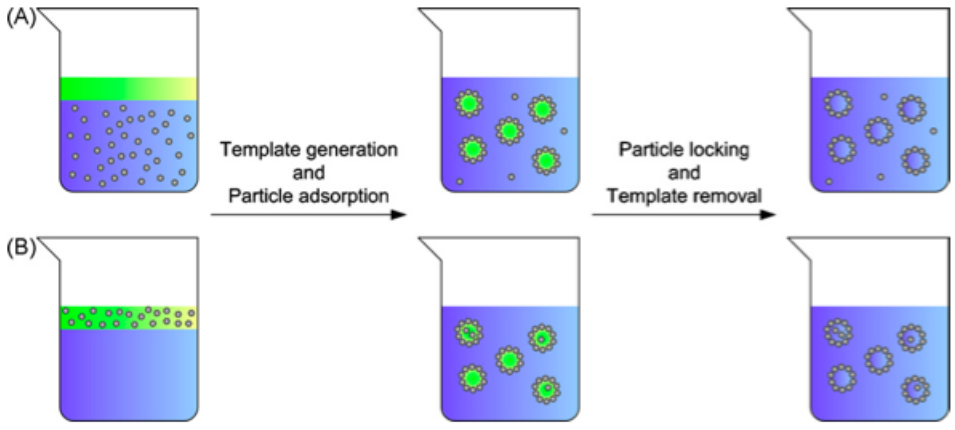

Figure 2.11 General methodology to produce colloidosomes[35]

2.6 Pickering Emulsion

The emulsion is a dispersive system consisting of two insoluble liquid phases, one of which is dispersed in the form of droplets in the other phase. However, if only droplets and continuous liquids are used, the interface of the system can be large, and the droplets will quickly get together and eventually make the two phases separate. Therefore, to obtain a stable emulsion, a class of material, emulsifier, must be added to the system. In 1903, Ramsden found that colloid particles could be used as emulsifiers when studying the protein dispersion system[62]. In 1907, Pickering undertook systematic research on the solid emulsion and stabilized emulsion. So the emulsion which is used to stabilise the solid particles of emulsion is called Pickering emulsion[61].

The hydrophile-lipophile balance (HLB) of the amphiphilic molecular surfactants shows in whether a particular surfactant stabilises oil-in-water (o/w) or water-in-oil emulsions (w/o). The packaging parameters have a definite effect on the solvent water of the polar head group of water on the oil / water interface and the oil phase of the hydrophobic tail[63]. For hydrophilic surfactants, the polar head group tends to occupy more space than the oil around the chain and the monolayer curve, giving a O / W emulsion. The case of hydrophobic surfactants is the opposite, and their lipophilic chain occupies more space than the head group, thus providing W / O emulsion.[63].

Compared with the traditional surfactants, the colloid particles adsorbed on the oil or air / water interface are not two parents, but surface active. For solid particles sitting on the oil and water interface, it is determined that the type of emulsion is the wettability of the particles.

The wettability of the particle is measured by the three-phase contact angle (θ) that the particle makes at the oil/water interface (see Figure 2.12). For hydrophilic particles, ($\theta < 90°$) the majority of the particle is absorbed in the water phase[64], thus stabilising o/w emulsions. For hydrophobic particles, ($\theta > 90°$) and the majority of the particles are absorbed in the oil phase. Importantly, when the oil/water volume fraction is 0.50, the relationship between θ and emulsion type (o/w or w/o) could be applied on the cases. However, the changing of the θ leads to the phase inversion[64].

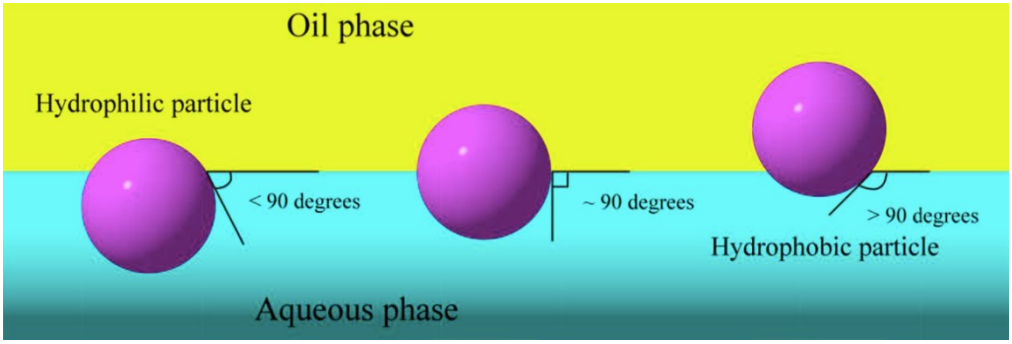

Figure 2.12 Homogeneous spherical particles at the oil-water interface. They can be hydrophilic (left), hydrophobic (right) and can have intermediate hydrophilicity (middle). Their contact angles depend on their surface hydrophilicity[64].

2.6.1 Influence of Solution pH Affecting Responsive Emulsions Stabilized by Microgel Particles

Richtering's group has built up a widely used of the PNIPAM-based microgels as stabilizers to prepare the responsive emulsions. Furthermore, they figured out the main effect of the pH environment on emulsion stability.[66-75] The PNIPAM-MAA microgel particles with both acidic and basic conditions were prepared by Richtering's group. The effect of polymer residue on the stability of the emulsion was also investigated. They found that the raw microgel particles synthesized under basic conditions would be more stable in a purified condition on the octanol-in-water

emulsions[73, 74]. There is only a small amount of MAA monomers could be incorporated the microgel particles when the microgel particles was prepared at high pH condition. Conversely, the MAA could be incorporated in to the micogel particles easily in low pH condition. This performance shows that the preparation of the efficient stimuli-responsive emulsion stabilisers needs the microgels particles with a suitable amount charges.[74]

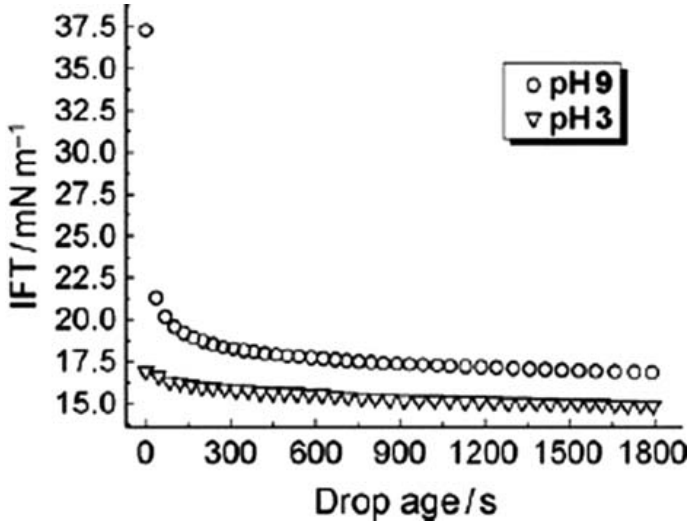

Figure 2.13 Decay of interfacial tension of a heptane–water interface as microgels adsorb at pH 3 and 9.[71]

Brugger and Richtering, mainly focused on PNIPAM-MAA microgel particles at heptane–water interfaces[72]. The interfacial tension was lowered by the microgel particles at both pH 3 and 9. It could be found that the emulsions prepared at high pH were more stable than those prepared at low pH. The results also indicated that the instable emulsion at low pH was not caused by desorption of microgel particles from the water–oil interface (Fig. 2.13).

2.8 Measurement Techniques

2.8.1 Dynamic Light Scattering (DLS)

Dynamic light scattering (DLS) is a technology to get the information of sample size by measuring the fluctuation of scattered light intensity. It is called "dynamic" because the molecules in the sample do not stop Brown movement. It is this motion that causes the scattering light to produce Doppler shift. A part of light is absorbed and part of the light is scattered when it comes to particles when it is propagated. If the molecule still does not move and the scattering light is elastic scattering, the energy frequency is constant, but the molecule is constantly undergoing a disorderly Brown movement. Therefore, when the molecules of the scattered light move towards the monitor, it is equivalent to sending the scattered photon to the monitor for some distance, so that the scattered light generated by the photon when the molecule is stationary is early enough to arrive at the monitor. That is, the frequency of scattering light increases in the view of the monitor. If the scattering light moves reversely to the monitor, it is equivalent to pulling the scattered photon away from the monitor, which results in the decrease of the frequency of the scattered light. Light scattering is to measure the diffusion rate of molecules in a solution based on this small frequency change.

The basic principle of particle size measurement based on the principle of dynamic light scattering is: The laser emitted by the laser irradiates the particles in the sample pool through the incident light path. The scattered light of the particles enters the photodetector by the receiving light path. Then the autocorrelation function of the light intensity is obtained by the digital correlator $G^2(\tau)$. The formula is:

$$G^2(\tau) = lim_{T\to\infty} \frac{1}{T}\int_0^T I(t)I(t+\tau)\,dt \quad (2.14)$$

Where, I(t) and I(t+τ) are scattered light intensity at t and t+τ time, respectively. And τ is the delay time. For the stationary process, it is advisable for t=0. According to the Siegert relation of Gauss beam, the relationship between the light intensity autocorrelation function $G^2(\tau)$ and the light field autocorrelation function $g^{(1)}(\tau)$ can be obtained:

$$G^2(\tau) = A\,[1+\beta\,|g^{(1)}(\tau)|^2] \quad (2.15)$$

Where A is the value of the light intensity autocorrelation function, when $\tau \to \infty$, it is often called the baseline and can be measured directly in the experiment. β is a parameter that reacts to the spatial coherence of the entire optical system, known as the spatial coherence factor, which is mainly determined by the optical properties of the system. For monodisperse particles,

$$G^2(\tau) = A\,[1+\beta\,exp(-2\Gamma\tau)] \quad (2.16)$$

Where, Γ is the characteristic decay rate, τ is the delay time. The relationship between Γ and scattering vector (q) can be described:

$$\Gamma = D_T q^2 \quad (2.17)$$

Where: D_T is diffusion coefficient. The scattering vector (q) can be described:

$$q=\frac{4\pi n}{\lambda_0}\sin(\frac{\theta}{2}) \quad (2.18)$$

Where λ is the wavelength of the light in the medium, n is the refractive index of suspension medium and θ is the scattering angle. The relation of diffusion is coefficient to particle size and can be achieved using the Stokes-Einstein Equation:

$$D_T = \frac{kT}{3\pi\eta d} \qquad (2.19)$$

Where, k is the Boltzmann's constant, T is the absolute temperature, η is the viscosity of the suspension liquid and d is the diameter of particles. Finally, the diameter of particles (d) can be described:

$$d = \frac{16\pi n^2 K_B T}{3\eta {\lambda_0}^2 \Gamma} \sin^2\left(\frac{\theta}{2}\right) \qquad (2.20)$$

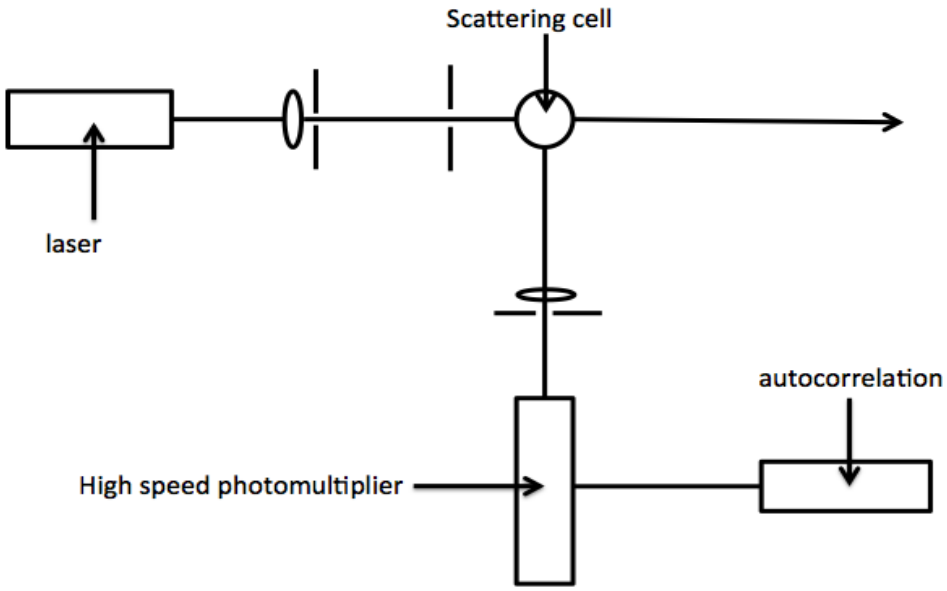

Figure 2.14 Apparatus for dynamic light scattering is illustrated schematically above. Label each of the components.

Usually, the measurement results obtained by DLS have smaller errors. The main reasons for the error are as follows: 1. The power output of a He-Ne laser is not constant. 2. The sample pool is not an ideal Colossus, therefore, the adjacent sides are

not completely vertical. 3. After adding a self focusing lens to the receiver, the light intensity can be increased, but due to the increase of the receiving surface, all light near 90 degrees is received, resulting in a certain error. 4. The change of indoor temperature also has a great influence on the experimental results. The change of temperature is mainly affected by the refractive index and viscosity of the solution.

2.8.2 Zeta potential measurement

The zeta potential is a measure of the electrostatic potential that resides in the electrical double layer surrounding the surfaces of particles in an aqueous dispersion[77]. The electrical double layer balances the surface charge of dispersed particles and consists of two regions: an inner Stern[78] layer where oppositely charged counter ions are effectively bound to the surface of the material in dispersion and an outer diffuse layer in which ions are associated with the surface but have mobility[77, 79].

Colloidal solution is a polyphase system. Dispersed phase-colloidal particles and dispersed medium are equal in numbers and opposite sign charge. Therefore, a double electric layer structure is established on the interface. When the colloid is relatively stationary, the whole solution is electrically neutral. However, under the influence of the external electric field, the potential difference is produced when the colloid particles and the dispersive medium move in reverse direction. This is called the zeta potential (ζ). The zeta potential (ζ) is one of the most important physical quantities that characterises the properties of the colloidal particles.

The electric potential is closely related to the stability of the colloid. The larger absolute value of zeta potential |(ζ)| shows that there is more particle charge and

greater repulsion between colloids and more stable colloids. The boundary of the dispersion stability of the particles in the aqueous phase is generally considered to be in +30mV or -30mV. If all the particles have a zeta potential of higher than +30mV or less than -30mV, the dispersion system should be more stable. When the zeta potential (ζ) is zero, the stability of the colloid is at its worst, and the precipitation can be observed at this time (see Table. 2.1). Therefore, it is necessary to understand the zeta potential (ζ) of the colloid.

Table 2.1 A standard of zeta potential ranges for colloidal particles in dispersed medium[79]

Zeta potential [mV]	Stability behaviour (colloid)
0 to ±5	Rapid flocculation
±10 to ±30	Incipient instability
±30 to ±40	Moderate stability
±40 to ±60	Good stability
±60 to ±100	Excellent stability

Under the action of external electric field, if the dispersed medium moves relative to the static dispersed colloidal particles, it is called electroosmosis. If the dispersed phase colloid moves relative to the dispersed medium, it is called electrophoresis. In essence, both electroosmosis and electrophoresis are the directional movement of charged particles under the action of an electric field. The zeta potential (ζ) can then be determined using the Henry equation:

$$V_c = \frac{2\varepsilon\zeta f(\kappa\alpha)}{3\eta} \qquad (2.21)$$

which relates the electrophoretic mobility (V_c), the dielectric constant (ε), the absolute zero-shear viscosity of the dispersion (η), the Henry function (f(κα)) and the ratio of

the particle radius to the Debye length (κα)[77]. The Henry function is either taken as 1.5 or 1.0 according to the Schmoluchowski approximation, or using the Huckel approximation[81].

In this thesis, Zeta potential measurement applied to microgels/nanogels particles with fluffy surface in dispersion should be considered using Ohshima's electrokinetic model as being covered by an ion-penetrable polyelectrolyte layer[82-84]. This model refers to latex particles with a core-shell structure. When being applied to microgel structures, this implies a conformation consisting of a relatively densely crosslinked, ion-impenetrable core and a lightly crosslinked polyelectrolyte surface layer that contains a higher proportion of ionic groups[83].

2.8.3 Fourier Transform Infra-Red (FTIR) spectroscopy

FTIR spectroscopy is a form of vibrational spectroscopy used to characterise materials by identifying the types of bonds present in the material. The FTIR involves five parts: the light generation system, which is composed of a light source, beam splitter, sample and so on to produce analysis of light loaded with sample information. The function of the interferometer is to make the light emitted by the light source be divided into two beams, resulting in a certain optical path difference. This is then used to generate the analytical light expressed in the spatial domain, that is, the interference light. The detector is used to detect interfering light. The sampling system, digitizing the interfering light detected by the detector through a digital to analog converter, and transfers this to the computer system. The computer system and display is used to transform the sample interference light function and the interference function of the light source to the intensity frequency distribution map.

Almost all organic compounds have an absorption in the infrared spectral range in addition to the single atom and the mononuclear molecules such as Ne, He, O_2, H_2, and et. Even if any materials are made by two compounds with different structures, they will not have the same infrared spectra, except for optical isomers, some high molecular weight polymers, and compounds with only slightly different molecular weights. Generally, the wavelength position and the intensity of the absorption band reflect the characteristics of the molecular structure, which can be used to identify the structure of unknown substances or determine their chemical groups. The absorption intensity of the absorption band is related to the content of molecular composition or chemical group, which can be used for quantitative analysis and purity identification. Because of the strong characteristic of infrared spectrum analysis, gas, liquid and

solid samples can be measured, and it has less consumption and fast analysis speed and does not destroy the characteristics of the samples.

The infrared spectrum belongs to the frequency doubling and main frequency absorption spectrum of the molecular vibrational spectrum, mainly due to the nonresonance of molecular vibration, which makes molecular vibration generated from the ground get to a high energy level state, and it has a strong ability to penetrate. Infrared light is mainly the frequency doubling and frequency absorption of the vibration of X-H (X = C, N, O) containing the hydrogen group, which contains information about the composition and molecular structure of most kinds of organic compounds. Types of bond deformations include stretching, bending, scissoring, rocking and wagging[85]. Planck's equation defines this frequency as $\nu = \Delta E/h$, where ΔE is the difference in energy between the upper and lower vibrational energy levels of the bond deformation and h is Planck's constant[86].

2.8.4 Scanning Electron Microscopy (SEM)

SEM images were obtained using the Philips FEGSEM XL30 instrument. The scanning electron microscope is composed of an electronic optical system, a signal collection and display system, a vacuum system and a power supply system. The basic principle of scanning electron microscopy is to scan the surface of the sample with a focused electron beam. First, the electron gun launches the electron beam. Then the electron beam is focused by three magnetic lenses. The function of the magnetic lens is to converge the electron beam, which reduces the beam spot of the electron beam. The electron beam then passes the scanning coil in the last stage lens through the device. The scanning coil scanned the incident electron beam onto the surface of the sample and made the picture tube synchronously scanned on the screen. When the electron beam is directed at the surface of the sample, a part of the energy is converted into heat energy, which may cause radiation damage to the sample. Another part of the energy reflects all kinds of useful information because of interaction between high-energy electrons and matter. A variety of information is generated on the sample, such as secondary electron, backscattered electron, Auger electron, X-ray, cathodoluminescence, absorbing electron and transmission electron (see Fig. 2.15).

There are two main electron: secondary electrons and backscattered electrons. Secondary electrons: the incident sheet makes the sample yard excite the electrons that are produced, and their energy is very low. Backscattered electrons: part of the incident electrons collide with the sample atoms and two change the direction of motion. They are scattered by the surface after repeated collisions, and they are therefore called backscattered electrons. Its energy is close to the energy of the incident electron. Finally, we detect the physical signals generated by the sample under the action of the incident electrons (mainly secondary electrons and

backscattered electrons), and output modulated signals onto the surface of the reaction samples. After the signal processing is amplified, the signal is transported to the kinescope. An information map that corresponds to the surface features of the sample is obtained on the screen.

In this thesis, SEM is used to observe the morphologies and size of samples, including MG particles, freeze-dried DX MGs and DX MG-colloidosomes. There are three major limitations to the application of SEM on these samples[87]. Firstly, most of the polymers have low electron density, and hence display at low contrast. Secondly, the polymers are poor in propagating the negative charges which significantly decrease the resolution. Thirdly, the incident beam will damage the soft surface of the samples. Therefore, all organic sample mentioned in this thesis are coated by a thin metal film (platinum or carbon) to increase the conductivity.

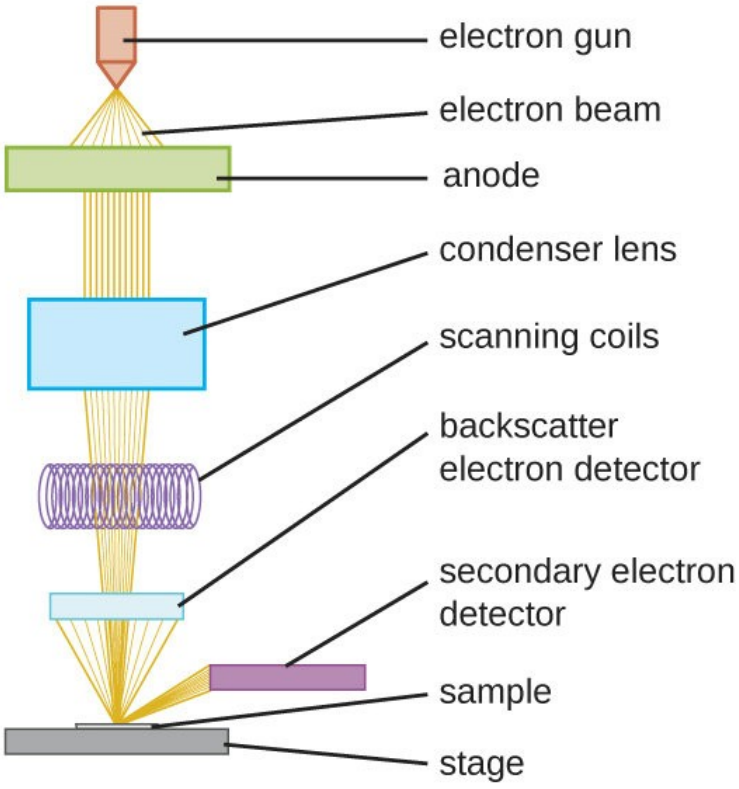

Figure 2.15 Schematic diagram of the SEM[87].

2.8.5 Transmission Electron Microscopy (TEM)

TEM is an electronic optical instrument with high resolution and high magnification, which is based on the electron beam with a short wavelength and illuminated by an electromagnetic lens. TEM is composed of three parts: The electronic optical system, the vacuum system and the power supply and control system. The electronic optical system is the core of the transmission electron microscope, and the other two systems provide support for the smooth running of the electronic optical system (see Fig. 2.16). The electron optical system is usually called the lens barrel. It is the core of the transmission electron microscope. Because of the same working principle, there are great similarities between the electron microscope and the optical microscope on the optical path structure. It is only in the electron microscope that the high energy electron beam is used instead of the visible light source, and the electromagnetic lens is replaced by the optical lens, and then the higher resolution is obtained. The electronic optical system is divided into three parts, that is, the source formation, the optics and the display section.

The function of the source formation is to provide an illuminated electron beam with high brightness, good coherence and stable beam flow. The electrons emitted by the thermionic cathodes move through the anode hole at high speed under the action of anode accelerating voltage and are gathered into a certain diameter spot by the concentrator in order to find the sample. It is composed mainly of an electron gun that emits electrons and accelerates electrons, condenser lenses converge electron beam and electron beam translation and tilt adjusting device. The imaging part is mainly composed of an object lens, a condenser lens, a projection lens, an object lens diaphragm and an electoral diaphragm. The condenser lens is used to shape the original electron beam. The objective lens is used to focus the electron beam through

the sample or to focus the electron beam through the sample. The projection lens is used to project the electron beam onto a fluorescent screen or to other display devices, such as the film. Display in part by the fluorescent screen and camera. After multiple magnifications of the lens, a high magnification image on the screen is displayed on the screen. The application of TEM in this thesis is to observe the size and structure of MG/NG particles and colloidosomes.

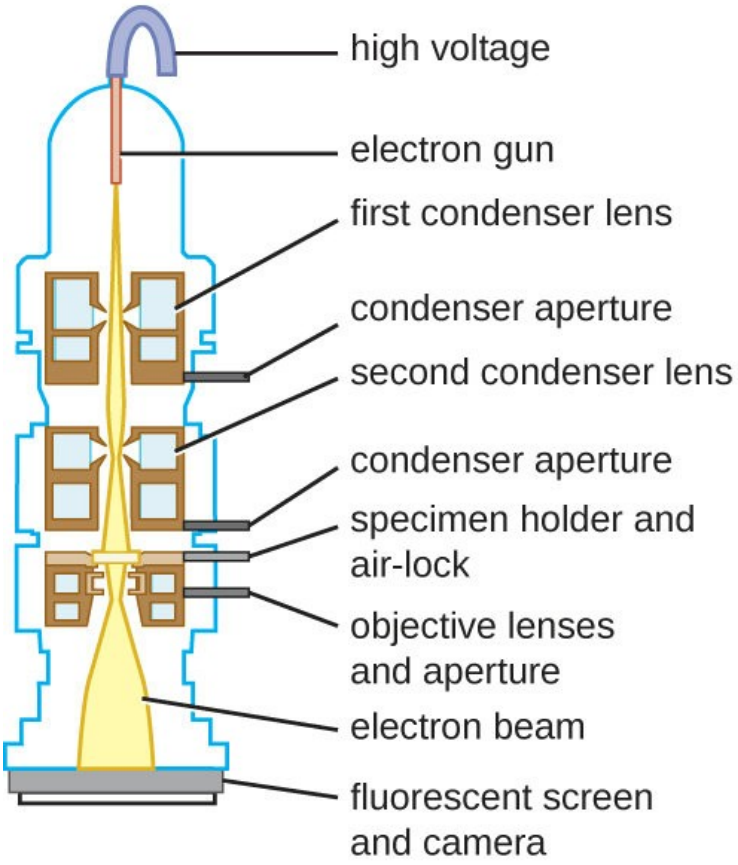

Figure 2.16 Schematic diagram of the TEM[87].

2.8.6 Confocal laser scanning microscopy (CLSM)

The invention of the confocal microscope originated in 1957. Minsky first expounded some basic principles of laser scanning confocal microscopy in his patent for the first time[17]. Because there was not enough intensity of the light source at that time, the image quality was not so ideal, so it was not brought to the attention of too many people at that time. In 1967, Egger successfully produced an optical cross-section with a confocal microscope for the first time[89]. In 1977, Wilson first described the nonlinear relationship between light and the atoms of the illuminated object and the Raman spectroscopy of the laser scanner[90]. In 1978, Brankenhoff invented a lens with high numerical aperture and applied the high numerical aperture lens to the laser confocal microscope[91]. In 1987, White and other immunofluorescent labelling methods were successfully uses to display the large molecular substances of embryos. This meant indicates that LSCM has become an important tool for scientific research[92].

A complete CLSM system consists of a major hardware and some imaging analysis software. The hardware includes a surface fluorescence microscope, laser source and cooling system, a positioning and scanning device, a resolution system, a computer control system and display and image output printing equipment. The software is composed of a three-dimensional image analysis system and three-dimensional image file management system.

CLSM uses a monochromatic laser as a light source and is attached to a light pinhole.

In addition, there is a pinhole in front of the detector. Pointolite scanned the photoelectric points after every pinhole was tested on the specimen focal plane. The spots on the specimen were detected in the pinhole and received as dots or lines by the

multiplier tube or cold electric coupler. The fluorescent images were quickly displayed on the computer's monitor screen. The position of the pinhole of the light source and the pinhole is conjugated to the focal plane of the objective lens. The point on the focal plane is focused on the pinhole of the light source and the pinhole. The points outside the focal plane are not detected in the pinhole imaging. This is called "confocal". The confocal image thus obtained is the optical cross section of the specimen, which overcomes the shortcomings of the blurred image of the ordinary microscope. Multi-channel CLSM can also display 3 different fluorescent light emitting wavelengths of fluorescent colors and 1 of mixed color images on the same screen, which has obvious advantages for studying the coexistence of 2 or more than 2 substances. By adjusting the Z value of the loading platform (the minimum distance is 0.1 M), the focal plane is located at different levels of the specimen, and the images of each optical cross-section of the specimen can be obtained by layer by layer, so as to achieve the purpose of optical sectioning. It is one of the most important functions of CLSM that a three-dimensional image of a thick specimen can be obtained through the optical slices produced by different focal plane surfaces. This technology will be used in the third and fourth chapters to verify whether the DX MGs-colloidosomes are hollow.

References

1. Wichterle, O.; LÍM, D., Hydrophilic Gels for Biological Use. *Nature* 1960, 185, 117.

2. Hsu, F. Y.; Tsai, S. W.; Wang, F. F.; Wang, Y. J., The Collagen-Containing Alginate/Poly(L-Lysine)/Alginate Microcapsules. *Artificial Cells, Blood Substitutes, and Biotechnology* 2000, 28, 147-154.

3. Lim, F.; Sun, A., Microencapsulated islets as bioartificial endocrine pancreas. *Science* 1980, 210, 908-910.

4. Matthew, H. W.; Salley, S. O.; Peterson, W. D.; Klein, M. D., Complex Coacervate Microcapsules for Mammalian Cell Culture and Artificial Organ Development. *Biotechnology Progress* 1993, 9, 510-519.

5. Hoffman, A. S., Hydrogels for biomedical applications. *Advanced Drug Delivery Reviews* 2012, 64, 18-23.

6. Mart, R. J.; Osborne, R. D.; Stevens, M. M.; Ulijn, R. V., Peptide-based stimuli-responsive biomaterials. *Soft Matter* 2006, 2, 822-835.

7. Saunders, B. R.; Vincent, B., Microgel particles as model colloids: theory, properties and applications. *Advances in Colloid and Interface Science* 1999, 80, 1-25.

8. Lally, S.; Bird, R.; Freemont, T. J.; Saunders, B. R., Microgels containing methacrylic acid: effects of composition on pH-triggered swelling and gelation behaviours. *Colloid and Polymer Science* 2009, 287, 335-343.

9. Johansson, C.; Hansson, P.; Malmsten, M., Interaction between lysozyme and poly(acrylic acid) microgels. *Journal of Colloid and Interface Science* 2007, 316, 350-359.

10. Keerl, M.; Pedersen, J. S.; Richtering, W., Temperature Sensitive Copolymer Microgels with Nanophase Separated Structure. *Journal of the American Chemical*

Society 2009, 131, 3093-3097.

11. Saunders, J. M.; Tong, T.; Le Maitre, C. L.; Freemont, T. J.; Saunders, B. R., A study of pH-responsive microgel dispersions: from fluid-to-gel transitions to mechanical property restoration for load-bearing tissue. *Soft Matter* 2007, 3, 486-494.

12. Saunders, B. R.; Laajam, N.; Daly, E.; Teow, S.; Hu, X.; Stepto, R., Microgels: From responsive polymer colloids to biomaterials. *Advances in Colloid and Interface Science* 2009, 147-148, 251-262.

13. Jia, X.; Yeo, Y.; Clifton, R. J.; Jiao, T.; Kohane, D. S.; Kobler, J. B.; Zeitels, S. M.; Langer, R., Hyaluronic Acid-Based Microgels and Microgel Networks for Vocal Fold Regeneration. *Biomacromolecules* 2006, 7, 3336-3344.

14. Varga, I.; Gilányi, T.; Mészáros, R.; Filipcsei, G.; Zrínyi, M., Effect of Cross-Link Density on the Internal Structure of Poly(N-isopropylacrylamide) Microgels. *The Journal of Physical Chemistry B* 2001, 105, 9071-9076.

15. Rodriguez, B. E.; Wolfe, M. S.; Fryd, M., Nonuniform Swelling of Alkali Swellable Microgels. *Macromolecules* 1994, 27, 6642-6647.

16. Freemont, T. J.; Saunders, B. R., pH-Responsive microgel dispersions for repairing damaged load-bearing soft tissue. *Soft Matter* 2008, 4, 919-924.

17. Flory, P. J., *Principles of polymer chemistry*. Cornell University Press: 1953.

18. Krause, S., Polymer Chemistry: An Introduction, 3rd Edition (Stevens, Malcolm P.). *Journal of Chemical Education* 2000, 77, 35.

19. Klingler, J., R. J. Hunter:Introduction to Modern Colloid Science, Oxford University Press, Oxford, New York, Melbourne, 1993. ISBN 0–19–855386–2, 338 Seiten, Preis: $ 14.95. *Berichte der Bunsengesellschaft für physikalische Chemie* 1995, 99, 591-592.

20. van Herk, A.; Heuts, H., Emulsion Polymerization. In *Encyclopedia of*

Polymer Science and Technology, John Wiley & Sons, Inc.: 2002.

21. Chern, C. S., Emulsion polymerization mechanisms and kinetics. *Progress in Polymer Science* 2006, 31, 443-486.

22. Thickett, S. C.; Gilbert, R. G., Emulsion polymerization: State of the art in kinetics and mechanisms. *Polymer* 2007, 48, 6965-6991.

23. Derjaguin, B., A theory of interaction of particles in presence of electric double layers and the stability of lyophobe colloids and disperse systems. *Progress in Surface Science* 1993, 43, 1-14.

24. Derjaguin, B.; Landau, L., Theory of the stability of strongly charged lyophobic sols and of the adhesion of strongly charged particles in solutions of electrolytes. *Acta physicochim. URSS* 1941, 14, 633-662.

25. Verwey, E., Theory of the stability of lyophobic colloids. *The Journal of Physical Chemistry* 1947, 51, 631-636.

26. Childress, A. E.; Elimelech, M., Effect of solution chemistry on the surface charge of polymeric reverse osmosis and nanofiltration membranes. *Journal of Membrane Science* 1996, 119, 253-268.

27. Stern, O., Theory of the electrical double layer.(In German.). *Electrochemistry* 1924, 30, 508-516.

28. Shaw, D., The colloidal state. *Introduction to Colloid and Surface Chemistry* 1992, 1-20.

29. Moreno, R.; Ferrari, B., Nanoparticles dispersion and the effect of related parameters in the EPD kinetics. In *Electrophoretic Deposition of Nanomaterials*, Springer: 2012; pp 73-128.

30. Hogg, R.; Healy, T. W.; Fuerstenau, D., Mutual coagulation of colloidal dispersions. *Transactions of the Faraday Society* 1966, 62, 1638-1651.

31. Yow, H. N.; Routh, A. F., Formation of liquid core–polymer shell microcapsules. *Soft Matter* 2006, 2, 940-949.

32. Napper, D. H., Steric stabilization. *Journal of Colloid and Interface Science* 1977, 58, 390-407.

33. Napper, D. H., *Polymeric stabilization of colloidal dispersions*. Academic Pr: 1983; Vol. 3.

34. Tan, B. H.; Tan, J. P. K.; Tam, K. C., pH-Responsive Nanogels: Synthesis and Physical Properties. In *Hydrogel Micro and Nanoparticles*, Wiley-VCH Verlag GmbH & Co. KGaA: 2012; pp 81-115.

35. Cloitre, M.; Borrega, R.; Monti, F.; Leibler, L., Structure and flow of polyelectrolyte microgels: from suspensions to glasses. *Comptes Rendus Physique* 2003, 4, 221-230.

36. Lyon, L. A.; Serpe, M. J., *Hydrogel micro and nanoparticles*. John Wiley & Sons: 2012.

37. Peppas, N. A.; Langer, R., New challenges in biomaterials. *Science-AAAS-Weekly Paper Edition-including Guide to Scientific Information* 1994, 263, 1715-1719.

38. Hu, Z.; Lu, X.; Gao, J.; Wang, C., Polymer gel nanoparticle networks. *Advanced Materials* 2000, 12, 1173-1176.

39. Hu, Z.; Lu, X.; Gao, J., Hydrogel opals. *Advanced Materials* 2001, 13, 1708-1712.

40. Supasuteekul, C.; Milani, A. H.; Saunders, J. M.; Lally, S.; Freemont, T.; Saunders, B. R., A study of hydrogel composites containing pH-responsive doubly crosslinked microgels. *Soft Matter* 2012, 8, 7234-7242.

41. Liu, R.; Milani, A. H.; Freemont, T. J.; Saunders, B. R., Doubly crosslinked pH-responsive microgels prepared by particle inter-penetration: swelling and

mechanical properties. *Soft Matter* 2011, 7, 4696-4704.

42. Velev, O.; Furusawa, K.; Nagayama, K., Assembly of latex particles by using emulsion droplets as templates. 1. Microstructured hollow spheres. *Langmuir* 1996, 12, 2374-2384.

43. Rossier-Miranda, F. J.; Schroën, K.; Boom, R., Mechanical characterization and pH response of fibril-reinforced microcapsules prepared by layer-by-layer adsorption. *Langmuir* 2010, 26, 19106-19113.

44. Biggs, S.; Williams, R.; Cayre, O.; Yuan, Q., Microcapsules and methods. Google Patents: 2008.

45. Dinsmore, A.; Hsu, M. F.; Nikolaides, M.; Marquez, M.; Bausch, A.; Weitz, D., Colloidosomes: selectively permeable capsules composed of colloidal particles. *Science* 2002, 298, 1006-1009.

46. Thompson, K. L.; Armes, S. P., From well-defined macromonomers to sterically-stabilised latexes to covalently cross-linkable colloidosomes: exerting control over multiple length scales. *Chemical Communications* 2010, 46, 5274-5276.

47. Yuan, Q.; Cayre, O. J.; Fujii, S.; Armes, S. P.; Williams, R. A.; Biggs, S., Responsive core− shell latex particles as colloidosome microcapsule membranes. *Langmuir* 2010, 26, 18408-18414.

48. Bon, S. A.; Chen, T., Pickering stabilization as a tool in the fabrication of complex nanopatterned silica microcapsules. *Langmuir* 2007, 23, 9527-9530.

49. Rossier-Miranda, F.; Schroën, C.; Boom, R., Colloidosomes: Versatile microcapsules in perspective. *Colloids and Surfaces A: Physicochemical and Engineering Aspects* 2009, 343, 43-49.

50. He, X. D.; Ge, X. W.; Wang, M. Z.; Zhang, Z. C., The preparation of composite microsphere with hollow core/porous shell structure by self-assembling of

latex particles at emulsion droplet interface. *Journal of colloid and interface science* 2006, 299, 791-796.

51. Cayre, O. J.; Noble, P. F.; Paunov, V. N., Fabrication of novel colloidosome microcapsules with gelled aqueous cores. *Journal of Materials Chemistry* 2004, 14, 3351-3355.

52. Croll, L. M.; Stöver, H. D., Composite tectocapsules via the self-assembly of functionalized poly (divinylbenzene) microspheres. *Pure and applied chemistry* 2004, 76, 1365-1374.

53. Noble, P. F.; Cayre, O. J.; Alargova, R. G.; Velev, O. D.; Paunov, V. N., Fabrication of "hairy" colloidosomes with shells of polymeric microrods. *Journal of the American Chemical Society* 2004, 126, 8092-8093.

54. Subramaniam, A. B.; Abkarian, M.; Stone, H. A., Controlled assembly of jammed colloidal shells on fluid droplets. *Nature materials* 2005, 4, 553-556.

55. Yang, X.; Chen, L.; Han, B.; Yang, X.; Duan, H., Preparation of magnetite and tumor dual-targeting hollow polymer microspheres with pH-sensitivity for anticancer drug-carriers. *Polymer* 2010, 51, 2533-2539.

56. Cardinal, C. M.; Francis, L. F.; Scriven, L., Drying and collapse of hollow latex. *Journal of Coatings Technology and Research* 2009, 6, 457-469.

57. Tani, T.; Takatori, K.; Pratsinis, S. E., Dynamics of hollow and solid alumina particle formation in spray flames. *Journal of the American Ceramic Society* 2004, 87, 523-525.

58. Sukhorukov, G.; Fery, A.; Möhwald, H., Intelligent micro-and nanocapsules. *Progress in Polymer Science* 2005, 30, 885-897.

59. Bhatia, S. N.; Chen, C. S., Tissue engineering at the micro-scale. *Biomedical Microdevices* 1999, 2, 131-144.

60. Freyman, T.; Yannas, I.; Gibson, L., Cellular materials as porous scaffolds for tissue engineering. *Progress in Materials Science* 2001, 46, 273-282.

61. Pickering, S. U., Cxcvi.—emulsions. *Journal of the Chemical Society, Transactions* 1907, 91, 2001-2021.

62. Ramsden, W., Separation of solids in the surface-layers of solutions and 'suspensions'(observations on surface-membranes, bubbles, emulsions, and mechanical coagulation).—Preliminary account. *Proceedings of the royal Society of London* 1904, 72, 156-164.

63. Aveyard, R.; Binks, B. P.; Clint, J. H., Emulsions stabilised solely by colloidal particles. *Advances in Colloid and Interface Science* 2003, 100, 503-546.

64. Binks, B. P., Particles as surfactants—similarities and differences. *Current opinion in colloid & interface science* 2002, 7, 21-41.

65. Kwok, M.-h.; Ngai, T., Responsive Particle-Stabilized Emulsions: Formation and Applications. In *Smart Materials for Advanced Environmental Applications*, 2016; pp 91-138.

66. Wiese, S.; Spiess, A. C.; Richtering, W., Microgel‐Stabilized Smart Emulsions for Biocatalysis. *Angewandte Chemie* 2013, 125, 604-607.

67. Richtering, W., Responsive emulsions stabilized by stimuli-sensitive microgels: emulsions with special non-Pickering properties. *Langmuir* 2012, 28, 17218-17229.

68. Liu, T.; Seiffert, S.; Thiele, J.; Abate, A. R.; Weitz, D. A.; Richtering, W., Non-coalescence of oppositely charged droplets in pH-sensitive emulsions. *Proceedings of the National Academy of Sciences* 2012, 109, 384-389.

69. Geisel, K.; Isa, L.; Richtering, W., Unraveling the 3D localization and deformation of responsive microgels at oil/water interfaces: a step forward in understanding soft emulsion stabilizers. *Langmuir* 2012, 28, 15770-15776.

70. Schmidt, S.; Liu, T.; Rütten, S.; Phan, K.-H.; Möller, M.; Richtering, W., Influence of Microgel Architecture and Oil Polarity on Stabilization of Emulsions by Stimuli-Sensitive Core–Shell Poly (N-isopropylacrylamide-co-methacrylic acid) Microgels: Mickering versus Pickering Behavior? *Langmuir* 2011, 27, 9801-9806.

71. Brugger, B.; Vermant, J.; Richtering, W., Interfacial layers of stimuli-responsive poly-(N-isopropylacrylamide-co-methacrylicacid)(PNIPAM-co-MAA) microgels characterized by interfacial rheology and compression isotherms. *Physical Chemistry Chemical Physics* 2010, 12, 14573-14578.

72. Brugger, B.; Rütten, S.; Phan, K. H.; Möller, M.; Richtering, W., The colloidal suprastructure of smart microgels at oil–water interfaces. *Angewandte Chemie International Edition* 2009, 48, 3978-3981.

73. Brugger, B.; Rosen, B. A.; Richtering, W., Microgels as stimuli-responsive stabilizers for emulsions. *Langmuir* 2008, 24, 12202-12208.

74. Brugger, B.; Richtering, W., Emulsions stabilized by stimuli-sensitive poly (N-isopropylacrylamide)-co-methacrylic acid polymers: microgels versus low molecular weight polymers. *Langmuir* 2008, 24, 7769-7777.

75. Brugger, B.; Richtering, W., Magnetic, Thermosensitive Microgels as Stimuli‐Responsive Emulsifiers Allowing for Remote Control of Separability and Stability of Oil in Water‐Emulsions. *Advanced Materials* 2007, 19, 2973-2978.

76. Walsh, A.; Thompson, K.; Armes, S.; York, D., Polyamine-functional sterically stabilized latexes for covalently cross-linkable colloidosomes. *Langmuir* 2010, 26, 18039-18048.

77. Clogston, J. D.; Patri, A. K., Zeta potential measurement. *Characterization of nanoparticles intended for drug delivery* 2011, 63-70.

78. Weiss, A.; Hartenstein, M.; Dingenouts, N.; Ballauff, M., Preparation and

characterization of well-defined sterically stabilized latex particles with narrow size distribution. *Colloid & Polymer Science* 1998, 276, 794-799.

79. Li, D., *Encyclopedia of microfluidics and nanofluidics*. Springer Science & Business Media: 2008.

80. Riddick, T. M., Control of colloid stability through zeta potential. *Blood* 1968, 10.

81. Tantra, R.; Schulze, P.; Quincey, P., Effect of nanoparticle concentration on zeta-potential measurement results and reproducibility. *Particuology* 2010, 8, 279-285.

82. Ohshima, H., Electrophoretic mobility of soft particles. *Journal of colloid and interface science* 1994, 163, 474-483.

83. Daly, E.; Saunders, B. R., Temperature–dependent electrophoretic mobility and hydrodynamic radius measurements of poly (N-isopropylacrylamide) microgel particles: structural insights. *Physical Chemistry Chemical Physics* 2000, 2, 3187-3193.

84. Ohshima, H., On the general expression for the electrophoretic mobility of a soft particle. *Journal of colloid and interface science* 2000, 228, 190-193.

85. Williams, D. H.; Fleming, I., *Spectroscopic methods in organic chemistry*. McGraw-Hill: 1980.

86. Young, R. J.; Lovell, P. A., *Introduction to polymers*. CRC press: 2011.

87. Gaillard, C.; Stadelmann, P. A.; Plummer, C. J.; Fuchs, G., Practical method for high ‐ resolution imaging of polymers by low ‐ voltage scanning electron microscopy. *Scanning* 2004, 26, 122-130.

88. Wischnitzer, S., *Introduction to electron microscopy*. Elsevier: 2013.

89. Egger, M. D., The development of confocal microscopy. *Trends in Neurosciences* 1989, 12, 11.

90. Wilson, T., Three‐dimensional imaging in confocal systems. *Journal of microscopy* 1989, 153, 161-169.

91. Brakenhoff, G.; Voort, H.; Spronsen, E.; Nanninga, N., Three‐dimensional imaging in fluorescence by confocal scanning microscopy. *Journal of microscopy* 1989, 153, 151-159.

92. White, J.; Amos, W.; Fordham, M., An evaluation of confocal versus conventional imaging of biological structures by fluorescence light microscopy. *The Journal of cell biology* 1987, 105, 41-48.

Chapter 3: Doubly crosslinked microgel-colloidosomes for pH-responsive capsule assembly using microgels as macro-crosslinkers

Abstract

In this chapter, it had mainly demonstrated is a general, convenient method to form the doubly crosslinked pH-responsive colloidosomes, which could lead to a new injectable cell delivery system or injectable scaffolds for intervertebral disc repair in the future. The colloidosomes were made by functionalized microgels particles poly(ethylacrylate-*co*-methacrylic acid-*co*-1,4-butanediol diacrylate)-glycidyl methacrylate (GMA-MGs). First of all, the non-functionalized microgels particles of poly(ethylacrylate-*co*-methacrylic acid-*co*-1,4-butanediol diacrylate) (MGs) and functionalized microgels particles (GMA-MGs) were prepared using emulsion polymerization and characterized by titration, scanning electron microscopy (SEM) and dynamic light scattering (DLS). Ethyl acetate was used at the oil phase. The oil/water interface promoted sufficient microgel deformation and interpenetration to enable covalent inter-linking of peripheral vinyl groups on the microgel particles via free-radical coupling using UV light. Uniquely, our method for DX MG-colloidosome preparation uses only one type of (colloidal) building block for shell assembly. The DX MG-colloidosomes were characterized using optical microscopy, confocal laser scanning microscopy (CLSM), transmission electron microscopy (TEM), DLS, and SEM. The morphology and the pH-triggered swelling properties of the DX MG-colloidosomes were investigated.

3.1 Introduction

The aim of this chapter was to develop a new concept which would use vinyl-functionalized single cross-linked microgels to prepare double crosslinked hollow particles with high internal porosity. Singly crosslinked pH-responsive microgel particles (SX microgels) have been studied extensively. Proof-of-principle studies have involved injection of IVDs with physically gelled singly cross-linked (SX) poly(ethylacrylate)-based microgel dispersions. More recently, those studies have involved double crosslinked microgels (DX MGs) form hydrogels with high modulus[1, 2]. DX MGs are hydrogels composed of MG particles that are covalently interlinked. A MG particle is a crosslinked polymer colloid particle that swells when the pH approaches its pK_a[3]. The DX MGs can be injectable and may support biomechanically meaningful loads[2]. However, as their modulus increases they become more brittle. A challenge that must be overcome is to increase the ductility of these high modulus DX MGs. Furthermore, the DX MGs are not internally porous and are not well designed for release. In this project we aimed to demonstrate a new concept in preparing DX MGs with high internal porosity. Here, DX MGs comprise of many interconnected voids and are connected using a Pickering emulsion approach[4]. The building block will be a MG colloidosome. Colloidosomes are a subgroup of microcapsules whose shells consist of coagulated or fused colloid particles[5]. The DX MG is related to, but different from, the DX hollow particle gels recently prepared by Bird et,al[6].

In Chapter 3, The colloidosomes were made by functionalized microgels particles poly(ethylacrylate-*co*-methacrylic acid-*co*-1,4-butanediol diacrylate)-glycidyl methacrylate (GMA-MGs). First of all, the non-functionalized microgels particles poly(ethylacrylate-*co*-methacrylic acid-*co*-1,4-butanediol diacrylate) (MGs) and functionalized microgels particles (GMA-MGs) were prepared. The uniform spherical pH-sensitive DX MG-colloidosomes were used as a simple, one-component method to prepare via UV initiation, which had a good morphology with high yield (see Scheme 3.1). The pH-triggered swelling property of DX MG-colloidosomes were also investigated.

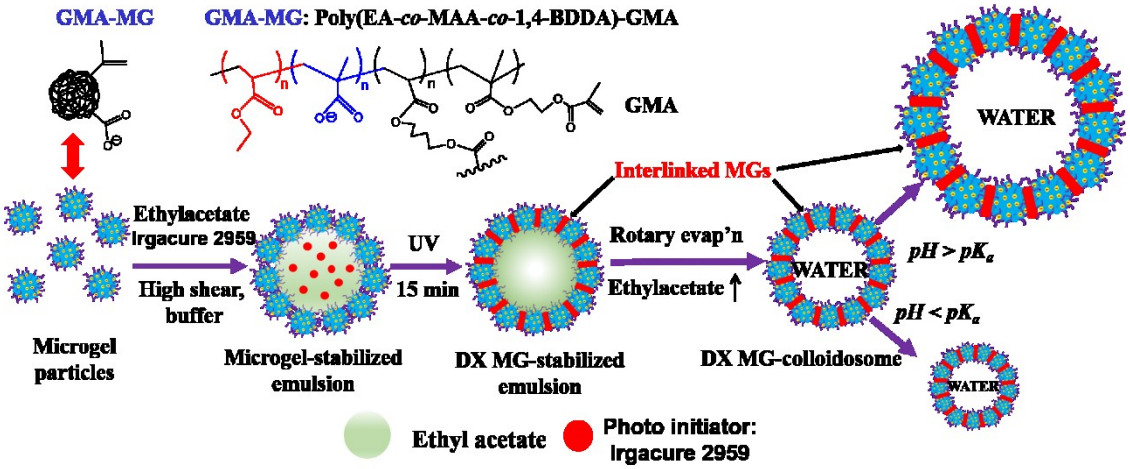

Scheme 3.1 Illustration of DX MG colloidosome preparation using pH-responsive MG particles.

3.2 Materials and Experimental Methods

3.2.1 Materials

Ethyl acrylate (EA, 99%), methyl methacrylate (MMA, 99%), methacrylic acid (MAA, 99%), 1-4 butaendiol diacrylate (1,4-BDDA, 90%), ethyleneglycol dimethacrylate (EGDMA, 98%), glycidyl methacrylate (GMA, 97%) and 2-hydroxy-4′-(2- hydroxyethoxy)-2-methylpropiophenone (photoinitiator, 98%) were purchased from Sigma-Aldrich and used as received. All water was of ultrahigh purity and was distilled and de-ionised.

3.2.2 Synthesis MGs using emulsion polymerisation.

A SDS solution (0.35 wt. %) was made using 1.81 g SDS in 517.52 g DI water. This was placed in a round bottomed flask fitted with a reflux condenser and mechanical stirrer. The solution was heated to 80°C in a water bath and purged with nitrogen gas for 30 min. A 289.85 g monomer mixture containing 66 wt.% EA (189.90 g), 33 wt.% MAA (97.06 g) and 1 wt. % BDDA (2.88 g) was made. A K_2HPO_4 solution (7 wt.%) was prepared using K_2HPO_4 (0.22 g) in water (2.94 g). An APS solution (5 wt.%) was prepared using APS (0.18 g) in water (3.33 g). 31.5 g of the mixture solution was added to a flask, and 3.15 g of K_2HPO_4 solution and 3.5 g of APS solution were then added. The temperature of the water bath was increased to 85°C and the mixture stirred for a further 30 minutes. Then 218.5 g of the monomer mixture was added at a constant rate using a pump over about 90 min. The reaction was continued with mechanical stirring in a nitrogen atmosphere at 85°C for a further 2 hours. The product was cooled in ice cold water, filtered through a 53 μm mesh and dialyzed in water for a total of 14 days, changing the fresh DI water twice daily.

3.2.3 Synthesis GMA-MGs

The functionalised MGs were made by adding the glycidyl methacrylate (GMA, 97%) into the E-BDDA microgels . The E-BDDA microgel dispersion had a polymer volume fraction of 22 wt. %. Microgel dispersion (100g, 10.0 wt.%) was prepared by mixing 45.2 g of EBDD microgel dispersion with 54.8 g of water in a round bottomed flask. GMA (16.77 g) was added to the flask. Due to the high concentration of the mixture, 50mL water was added after the adding the GMA. The pH was controlled before adding the alkaline solution. The mixture was then heated to 50°C in an oil bath and mechanically stirred for 8 hours. After the reaction, the mixture was taken out and filtered through a 53 μm mesh and diluted to an approximately 300 mL total volume with water in a separating funnel. Adding the same volume of chloroform into the separating funnel, the mixture was 'washed' by shaking the funnel for about 5 minutes. The funnel was suspended over an empty beaker for a few minutes to allow the mixture to separate before opening the tap to drain off the chloroform. Another roughly equal volume of chloroform was added to the separating funnel, and the procedure was then repeated twice more. After the final chloroform wash, the contents of the separating funnel were placed in another round bottomed flask and attached to a rotary evaporator. This was used to remove the rest of the chloroform at room temperature.

3.2.4 Preparing colloidosomes

The pH-responsive vinyl-functionalised microgels used in this study were poly(ethylacrylate-*co*-methacrylic acid-*co*-1,4-butanediol diacrylate)-glycidyl methacrylate (poly(EA-*co*-MAA-*co*-1,4-BDDA)-GMA). The GMA-MGs particles were used to stabilise ethyl acetate-in-water emulsions (Scheme 1), which contained a UV photoinitiator (2-hydroxy-4′-(2-hydroxyethoxy)-2-methyl- propiophenone). The role of the photo initiator was to covalently "stitch together" the MG building blocks at the oil-water interface. After UV irradiation the ethyl acetate was removed by rotatory evaporation at room temperature to give DX MG-colloidosomes.

3.2.4.1 Method 1: Preparation of MG-stabilised emulsions using low photoinitiator concentration

Photoinitiator (2.0 mg, 0.0089 mmol.) was dissolved in ethylacetate (2.0 ml) and the oil phase added to 4.0 ml of water and 0.3 ml of GMA-MG dispersion (5.0 wt.%). The emulsion was sheared at 9,500 rpm for 30 s using a Silverson L4R high shear mixer equipped with a micromixing head and it was kept cool in an ice-water bath.

3.2.4.2 Method 2: Preparation of MG-stabilised emulsions using high photo initiator concentration

Photoinitiator (10.0 mg, 0.045 mmole) was dissolved in ethylacetate (1.0 ml) and the oil phase added to 3.5 ml of buffer solution (pH = 6.8) and 0.5 ml of GMA-MG dispersion (5.0 wt.%). The emulsion was sheared at 10,500 rpm for 120 s using and Silverson L4R high shear mixer equipped with a micromixing head and till keep in ice-water bath cooling.

3.2.4.3 Preparation of doubly crosslinked microgel colloidosomes

Both of Method 1 and Method 2 emulsions were placed in a petri dish (diameter ~ 5 cm) which was sealed with parafilm and the sample was UV irradiated for 10 min at 254 nm using a UV Crosslinker instrument (Ultra-violet Products LtD). Then ethylacetate was subsequently removed by rotary evaporation at room temperature to give a dispersion of DX MG-colloidosomes.

3.2.5 Physical Measurements

Optical images were obtained using an Olympus BX41 microscope. Titration measurements were performed using a Mettler Toledo titration unit in the using a supporting electrolyte (0.1 M NaCl). Dynamic Light Scattering (DLS) measurements were obtained using a Malvern Nano ZS instrument. All measurements were conducted using 0.1M buffer solutions. SEM measurements were obtained using a Philips XL30 FEG SEM instrument. Dispersions of particles were deposited on SEM stubs at room temperature. The samples were coated by platinum or carbon. The number-average particle sizes were measured with Image J software (National Institutes of Health) and at least 100 particles were measured. Confocal laser scanning microscopy (CLSM) images were obtained using Broadband Confocal Leica TCS SP5. The DX MG-colloidomes were labelled by Rhodamine B. Rhodamine B was dissolved in water (at a concentration of 2*10-9 M). DX MG-colloidosomes were then dispersed in the Rhodamine B solution before being examination.

3.3 Results and Discussion

3.3.1 Singly crosslinked microgel characterization and pH-dependent swelling

It is possible to study the morphology of microgel particles by SEM. Fig. 2 shows SEM images of microgel particles before and after being functionalized. High magnification SEM images of both MGs and GMA-MGs (Fig. 3.1) show that the particles are spherical. It has been shown previously[3] that polystyrene microgel particles dispersed in an organic solvent can deform to give a "pancake" morphology as described by Saunders et，al.[7] When observed under SEM. However, this particle deformation was not apparent for either of these microgels in any of the SEM images obtained obviously in this work. But only SEM at side angle could support this. The number-average particle size of MGs (Fi|g. 3.1a) from SEM was 72 nm (coefficient of variation, CV = 15%). The number-average particle size of GMA-MGs (Fig. 3.1(b) from SEM was 73 nm (CV = 12%). The morphology of particles for MG can be compared before and after functionalisation as well. It is important to ensure that functionalisation does not affect the morphology and size of particles too much.

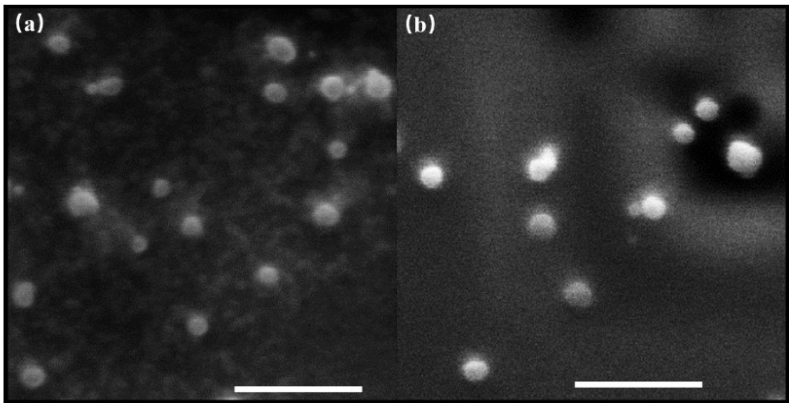

Figure 3.1 (a) SEM image of dried MGs. (b) SEM images of dried GMA-MGs. Microgel concentrations before drying were control at 5 x 10^{-6} wt.%. The scale bars are 500 nm.

3.3.2 Measuring microgels particle size using DLS

DLS was used to determine the z-average diameter (d_z) of SX MG particles at different pHs before and after functionalisation. The variation of d_z with pH can be seen in Fig. 3.2. The particle size increased with increasing pH, which is expected for pH responsive microgels containing carboxylic acid groups.

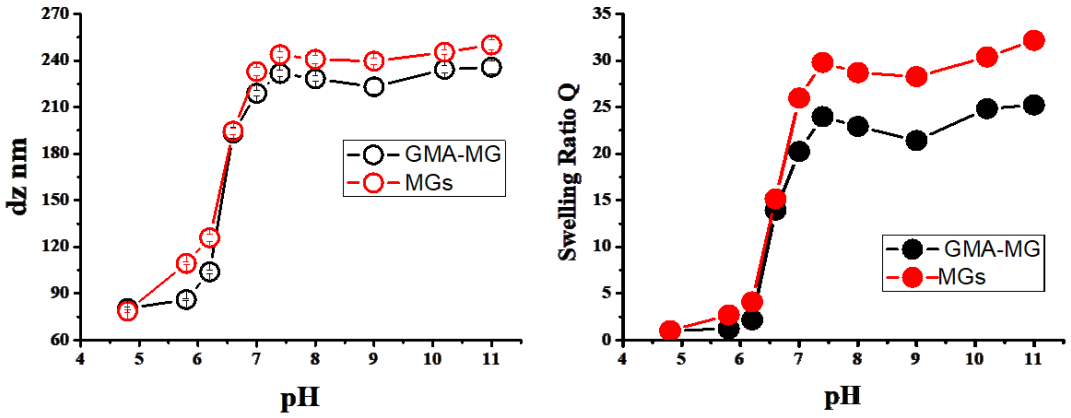

Figure 3.2 (a) showed the DLS results of an average hydrodynamic diameter vs. pH of MGs and GMA-MGs. (b) The average swelling ratio vs pH for MGs and GMA-MGs.

The pH-dependence of the mean diameter and the mean volume swelling ratio (Q) of the MGs and GMA-MGs was shown in Fig. 3 (a) and (b), respectively. Significant pH-triggered swelling occurred of MGs and GMA-MGs at a pH 6.5 and 6.4, respectively. Then pH-triggered swelling of MGs and GMA-MGs became almost constant after pH=7.4. When the pH value was above 9, they continued to show a slight increase in d_z with pH increased (Fig. 3.2). As a result of this, the swelling ratios of MGs at pH values above ~6.5 were greater than those of the GMA-MGs (Fig. 3).

3.3.3 Potentiometric titration

The titration data for these two microgels (Fig. 3.3) showed that the mean MAA content of MGs was 35.64 % and GMA-MGs was 27.16 % (Table. 1). Potentiometric titration data also showed that the GMA-MGs particles contained 8.5 mol. % of GMA. These results were expected, as the GMA reacts with the –COOH groups of some of the MAA molecules at the surface of the MGs particles. This functionalises the particles, reducing the total number of ionic –COOH groups with the microgel particles and thus reducing the titration value of MAA for GMA-MGs. However, this decrease in the number of ionic groups in GMA-MGs meaning that there were fewer groups within the particles to be ionized from pH changes, and the particles do not decrease in size as much or as the non-functionalised MGs particles with high concentrations of –COOH (Fig. 3.2).

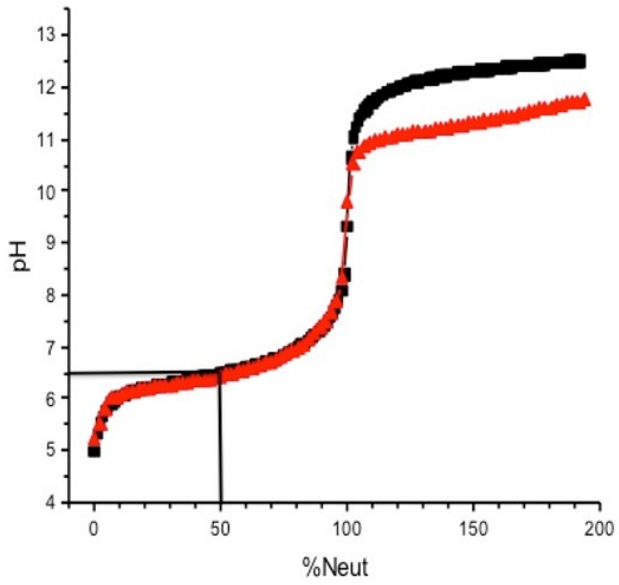

Figure 3.3 Potentiometric titration data for MGs (black) and GMA-MGs (red).

It was expected that the pK_a would increase for GMA-MGs due to more hydrophobic group (GMA) and less polar microenvironment. However, the pK_a for GMA-MGs slightly decreased after functionalization (Table. 3.1). This is possibly due to after functionalisation changes in complex thermodynamic factors, which facilitate deprotonation of carboxylic acid groups.

Table 3.1 Compositions and characterisation data of microgels

Particles	Mol % GMA[a]	$d_{n(SEM)}$[b]/ nm	$d_{(4.8)}$/nm	$d_{h(10)}$/nm	$Q_{(10)}$[c]	pK_a	Mean MAA[a] %
MG	——	72 [15][d]	78.64 ± 0.89	245.4 ± 1.39	30	6.5 ± 0.1	35.64 ± 1.14
GMA-MG	8.5	73 [12] [d]	80.35 ± 1.02	234.4 ± 2.54	25	6.4 ± 0.1	27.16 ± 0.88

[a] Calculated from the difference in the mol. % GMA and MAA before and after functionalisation. [b] Number- average diameters determined from SEM images. [c] The swelling ratio of MG and GMA-MG at pH10 determined from DLS. [d]

3.3.4 DX MG-colloidosomes prepared using method 1.

Under the optical microscope, the spherical particles were found (Fig. 10a). The swelling DX MG-colloidosomes were confirmed as well (Fig. 10 (b) (c) and (d)).

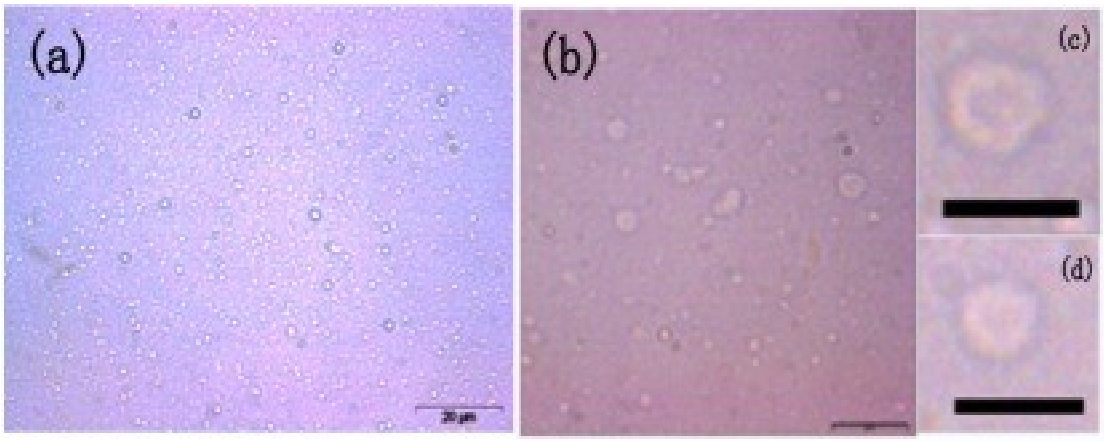

Figure 3.4 (a) Optical micrographs of DX MG-colloidosomes; (b) to (d) are optical micrographs of swelling DX MG-colloidosomes (pH 9.0). The scale bar in (a) and (b) are 20 μm; both scale bars in (c) and (d) are 10 μm.

Spherical particles were confirmed, whereas the MGs-based shell and hollow central were not to be found clearly in Fig. 5 (a). According to optical microscopic images, the average diameter of the DX MG-colloidosomes was 2.0 um. When the pH of DX MG-colloidosomes dispersion was increased to 9.0, there were some of the DX MG-colloidosomes that were clearly swollen Fig. 3.4(b). According to these images, the swollen hollow particles had an average diameter of ~8.7 μm. The hollow center and the thickness of shell could be viewed more clearly in Fig. 3.4(c) and (d). The thickness of the shell was around 2.0 μm. In summary, the yield of swollen colloidosomes was low, which could be viewed from Fig. 3.4(c) and (d)was low and the pH-responsive swelling property was not good using method 1 of forming DX MG-colloidosome. A challenge had to be overcome was to improve the high yield of

the colloidosomes. The key aim was to increase the adsorption capacity between GMA-MGs and the oil/water interface.

3.3.5 A brief study of Pickering emulsion with pH-Responsive Behaviors.

Following the reasoning of method 1, a primary study of Pickering emulsion was conducted. here, we use method 2 without adding the photo initiator. This involved addition of the GMA-MGs particles to ethyl acetate and different buffer solution mixtures followed by high shear which resulted in stable oil-in-water emulsions with pH-dependent colloidal stabile (Fig. 3.5).

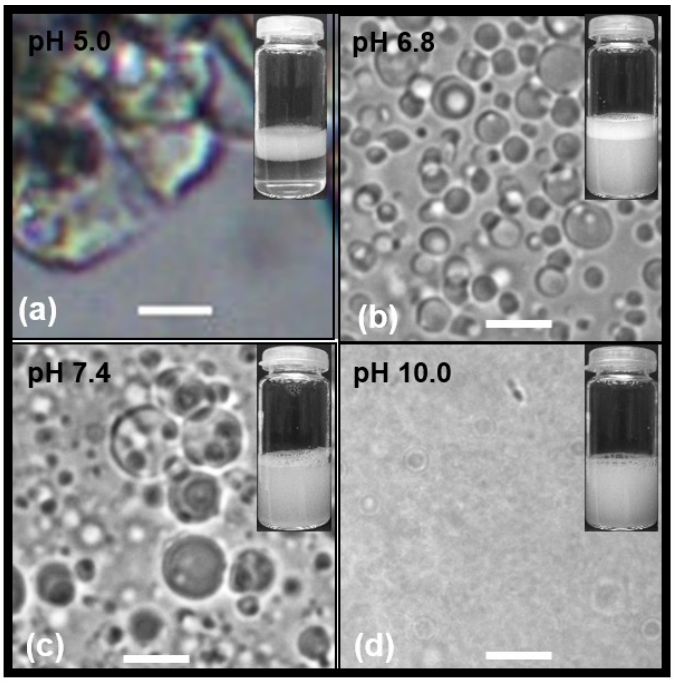

Figure 3.5 Optical micrographs (a) to (d) of pickering emulsions prepared by 1.0 ml ethyl acetate oil and 4.0 ml of 0.63 wt% aqueous GMA-MGs with buffer (a) pH 5, (b) pH 6.8, (c) pH 7.4 and (d) pH 10 buffer, respectively. The mixtures were homogenized for 2 minutes at 10500 rpm and allowed to stand for 10 min before optical micrographs and digital photographs of the vials were recorded as inset. The

scale bars were 10 μm.

The surface charge and partial wettability of the Pickering emulsifier are key parameters that control the type and stability of the Pickering emulsions[8]. In the discussion on emulsion stability, only coalescence that leads to phase separation is considered to be destabilisation of the emulsion droplets. Therefore, the responsive properties of modified particles were correlated to the dispersion pH, which can be exploited for stabilizing emulsions.[9,10, 11]

As a reference, we prepared the four different Pickering emulsion (Fig. 3.5). At lower pH 5 (Fig. 3.5(a)) the emulsions formed the cream rapidly and the droplets aggregated. It had a poor stability when the microgel particles were in the collapsed state as had been reported[12]. However, at pH of 6.8 the GMA-MG-stabilised O/W droplets were colloidally stable (Fig. 6 (b)) and did not cream over 24 h. The average droplet diameter for the emulsion droplets at pH 6.8 was 3.5 μm (CV = 36%). At pH values greater than 7.4 the smaller droplets became less visible (Fig. 3.5(c)) and at pH 10 droplets were not able to be visualised clearly by optical microscopy (Fig. 3.5(d)). At high pH the GMA-MG particles were too hydrophilic to adsorb strongly into the interface. At pH 6.8 the MG particles were less hydrophilic due to a lower extent of GMA-MG neutralisation (Fig. 3.5) and they provided good emulsion stability (Fig. 3.5(b)). The latter emulsions did not phase separately over a period of 24 h. In summary, we selected pH 6.8 buffer to prepare the DX MG colloidosomes due to the good stable condition of the precursor emulsions and the higher yield of colloidosoemes.

3.3.6 Morphological Characterisation of DX MG-colloidosomes prepared by method 2.

The morphology of the DX MG-colloidosomes was probed using several complementary microscopy techniques (Fig. 7 to Fig. 11). DX MG-colloidosome morphology was probed directly by optical microscopy (Fig. 3.6(a)).

3.3.6.1 Optical microscope

Firstly, optical micrographs obtained at pH 6.4 (Fig. 3.6(a)) revealed the colloidosomes were hollow. The number-average diameter of colloidosomes was measured as 1.7 μm (CV = 22 %). Secondly, by contrast, the number-average size of parent MG-stablised emulsion (Fig. 3.5(b)) was larger, which was 3.5 μm (CV = 36%). A reason for this may be that following the double crosslinking reaction. The pH of colloidosomes would be slight decreased from 6.8 to 6.4 after the DX MG-colloidosomes formation. The final of pH 6.4 was equal to the pK_a of GMA-MG. The pH decreased to 6.4 corresponding to a major decrease in the diameter of the MG particles (Fig. 3a). Another reason was that the oil phase was removed by rotary evaporation. Consequently, the diameter of final DX MG-colloidosomes (1.7 μm) was smaller than before UV crosslinking (d=3.5 μm). This topic is also considered in chapter. 4.

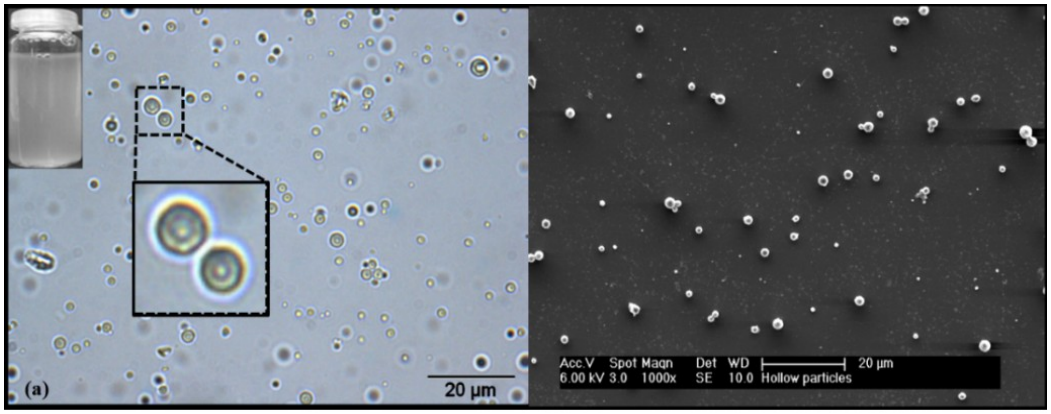

Figure 3.6 (a) Optical microscope of DX MG-colloidosomes prepared by method 2. (b) SEM image of DX MG-colloidosomes prepared by method 2.

3.3.6.2 Confocal laser scanning microscope

DX MG-colloidosomes morphology was probed using a confocal laser scanning microscope (CLSM) with Rhodamine B labelling (Fig. 3.7 and Fig.3.8). We used confocal laser scanning microscopy images to get evidence that the particles were hollow and also of the thickness of the shell. The DX MG-colloidosomes were made by poly (EA-MAA-BDDA) as written in Scheme. 1. Then the functionalised MG was used to covalent inter-linking of the peripheral vinyl group on the microgels particles via free-radical coupling initiating by the photo initiator (Scheme. 1). According to the chemical structure of microgels particles, they had COOH in the chain of MAA with some $-COO^-$. The Rhodamine B would have the positive charge, which would have been adsorbed by the COO^- groups.

From the CLSM images in Fig. 3.7, first of all, the DX MG-colloidosome particles using (method 1 (Fig. 3.7(a) and (b)) and method 2 (Fig. 3.7(c) and (d)) were spherical. Both method 1 and method 2 of the DX MG-colloidosomes (Fig. 3.7) were confirmed that they were hollow particles. The microgel-based shell of the DX MG-colloidosomes could also be confirmed clearly under the CLSM as well. Method 1,

from Fig. 3.7(a) and (b), showed the number average diameter of the colloidosomes was 1.96 μm and the thickness of the shell was ~0.12 μm. The number average diameter of the GMA-microgel particles was 73 nm by SEM in Fig. 3.1. It was not clear whether the shell of DX MG-colloidosome using method 1 consisted of multiple layers or of a single layer. For method 2, from Fig. 3.7(c) and (d), by contrast with Fig. 3.7(a) to (b), it was not easy to see that all of the colloidosomes were hollow particles nature and measure the thickness of the shell.

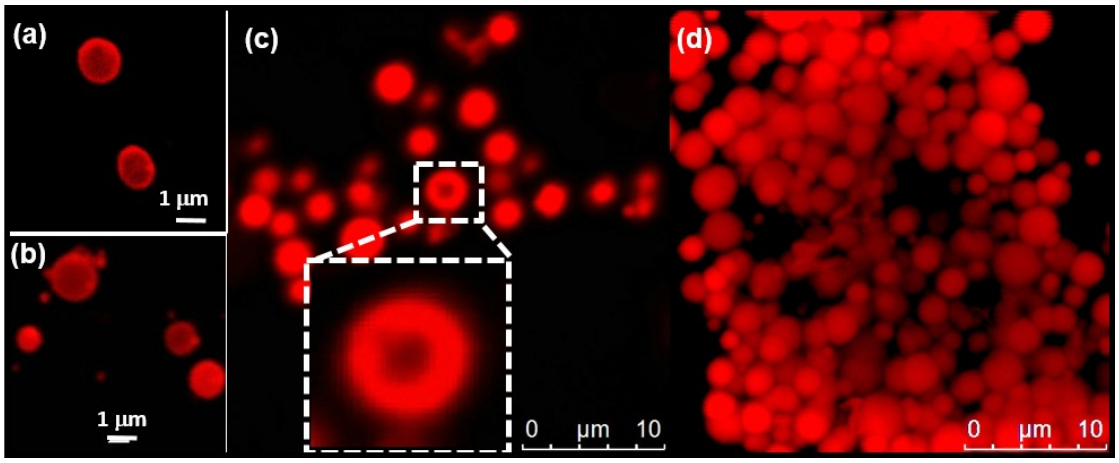

Figure 3.7 Images of confocal laser scanning microscopy (CLSM), which were dyed by Rhodamine B. (a) to (b) are prepared by method 1. (c) and (d) were prepared by method 2.

Furthermore, the sequential z-scanning images of CLSM were obtained (Fig. 3.8) which showing that the thickness of the shell of DX MG-colloidosome was ~1 μm in pH 7.4 buffer using method 2. These images proved that the shell contained multiple layers of microgels particles and that they were hollow particles nature. It has to be mentioned that the sample in Fig. 3.8 had been swollen under the pH 7.4 buffer solution.

Considering the formative conditions used to prepare the DX MG-colloidosomes. Method 1 and method 2 used lower (0.15) and higher (0.40) mass ratio of the photo initiator to GMA-MGs, respectively. The method 1 and method 2 used water without added buffer and only buffer (pH 6.4), respectively. Interestingly, these different conditions between method 1 and method 2 led to the DX MG-colloidosome obtaining a thicker shell (Fig. 3.8(c) and (d)) and higher yields by using method 2.

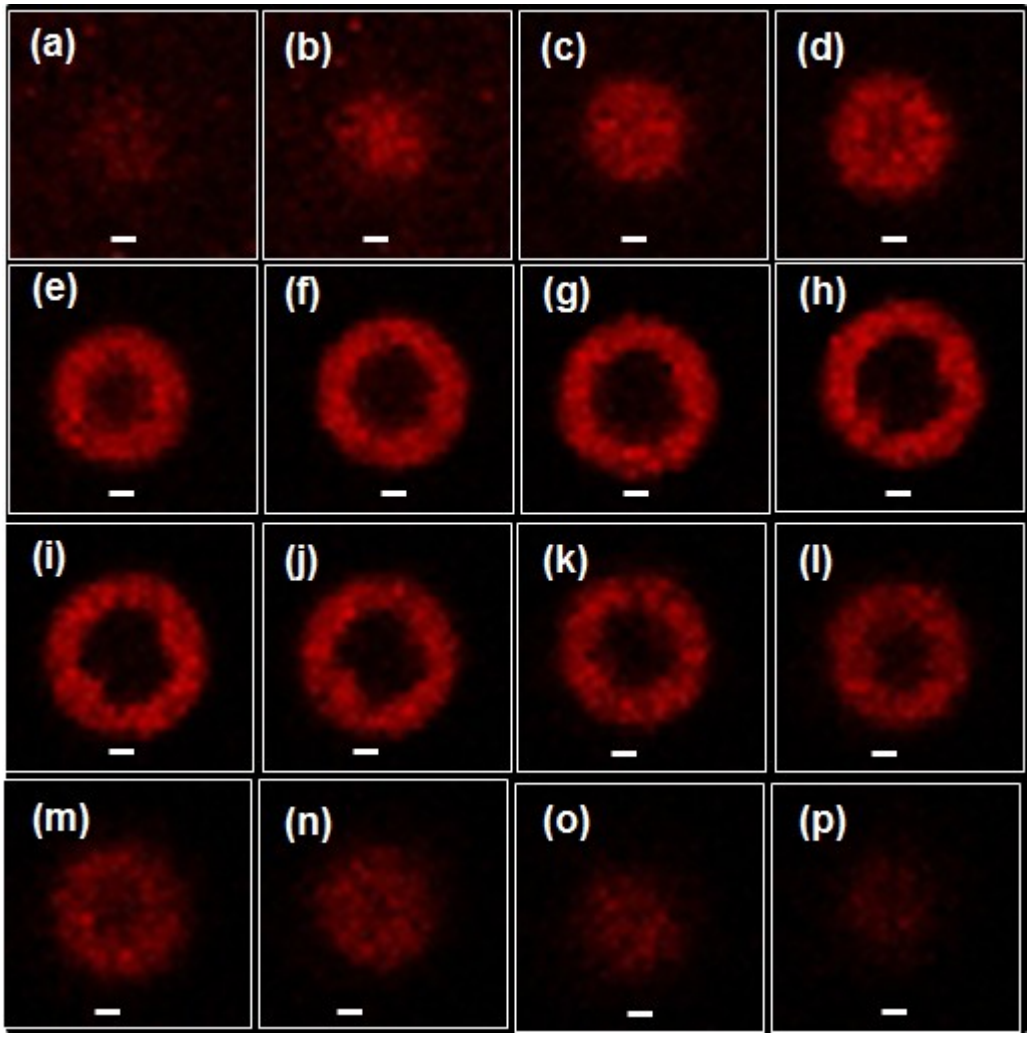

Figure 3.8 Sequential z-scanning CLSM images obtained for an individual DX MG-colloidosome, which prepared by method 2. The top surface is shown in (a) and the image plane moves towards the bottom of the colloidosome from (a) to (p). The scales bars are 1 um. The pH during these experiments was 7.4.

3.3.6.3 Scanning electron microscopy

DX MG-colloidosomes morphology was also investigated with a at higher magnification microscope using SEM (Fig. 3.9). According to the SEM images, first of all, the spherical morphology of DX MG-colloidosomes could be confirmed from both of the (Fig. 3.6(b) and Fig. 3.9 of method 2. The SEM images in Fig. 10 were taken using method 2. Compared with the method 1, method 2 had a lower polydispersity (Fig. 3.6(b Most of the microgles particles were formed the hollow particles. Colloidosome morphology was investigated at a higher magnification using SEM (Fig. 3.9(a)). The individual colloidosomes had a crumpled appearance. The highest magnification images clearly showed the presence of GMA-MG particles at the surface (Fig. 3.9(b)). Because the DX MG colloidosomes did not redisperse when the pH increased, it is certain that the MG particles were covalently inter-linked. These data confirm that the shells were comprised of MG particles. The fact that the colloidosomes retained significant three-dimensional morphology supports the view that the shells contained multiple layers of DX MGs.

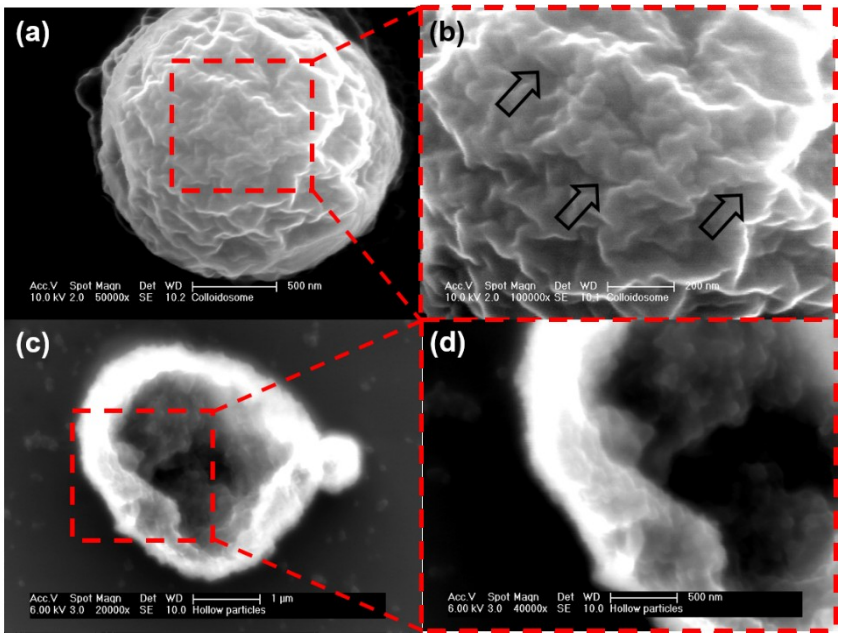

Figure 3.9 SEM images of dried hollow particles using method 2.

The high magnification images (Fig. 3.9(c) and (d)) clearly showed the formation of the shell. These images (Fig. 3.9(c) and (d)) were an incomplete particle. That was a very important evidence to prove that the particles what we made were hollow particles and how thick of the shell it was. The small particles were clearly found on the shell and the shell was calculated at about 700 nm.

3.3.6.4 Transmission electron microscopy

We further probed the morphology of DX microgel-colloidosome using TEM (Fig. 3.10). A larger extent of electron scattering (and hence MG) density was evident at the colloidosome periphery. The microgels based shell of c the olloidosome was confirmed again by the individual colloidosome on the left bottom corner indicated by the red arrow. The colloidosome clusters (arrows) showed an elliptical interface (window) between two adjoining colloidosomes that confirmed the natural hollow particles morphology. At the same time, the size of colloidosomes can be measured which is around 1.5um as well. This value is similar to those obtained using an optical microscope ~1.7 μm (Fig. 3.6(a)) and SEM (Fig. 3.9).

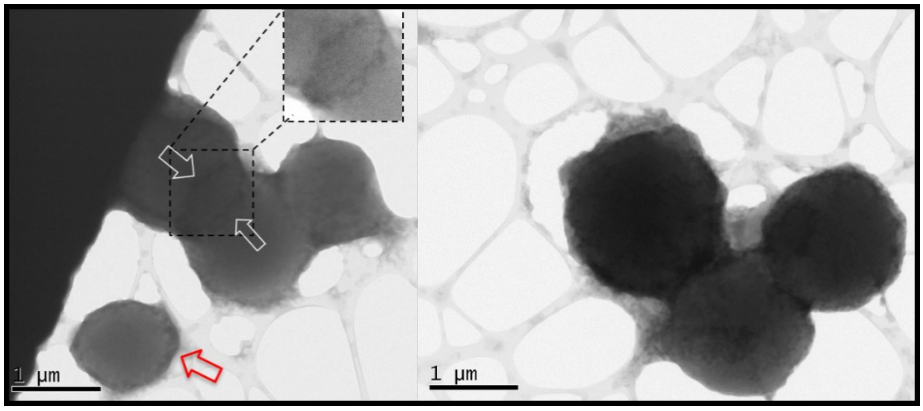

Figure 3.10 TEM images of E-BDD-GMA DX MG colloidosomes. The arrows (and inset) show a window formed by contact between two hollow particles. The red arrow indicates an individual colloidosomes.

3.3.7 Colloidosome swelling property characterisation.

There are few literatures reported about the pH-responsive microgel colloidosome swelling properties of this type of microgel-colloidosome[13, 14]. Because the microgel particles had a strong pH-triggered swelling and the swelling property of microgels before and after being functionlised were investigated (Fig.3.1) using DLS. It is possible to study the swelling property of DX microgel-colloidosome particles by DLS, as with reports for related systems; both initially small particles and colloidosomes were present.

In Fig. 3.11(a), the DLS data was measured for the DX MG-colloidosomes dispersions at three different pH values. From top to bottom (Fig. 3.11(a)), they were pH 6.4 (blue curve), 8.0 (green curve) and 10 (red curve). All of the curves had a weak peak on the left and a strong peak on the right. The smaller peaks on the left were due to the GMA-MGs particles and the strong peaks on the right were due to the DX MG-colloidosomes. All the peaks were shifted by increasing the pH value (Fig. 3.11(a)). Comparing the area of the small diameter and large diameter peaks, The results showed that only about 5% of the initially GMA-MGs particles still remained after the preparation of the DX MG-colloidosomes, meanwhile, the DX MG-colloidosomes were present at the highest vol% (about 95%) at all pH values measured.

In Fig. 3.11(a), the GMA-MGs had shown the pH-triggered swelling property when the pH was higher than pKa (6.4), which is indicated by the small peak. The strong peak shown on the top (blue curve) showed that the diameter of the DX MG-colloidosomes was ~1440 nm, which was smaller than that shown under the optical microscope (Fig. 3.6(a) and Fig. 3.11(b)). The result is expected because the best

resolutions for the optical microscopy were in size range greater than 1 mm. But the light scattering technique of DLS is able to detect particles across the length scale of 1 to 10 000 nm. The DLS was best suited to detect the smaller colloidosomes in this research. In Fig. 3.11(a), the large peak was shifted to 5310 nm (red curve) when increasing the pH of DX MG-colloidosomes to 10. The value of swelling ratio ($Q = (d_{pH10}/d_{pH6.4})^3$) could be calculated for DX MG-colloidosomes at about 50 at pH 10. This result could shows the DX MG-colloidosomes had a strong pH-triggered swelling property as well as GMA-MGs.

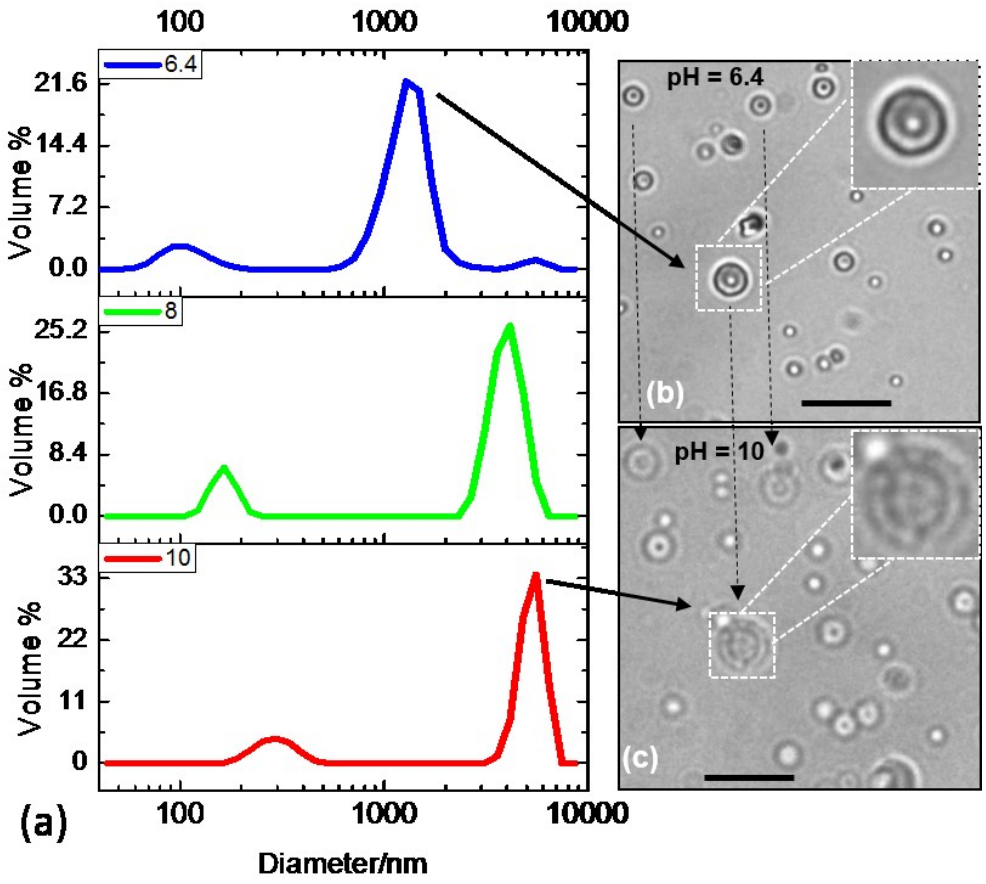

Figure 3.11 DLS data measured at various pH values (a) for DX MG-colloidosomes. (b) and (c) show optical micrographs for the colloidosomes at pH 6.4 and 10, respectively. The arrows show colloidosomes that did not change position when the pH increased. Scale bar = 10 μm.

The pH-triggered swelling property of the DX MG-colloidosome was probed using an optical microscope directly (Fig. 3.11 (b) and (c)). In this experiment, a drop of DX MG-colloidosome dispersion (pH 6.4) was prepared on the glass slide and covered by a piece of glass under the optical microscope. Some droplets of pH 10 buffer solutions were added from the edge of the glass slide. Several DX MG-colloidosomes were washed out by the addition of the buffer solution. Some of the colloidosomes had adsorbed on the glass slide which prevented their motion upon addition of the buffer solution (Fig. 3.11(b)). These absorbed DX MG-colloidosomes provided a good chance to directly track their diameter changes with increasing pH. Compared to the DX MG-colloidosome in Fig. 3.11(b) and (c), the DX MG-colloidosome (Fig. 3.11(c)) became larger and more transparent. The large DX MG-colloidosome (inset) had a diameter of ~4.0 μm at pH 6.4 (Fig. 3.11(b)) and this increased to ~6.0 um at pH 10 (Fig. 3.11(c)). Even though the relative diameter increase was lower than that under the DLS, the data had confirmed the pH-triggered selling property of the DX MG-colloidosome. The totally time of swelling transition was 2s. This confirmed the DX MG-colloidosome could respond rapidly to pH increases at the same as the GMA-MGs particles. Also, the DX MG-colloidosomes did not redisperse after increasing the pH above the pK_a of GMA-MGs particles. This confirmed that the GMA-MGs particles were covalently inter-linked with an interfacial DX MG hydrogel layer. As a comparative control experiment, the non-vinyl funtionalised mirogel particles and non-crosslinking funtionalised microgel particles were used to form colloidosomes. These colloidosomes dispersed when the pH was increased above the pKa of microgel particles.

3.4 Conclusion

In summary, we used a simple, one-component method to make uniform spherical pH-sensitive DX MG-colloidosomes, which had a good morphology and high yield. The DX MG-colloidosome had a strong pH-triggered swelling property and could be swollen when the pH value was changed to as the same as the microgle particles. In this study, this data could also confirm that the microgel particles peripheral chains do interpenetrate at the oil/water interface and could be interlinked directly if the peripheral chains have vinyl groups. The DX MG-colloidosome was stable and did not redisperse when the pH increased. Here, this study provided proof-of-principle design for pH-responsive DX MG-colloidosomes from microgels.

Reference

1. Liu, R.; Milani, A. H.; Freemont, T. J.; Saunders, B. R., Doubly crosslinked pH-responsive microgels prepared by particle inter-penetration: swelling and mechanical properties. *Soft Matter* 2011, 7, 4696-4704.

2. Milani, A. H.; Freemont, A. J.; Hoyland, J. A.; Adlam, D. J.; Saunders, B. R., Injectable doubly cross-linked microgels for improving the mechanical properties of degenerated intervertebral discs. *Biomacromolecules* 2012, 13, 2793-2801.

3. Saunders, B. R.; Vincent, B., Microgel particles as model colloids: theory, properties and applications. *Advances in colloid and interface science* 1999, 80, 1-25.

4. Geisel, K.; Isa, L.; Richtering, W., Unraveling the 3D localization and deformation of responsive microgels at oil/water interfaces: a step forward in understanding soft emulsion stabilizers. *Langmuir* 2012, 28, 15770-15776.

5. Yow, H. N.; Routh, A. F., Formation of liquid core–polymer shell microcapsules. *Soft Matter* 2006, 2, 940-949.

6. Bird, R.; Tungchaiwattana, S.; Freemont, T.; Saunders, B. R., Doubly crosslinked hydrogels prepared from pH-responsive vinyl-functionalised hollow particle dispersions. *Soft Matter* 2012, 8, 3062-3066.

7. Saunders, J. M.; Tong, T.; Le Maitre, C. L.; Freemont, T. J.; Saunders, B. R., A study of pH-responsive microgel dispersions: from fluid-to-gel transitions to mechanical property restoration for load-bearing tissue. *Soft Matter* 2007, 3, 486-494.

8. Tang, J.; Lee, M. F. X.; Zhang, W.; Zhao, B.; Berry, R. M.; Tam, K. C., Dual responsive pickering emulsion stabilized by poly [2-(dimethylamino) ethyl methacrylate] grafted cellulose nanocrystals. *Biomacromolecules* 2014, 15, 3052-3060.

9. Tang, M.; Wang, X.; Wu, F.; Liu, Y.; Zhang, S.; Pang, X.; Li, X.; Qiu, H., Au

nanoparticle/graphene oxide hybrids as stabilizers for Pickering emulsions and Au nanoparticle/graphene oxide@ polystyrene microspheres. *Carbon* 2014, 71, 238-248.

10. Li, J.; Stöver, H. D., Doubly pH-responsive pickering emulsion. *Langmuir* 2008, 24, 13237-13240.

11. Morse, A. J.; Dupin, D.; Thompson, K. L.; Armes, S.; Ouzineb, K.; Mills, P.; Swart, R., Novel Pickering emulsifiers based on pH-responsive poly (tert-butylaminoethyl methacrylate) latexes. *Langmuir* 2012, 28, 11733-11744.

12. Richtering, W., Responsive emulsions stabilized by stimuli-sensitive microgels: emulsions with special non-Pickering properties. *Langmuir* 2012, 28, 17218-17229.

13. Gong, Y.; Zhu, A. M.; Zhang, Q. G.; Ye, M. L.; Wang, H. T.; Liu, Q. L., Preparation of Cell-Embedded Colloidosomes in an Oil-in-Water Emulsion. *ACS Applied Materials & Interfaces* 2013, 5, 10682-10689.

14. Morse, A. J.; Madsen, J.; Growney, D. J.; Armes, S. P.; Mills, P.; Swart, R., Microgel Colloidosomes Based on pH-Responsive Poly(tert-butylaminoethyl methacrylate) Latexes. *Langmuir* 2014, 30, 12509-12519.

Chapter 4: Pickering emulsions stabilized by pH-responsive microgels and their scalable transformation to robust sub-micrometer colloidoisomes with selective permeability

In the last chapter, we prepared pH responsive DX MG-colloidosomes with a clean, simple and faster method. But it have following disadvantages: 1. we have not established the best condition for preparing pH responsive DX MG-colloidosomes. 2. the output of the experiment is very small, which is not suitable for the next application and research. 3. we have not studied the drug loading and release of the colloidosomes. Therefore, in this chapter, we mainly solve the above three problems.

Abstract

Colloidosomes are micrometer-sized hollow particles that have shells consisting of coagulated or fused colloid particles. Our method used covalent inter-linking of vinyl-functionalised microgel particles adsorbed into oil droplets to form shells of doubly crosslinked microgels (DX MGs). The initially established method for pH-responsive hollow particle preparation is not compatible with scale up, which limits its potential for use. In this study, we established the best conditions to prepare the stable Pickering emulsion which used an ethylacrylate based microgels (EA-MGs) system. After that, we demonstrated a general, gram scale method to form the doubly crosslinked pH-responsive colloidosomes, which are strongly pH-responsive and exhibited a major pH-triggered swelling response in the physiological pH region. It is also shown that the doubly crosslinked pH-responsive colloidosomes have selective pore size, which can be varied by changing the pH environment. The properties of these microgel-colloidosomes dispersions imply that they have good potential for future application as injectable gels for release and delivery applications.

4.1 Introduction

MG particles are crosslinked polymer particles that swell when the pH approaches the pK_a of the particles Richtering and Saunders [1]. Colloidosomes are microcapsules whose shells are composed of colloidal particles[2-7]. The first report about the production of colloidosomes was the pioneering work of Velev et al[8, 9], while Dinsmore et al[10, 11] coined the phrase "colloidosomes". In recent years, the release of larger encapsulated materials from such traditional colloidosomes relies on external triggers to break and open the shell of the colloidosomes. The limitations highlight the need for a flexible technique to fabricate colloidosomes that enables both control of the permeability to small species and a good sensitivity to a release trigger. While colloidosomes prepared using microgels have been reported[12]. There are very few examples where the pore-size can be controlled. The motivation for the present work was to demonstrate that scale-up of our previous microgel colloidsomes, which are termed as doubly crosslinked microgel (DX MG) colloidosomes, was possible and that they could provide size-selective permeation. The hypothesis tested in this study is that microgel colloidosomes are highly permeable due to interstitial spaces for solutes that are smaller than the interstitial size.

Microgel colloidosomes have been fabricated using microgels assembly at liquid-liquid interfaces[2, 10, 13-16]. To be successfully prepare microgel colloidosomes, microgel-stabilised emulsions need to be prepared first[17]. However, a limitation of previous methods used to prepare microgel-colloidosomes[4, 13, 18] was that the construction of microgel based colloidosomes needs more than one component[10]. The microgels on the oil-water interface need to be linked together by an additional small molecule or croslinker[13]. In previous work, we demonstrated that a pH-responsive

microgel-colloidosomes was prepared using vinyl functionalised microgel particles as the only (colloidal) building block via UV- irritation, because of the lower scale of the DX MG colloidosomes prepared by UV- irritation. In this study, we overcome the limitation of small-scale preparation and also demonstrate that the permeability of the microgel-colloidsomes with pH. The approach used to prepare our DX MG-colloidosomes is shown in Scheme 4.1. This approach involves pH-responsive vinyl-functionalised microgels as the same as the microgels in chapter 3. Our working hypothesis was that the oil/water interface would promote sufficient microgel deformation and interpenetration to enable covalent inter-linking of peripheral vinyl groups on the microgel particles via free-radical coupling. Uniquely, our method for DX MG-colloidosome preparation uses only one type of (colloidal) building block for shell assembly. And the key intermediate is microgel-stabilized emulsions[17].

Microgel-stabilized emulsions were first reported by Richtering. The term "Mickering emulsion" was introduced by Richtering in order to stress similarities and differences to Pickering emulsions stabilized by rigid particles[19]. The stabilization of the Mickering emulsions does not depend on electrostatic repulsion although the presence and location of charges are relevant. The stabilization of Mickering emulsions needs to the swollen microgels at the oil-water interface, which depends not only on the solvent's polarity but also on microgel morphology[19].

In this study we have demonstrated construction of DX MG-colloidosomes without having to use an additional linking monomer. The DX MG-colloidosomes were strongly pH-responsive and exhibited a major pH-triggered swelling response in the physiological pH region which further supports the view that they have good potential for biomaterial applications.

The permeability of colloidosomes for encapsulated species, which is critically dependent on the size of the interstitial pores between the particles in the shell, can be made through the variation of the size of the colloidal particles on the shell[10, 20-23]. The ability to vary the pore size of the colloidosomes makes them suitable for a wide variety of applications in some industry area. In this study, we use only one type of microgel particles as the nature shell materials which have the strong pH-responsive property and that could lead to self-modified pore size of the shell of the colloidosomes.

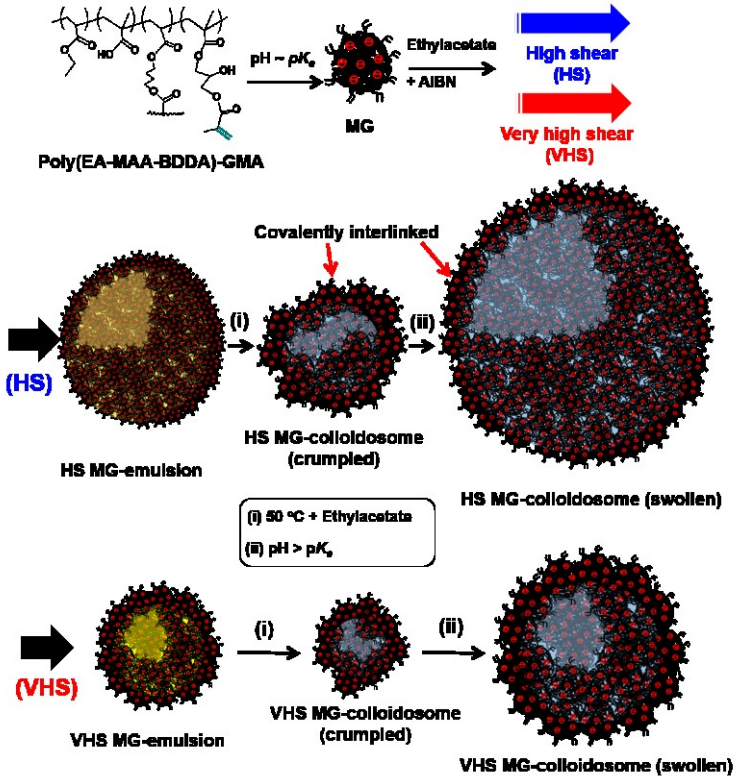

Scheme 4.1 Preparation of pH-responsive colloidosomes using microgels. Poly (EA-MAA-BDDA)-GMA MGs stabilized ethylacetate-in-water emulsions containing AIBN and were heated to covalently interlink the MGs via free-radical coupling of surface vinyl groups. HS or VHS mixing was used to control the emulsion and colloidosome size. The removal of ethylacetate formed crumpled colloidsomes that subsequently swelled when the pH was increased to above the pK_a.

4.2 Experimental

4.2.1 Materials

Ethyl acrylate (EA, 99%), methacrylic acid (MAA, 99%), 1-4 butaendiol diacrylate (BDDA, 90%), glycidyl methacrylate (GMA, 97%), 2,2′-azobis(2-methylpropionitrile) (AIBN, 98%) were purchased from Sigma and used as received. Rhodamine B, fluorescein, Nile Red, Coumarin 6 and all of the fluorescein isothiocyanate (FITC)-labeled were purchased from Sigma and used as received. All water was of ultrahigh purity de-ionised quality.

4.2.2 Synthesis reactions

4.2.2.1 Synthesis of poly (EA-MAA-BDDA-GMA) microgel using emulsion polymerisation

The synthesis of this microgel was conducted using the emulsion polymerisation method according to a previously published method[24]. Briefly, a mixed solution (250 g) containing EA (167 g, 1.88 mol), MAA (83 g, 0.83 mol), BDDA (2.5 g, 0.01 mol) was prepared. A total of 31.5 g of the co-monomer solution was used for the seed formation. The latter solution was added to water (518 g) containing SDS (1.8 g, 6 mmol) and then K_2HPO_4 (3.15 g of a 7 wt.% aqueous solution) and APS (10 g of a 2 wt.% solution) were added. The seed was prepared at 80 ˚C with mechanical stirring under nitrogen for 30 min. The remaining monomer solution was added at a uniform rate over a period of 2 h. The reaction was continued for a further 2 h. The product was purified by extensive dialysis using water. Vinyl-functionalization of the microgel also followed a method described earlier[24]. Briefly, GMA (16.66 g) was added to the microgel dispersion (100 g, 10 wt.%) and the reaction performed at pH 5.2 for 8 h.

Excess GMA was removed by repeated washing with chloroform. Residual chloroform was removed using rotary evaporation. The GMA-functionalized microgel is referred to as MG.

4.2.2.2 Preparation of MG-stabilised emulsions

The following preparation method was used to investigate the stability of MG-stabilized emulsions. An aqueous phase (4.0 ml) was prepared that contained buffer at specific pH values and MG dispersions with a range of particle concentrations. Ethyl acetate (1.0 ml) was added to the aqueous phase (to give an oil phase volume fraction of 20 vol.%) and the mixture was sheared at 10,500 rpm for 120 sec using a Silverson L4R high shear mixer equipped with a 3/8" Mini-Micro tubular mixing unit.

4.2.2.3 Small-scale DX MG colloidosome preparation

AIBN (0.01 g, 0.061 mmol) was dissolved in ethyl acetate (1.0 ml). An aqueous phase (4.0 ml) was prepared that contained buffer (pH 6.4) and MG dispersion (0.60 wt.%). The AIBN / ethyl acetate solution was added to the aqueous phase and the mixture sheared at 10,500 rpm for 120 sec to give using a Silverson L4R high shear mixer with the geometry described above. The emulsions were placed in a round-bottomed flask with a condenser and heated with an oil bath for 180 min at 50 ^{o}C. Ethyl acetate was subsequently removed by rotary evaporation at room temperature to give a dispersion of DX MG-colloidosomes. Excess AIBN was removed by chloroform washing. Residual chloroform was removed out using rotary evaporation. The yield of colloidosomes was 79%. Further details concerning the small-scale preparations are given in Table 1.

4.2.2.4 Large-scale DX MG colloidosome preparation

AIBN (0.60g, 3.66 mmol) was dissolved in ethyl acetate (60.0 ml). An aqueous phase (240 ml) was prepared that contained buffer (pH 6.4) and MG dispersion (0.60 wt.%). The AIBN / ethyl acetate solution was added to the aqueous phase and sheared at 10,500 rpm for 120 sec to give a MG-stabilised emulsion using a Silverson L4R high shear mixer equipped with a ¾" tubular work head and a square holed high shear screen. The emulsions were placed in a round-bottomed flask which was sealed and heated in an oil bath for 6 h at 52 ^{o}C. Ethyl acetate and AIBN were removed by rotary evaporation as described above. The yield of colloidosomes was 74% (Table 1).

4.2.3 Characterization methods

4.2.3.1 Physical Measurements

Optical images were obtained using an Olympus BX41 microscope and white transmitted light. Titration measurements were performed using a Mettler Toledo titration unit with a supporting electrolyte (0.1 M NaCl). Dynamic Light Scattering (DLS) measurements were obtained using a Malvern Nano ZS instrument. All measurements were conducted using 0.1M buffer solutions. SEM measurements were obtained using a Philips XL30 FEG SEM instrument. Dispersions of particles were deposited on SEM stubs at room temperature. The samples were coated by platinum or carbon. The number-average particle sizes were measured with Image J software (National Institutes of Health) and at least 100 particles were measured. Confocal laser scanning microscopy (CLSM) images were obtained using Broadband Confocal Leica TCS SP5. The DX MG-colloidomes were labelled by Rhodamine B.

Rhodamine B was dissolved in water (at a concentration of $2x10^{-9}$ M). DX MG-colloidosomes were then dispersed in the Rhodamine B solution before examination. UV-vis spectroscopy was performed using a PerkinElmer Lambda 25 UV-visible Spectrometer. Surface tension was performed using a Krüss Drop Shape Analysis (DSA100).

4.2.3.2 DX MG-colloidosome permeability studies

Confocal laser scanning microscope (CLSM) was used to analyse capsule permeability towards fluorescein and different molecular weights of FITC-dextran. DX MG-colloidosome dispersions prepared using the large-scale method (1.0 mL, 0.45 wt.%) were added to vials containing fluorescein or FITC-dextran aqueous solutions (1.0 mL) at a concentration of 0.10 wt.% and the diluted dispersions were imaged at specific time intervals.

4.3 Results and Discussion

4.3.1 Study of GMA functionalised MGs

The pH-responsive vinyl-functionalised microgels used in this study was poly(EA-*co*-MAA-*co*-1,4-BDDA)-GMA. The number-average particle size from SEM (Fig. 4.1a, inset) was 84 ± 15 nm. It can be seen from Fig. 4.1a that the GMA-MGs particles showed a strong pH-triggered increase of the hydrodynamic diameter (d_h). From this data an estimated volume-swelling ratio at pH 10 of ~ 34 was calculated using $Q = (d_{h(pH=10)} / d_{h(pH=5)})^3$. Potentiometric titration data (Fig. 4.1b) showed that the GMA-MGs particles contained 32.0 mol % MAA and 7.0 mol % of GMA and had a pK_a of 6.2. pH-dependent change of zeta potential (ζ) was measured (Fig. 4.1c). The zeta potential (ζ) of GMA-MGs increased sharply when pH achieved pK_a of 6.2 and kept a constant value beyond a pH above 6.6. The MG particles were in their collapsed (latex) form at pH values less than their respective pK_a values. The zeta potential (ζ) data (Fig. 1b) was used to qualitatively assess the change in the extent of charge at the periphery of the MGs. Accordingly, the MGs were negatively charged at all pH values studied. The ζ magnitude for the MGs increased when the pH increased and approached the pK_a of 6.2 due to pH-triggered COO^- formation. The MGs became surface active as the pH approached the pK_a (Fig. 4.1d). It followed that the MGs became more amphiphilic. These data are the first surface tension data reported for this class of MGs to our knowledge. The surface activity of the MGs was due to a combination of hydrophobicity from EA and the polymer backbone and polar groups from COO^- groups. The lowest γ value obtained (44 mN/m at pH 6.6) is similar to surface tension values reported by Mourran et al.[25] for poly(*N*-vinylcaprolactam)/poly(*N*-isopropylacrylamide) microgels.

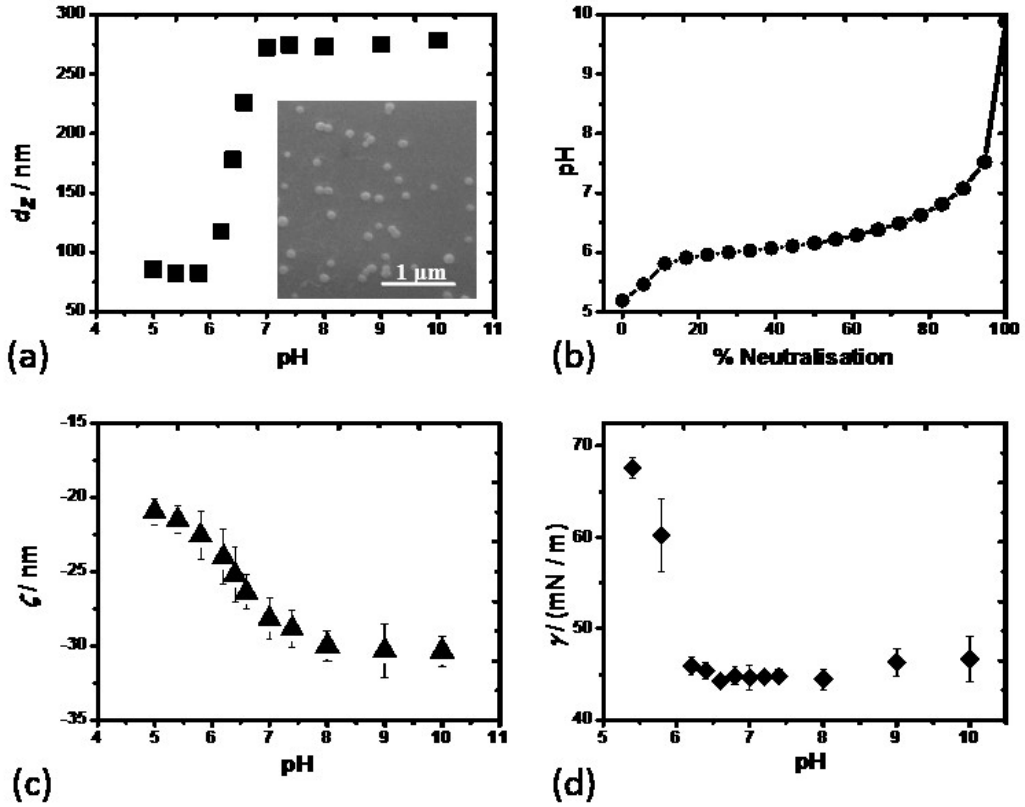

Figure 4.1 (a) z-average diameter (d_z), (b) potentiometric titration data, (c) zeta potential (ζ), and (d) surface tension data (γ) for the GMA-MGs. The inset shows an SEM image of the GMA-MGs particles.

4.3.2 The effect of pH on MG-stabilised emulsion formation

We first investigated the effect of pH on MG-stabilised emulsion formation. The conditions required to form stable Pickering emulsions using 84 nm GMA-MGs particles with ethyl acetate as the oil phase have been reported in pervious paper[24]. It was shown that the stability of Pickering emulsions depends on the solution pH. Richtering's group has extensively employed PNIPAM-based microgels as stabilizers for making responsive emulsions[12, 17, 19, 26-28]. They illustrated that microgel particles need to carry a certain amount of charges to be efficient stimuli-responsive emulsion

stabilizers. Schmidt et al. found that the presence of charges in the microgel particle is important for obtaining stable emulsions, whilst the location of charges is not relevant[19]. Whilst MG-emulsions related to those studied here were briefly investigated in the earlier study.[29] In Chapter3, only studied at 3 pH values using a fixed MG concentration were studied. Here, we studied 8 pH values as well as the effect of shear.

In this study, at above pH 6.4, stable emulsions were obtained with mean droplet diameters of approximately 3300 nm (Fig. 4.2 (c) to (h)). At below pH 6.4, unstable emulsions were obtained, as evidenced by the optical microscopy images in (Fig. 4.2 (a) and (b), indicating that the emulsion destabilization at pH 6.0 and 6.2 resulted in the droplet diameters increasing. This was because the pH was below the pK_a of GMA-MGs. Hence, the GMA-MGs is collapse due to less presence of charges, eventually leading to the breakage and coalescence of the emulsion droplets. However, at high pH, the stable emulsion droplets absorbed by swollen GMA-MGs particles would be under a balance between attractive and repulsive forces. According to Schmidt's study, when the microgel particles were not strongly swollen and less deformable, no stable emulsions were formed. However, when the swelling and the deformability was enhanced, stable emulsions were obtained[19]. But in my study, with the increasing of pH, the yield of double crosslink colloidosoems would be decreased, due to the stronger electrostatic repulsion and deformability. The DLS (Fig. 4.1a) and zeta potential (Fig. 4.1c) data show that pH 6.4 corresponded to MG particles that were partially swollen with intermediate charge. We propose that these conditions resulted in inter-MG overlap for the MGs adsorbed to the droplet surfaces. Consequently, stable emulsions could not be prepared at pH values lower than 6.4 due to the lack of charge on the MGs as judged by the zeta potential data (Fig. 4.1c) and

their poor surfactant-like properties as judged by the surface tension data (Fig. 4.1d). Therefore, the best pH environment for stable emulsion droplets and double crosslink colloidosomes was 6.4.

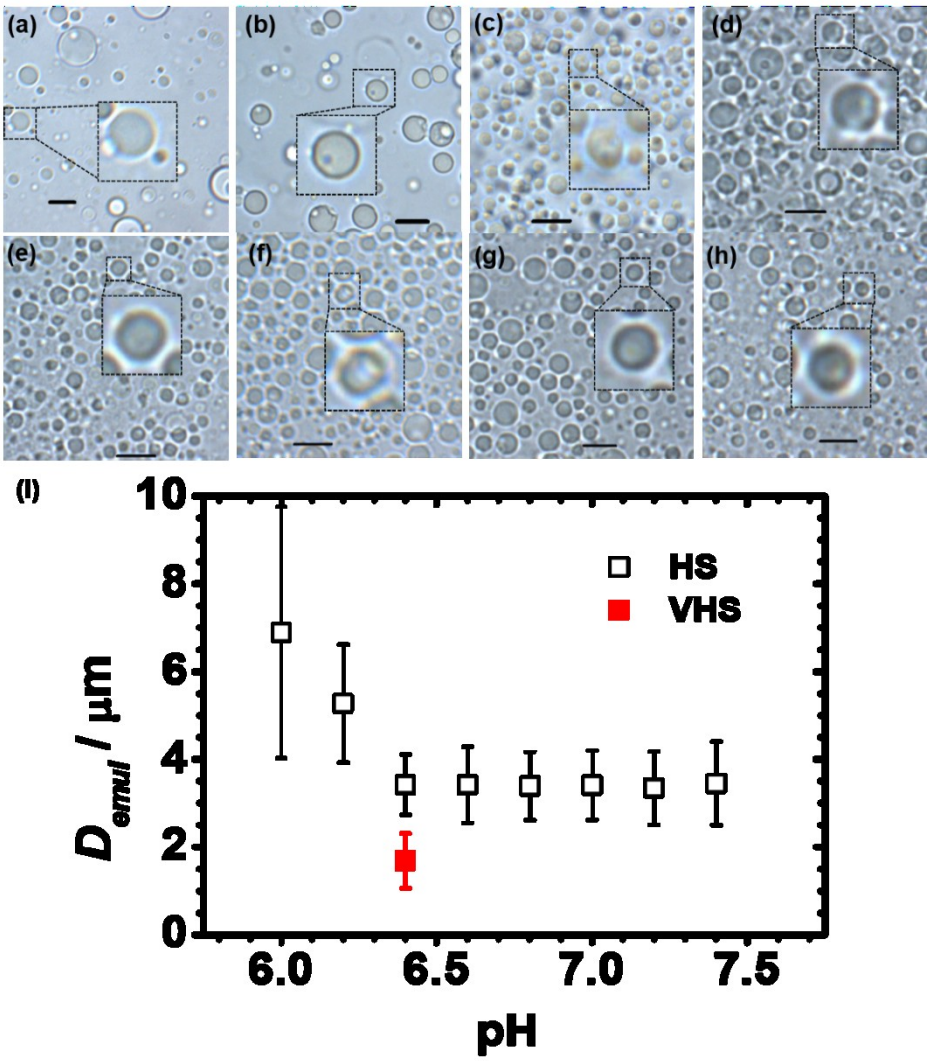

Figure 4.2 Optical micrographs of MG-stabilised EA-in-water emulsions prepared at pH values of (a).6.0, (b).6.2, (c).6.4, (d) 6.6, (e) 6.8, (f) 7.0, (g) 7.2 and (h) 7.4. The insets show expanded views of the emulsions. The MG concentration was 0.6 wt.% The scale bars are 10 μm. (i) shows the variation of the number-average diameter with pH values for the emulsions.

The effect of pH Fig. 4.3 on the stability of the MG-emulsions to creaming and phase

separation was examined visually after 5 min, 1 h and 24 h. In all cases the droplets had creamed after 24 h. Importantly, there was no evidence of phase separation, which suggests that the MGs remained strongly adsorbed to the oil/water interface. Especially, from pH 6.8, the droplets had creamed easier after 5 min due to being the mostly swollen with intermediate charge (Fig. 4.1a) and stronger surface activity.

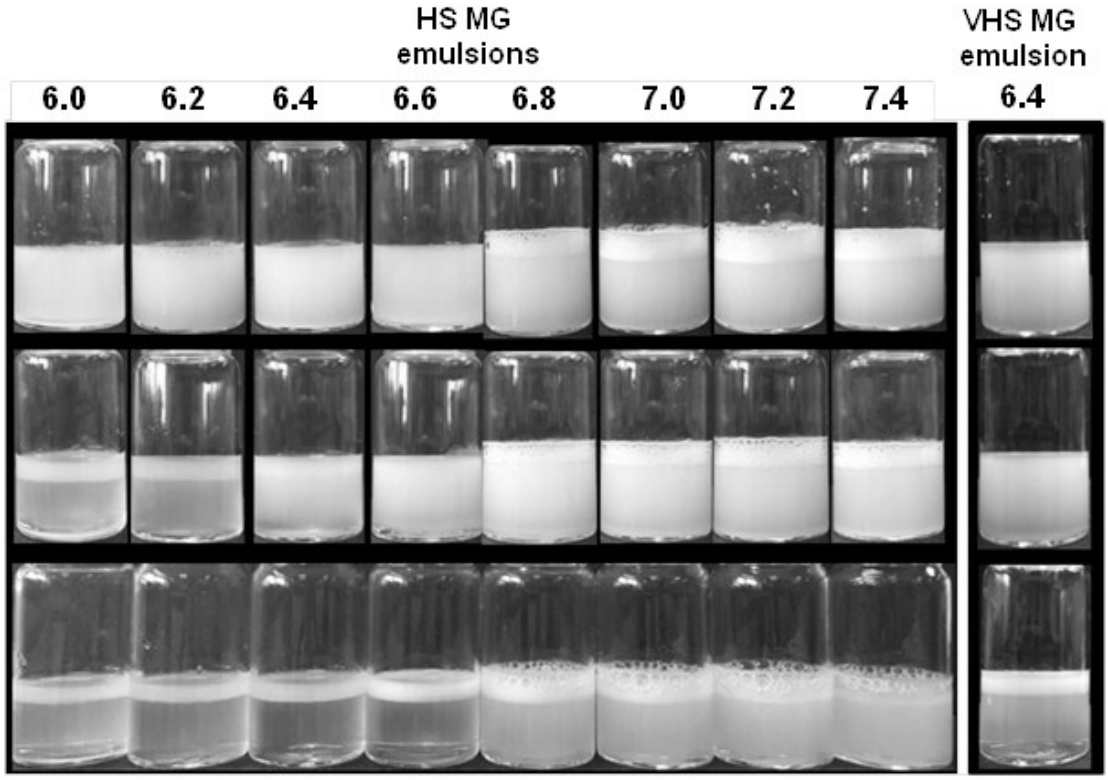

Figure 4.3 MG stabilised ethyl acetate-in-water (oil phase volume fraction = 0.20) emulsions at different times. The MG concentration was 0.6 wt.% and the pH is shown above the vials. The times after emulsification when the images were taken are 5 min (top row), 1 h (middle row) and 24 h (bottom) row. The tube diameters were 23.12 mm.

4.3.3 The effect of concentration on MG-stabilised emulsion formation

Having established that a pH of 6.4 was required to achieve a minimum emulsion size we then investigated the effect of MG concentration. The concentration dependence of the ethyl acetate oil droplet diameter was investigated using equal volumes of oil with aqueous dispersions containing various concentrations of particles at pH 6.4. Fig. 4.4 shows the number-average emulsion droplet diameter obtained for a series of GMA-MG dispersions at concentrations of 0.024 wt. % to 1.32 wt. %, the droplet optical images in each case are displayed (Fig. 4.4a to h). At low particle concentrations, unstable emulsion droplets are formed with small quantities of excess particles present in the aqueous phase. The emulsion droplets size increased sharply with the decreasing of GMA-MGs concentration below 0.36 wt. % (Fig. 4.4i). The lower amount of GMA-MGs particles could not stay on the interface of oil and water due to the free oil droplets accelerating the coalescence of emulsion droplets. The emulsion droplets size becomes approximately constant (3300 nm) above particle concentrations of 0.36 wt %, with the excess GMA-MGs particles remaining in the lower aqueous phase. These observations are similar to those emulsions made by Fielding et al[30]. This conjecture raises the interesting question of the likely arrangement of the MGs at the ethylacetate/water interface.

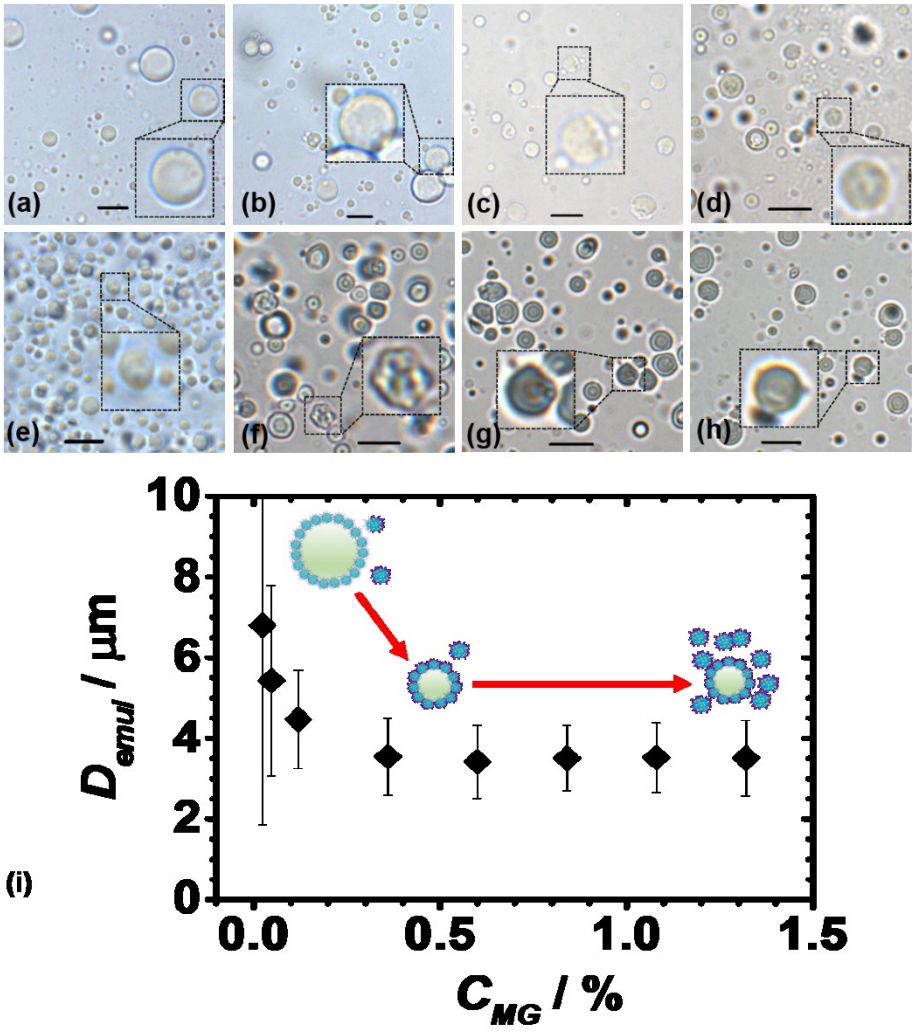

Figure 4.4 Optical micrographs of MG-stabilised EA-in-water emulsions were prepared at MG concentrations of (a) 0.024, (b) 0.048, (c) 0.12, (d) 0.36, (e) 0.60, (f) 0.84, (g) 1.08 and (h) 1.32 wt.% The scale bars are 10µm. (i) shows the average size data measured at various concentration of MGs. The cartoon depicts the proposed change from surface saturated to excess MGs with increasing MG concentration.

The effect of concentration of MGs (Fig. 4.5) on the stability of the MG-emulsions to creaming and phase separation was examined visually after 5 min, 1 h and 24 h. In all cases the droplets had creamed after 24 h. Importantly, there was no evidence of phase separation, which suggests that the MGs remained strongly adsorbed to the oil/water interface. The aqueous phases (bottom of tubes) for the emulsions were

prepared using relatively high concentration $_{GUO}$of MGs values (1.08 and 1.32%) and they remained turbid after 24 h (Fig. 4.5), which is attributed to residual MG particles.

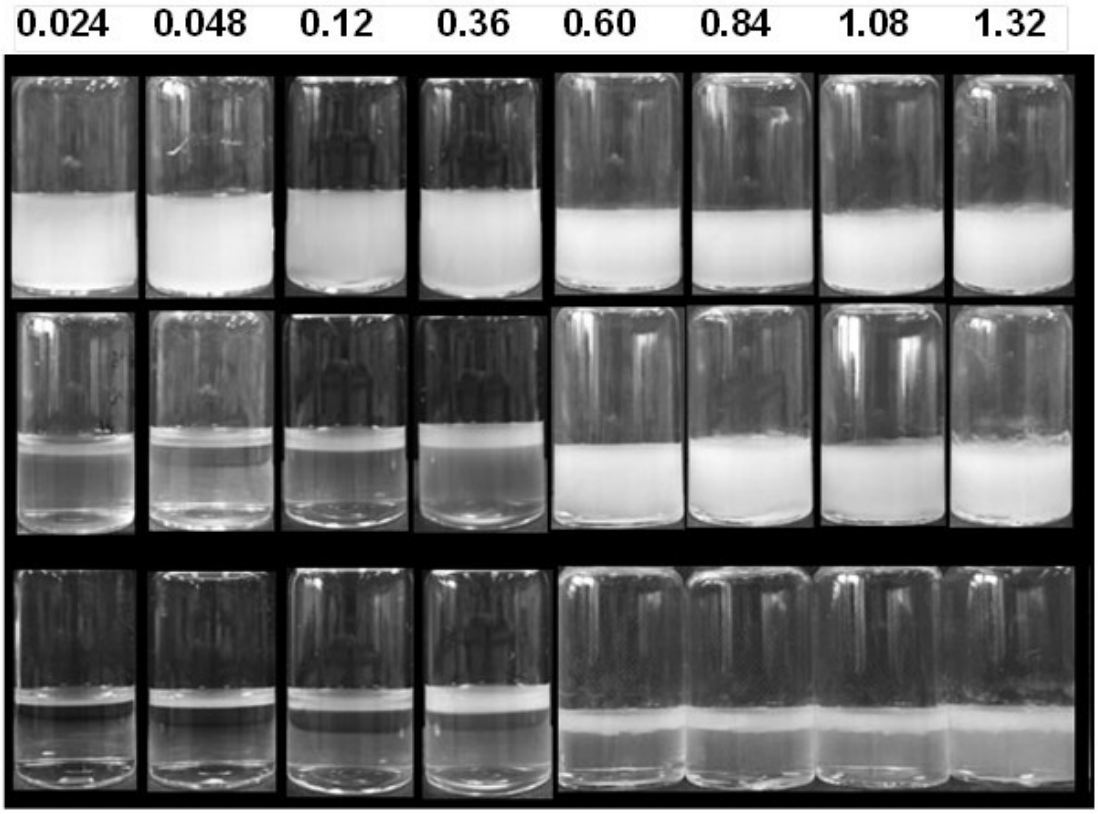

Figure 4.5 MG stabilised ethyl acetate-in- water (oil phase volume fraction = 0.20) emulsions at different times. The pH was 6.4 and the MG concentration is shown above the vials. The times after emulsification when the images were taken are 5 min (top row), 1 h (middle row) and 24 h (bottom) row. The tube diameters were 23 mm.

Combining the DLS and vials data, they clearly show that the stabilization of the microgel-stabilized emulsions depends not only on the microgel surface charges and morphology but also on the concentration. The selected condition for preparing stable emulsion in the rest of the chapter is 0.6 wt.% GMA-MGs dispersed in pH 6.4.

4.3.4 Estimating the nominal fractional coverage of oil droplets by microgel particles

An interesting fundamental question related to the emulsion stabilisation mechanism concerns the fractional coverage of droplet surface by the MGs. The nominal fractional coverage was calculated (θ_{cal}) using a geometric approach. Each oil droplet was assumed to be covered by a MG particles that were spherical and had a contact angle of 90^{o} at the oil/water interface (See Fig. 4.6).

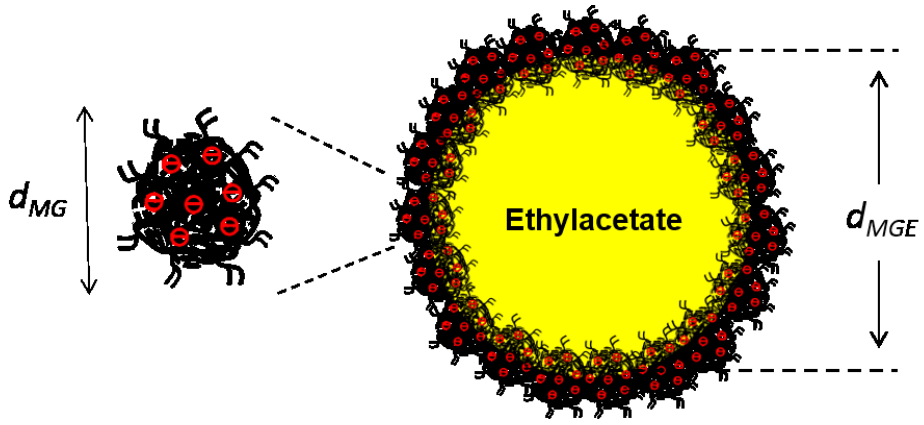

Figure 4.6 Simplified model for MG particles adsorbed to an oil droplet.

The approach used in order to derive an expression for θ_{cal} was to: (a) obtain an expression for the total surface area of the emulsion droplets ($A_{MGE(T)}$); (b) obtain an expression for the total cross-sectional area of the adsorbed MG particles ($A_{X,MG(T)}$) and (c) use the ratio of the expressions from parts (a) and (b) to arrive at the final equation for θ_{cal}.

For part (a), the parameter $A_{MGE(T)}$) was calculated from the average droplet diameter (d_{MGE}) and volume fraction of oil phase present (ϕ_o) using

$$A_{MGE(T)} = n_{MGE}(\pi d_{MGE}^2) \qquad (4.1)$$

Where n_{MGE} is the number of emulsion droplets present.

$$n_{MGE} = \frac{6\phi_o V_E}{\pi d_{MGE}^3} \quad (4.2)$$

Where V_E is the emulsion volume. Combining equations 1 and 2 gives:

$$A_{MGE(T)} = \frac{6\phi_o V_E}{d_{MGE}} \quad (4.3)$$

For part (b), the parameter $A_{X,MG(T)}$ was determined from the MG diameter at the pH of the emulsion (d_{MG}) and the number of MG particles present (n_{MG}) using

$$A_{MG(T)} = n_{MG}\left(\frac{\pi d_{MG}^2}{4}\right) \quad (4.4)$$

The value for n_{MG} can be determined from the total volume of MG present in the emulsion and the volume of a collapsed MG particle with a diameter of $d_{MG(c)}$ using

$$n_{MG} = \frac{6V_E(1-\phi_o)\left({}^{C_{MG}}/_{100}\right)}{\pi d_{MG(c)}^3} \quad (4.5)$$

Where C_{MG} is the concentration of MG and the density of the MG particles present (w/w%). Inserting equation 4.5 into 4.4 gives

$$A_{MG(T)} = \frac{3V_E(1-\phi_o)\left({}^{C_{MG}}/_{100}\right)d_{MG}^2}{2d_{MG(c)}^3} \quad (4.6)$$

For part (c), the ratio of equations (4.6) and (4.3) gives:

$$\theta_{cal} = \frac{1}{4}\left(\frac{d_{MG}^2 d_{MGE}}{d_{MG(c)}^3}\right)\left(\frac{1-\phi_o}{\phi_o}\right)\left(\frac{C_{MG}}{100}\right) \quad (4.7)$$

We can then calculate a value for θ_{cal} of 1.18 using d_{MG} = 178 nm (pH 6.4), $d_{MG(c)}$ = 82 nm, d_{MGE} = 3,420 nm, ϕ_o = 0.20 and C_{MG} = 0.60 wt.%.

4.3.4 Scale up of colloidosomes fabrication

Due to the limitation of scaling up using UV-initiated, we needed to change from a UV-initiated approach to a thermal approach, which required use of AIBN in the ethyl acetate and heating of the emulsion to 55 ^{o}C. The following in Table 4.1 and Table 4.2 shows the details of the scaling up of colloidosome fabrication.

Table 4.1 Characterisation data for scaling up of colloidosome fabrication in this work.

Code [a]	**volume ml**	**Initiator mass g**	**Buffer volume ml**	**Mass of MGs g**	**Mixing speed rpm & time s**	**Yield / g**
Small scale (HS)	1.0	0.01	4	0.024	10000 & 120	0.019
Large scale (VHS)	60.0	0.60	240.0	1.44	10000 & 120	1.071

[a] HS and VS refer to high shear and very high shear, respectively.

4.3.4.1 Calculation of the shear rate during emulsification

The following equation was used[31] to estimate the rotor tip speed (V) for the mixer geometry used to prepare the emulsions.

$$V = \pi D n \qquad (4.8)$$

For the above equation D and n are the rotor diameter and rotational speed, respectively. The value for V together with the gap distance (g) was then used to calculate the shear rate (s) using equation (S2)[31].

$$s = \frac{V}{g} \qquad (4.9)$$

Table 4.2 shows the values used for the parameters in order to calculate s for the two mixing geometries used in this study.

Table 4.2 Parameters used for the calculation of shear rate

Mixer type	**Code**[a]	***D* / mm**	***g* / mm**	***n* / (rev s^{-1})**	***V* (m s^{-1})**	**s/ s^{-1}**
Mini-micro	HS	7.64	0.26	175	4.2	16,150
Tubular	VHS	31.32	0.21	175	17.2	82,000

[a] HS and VS refer to high shear and very high shear, respectively.

4.3.5 Morphological and swelling characterisation of DX MG-colloidosomes prepared by small scale (HS)

The morphology of the DX MG-colloidosomes was probed using several complementary microscopy techniques (Fig. 4.7a to d). DX MG-colloidosome morphology was probed directly by an optical microscope (Fig. 4.7c). The optical micrographs obtained at pH 6.4 (Fig. 4.7c) revealed that the colloidosomes were hollow. The number average diameter and the thickness of the shell of the colloidosomes in the same condition had been measured by ImageJ software was 1.8 μm (CV = 21%) and was ~ 460 nm, respectively. DX MG-colloidosomes morphology was probed using CLSM with Rhodamine B labeling (Fig. 4.7a). We used CLSM images to get evidence that the particles were hollow and also to show the thickness of the shell. MG-colloidosome could also be confirmed clearly under the CLSM as well. It is interesting that the wall thickness of the DX MGs (460 ± 120 nm) is much larger than the diameter of MG particles (84 ± 6 nm, from Fig. 4.1). The individual colloidosomes had a crumpled appearance (Fig. 4.7(b)ii). The highest magnification images clearly showed the presence of MG particles at the surface (Fig. 4(b)i). Because the DX MG colloidosomes did not redisperse when the pH increased it is certain that the MG particles were covalently inter-linked. The high magnification images (Fig. 4.7b iii and Fig. 4.7(b) iv) clearly showed the formation of the shell. These images (Fig. 4.7(b) iii and iv) comprised of a folded colloidosome which enabled a clear view of the shell. This was very important evidence to prove that the particles what we made were hollow and it helped to determine how thick of the shell was. The small particles were clearly found on the shell and the shell was calculated at about 400 nm, which is similar to the measured thickness from optical images. The SEM image (Fig. 4.7(b) iv) clearly shows MG particles at the surface. Interestingly,

holes (or interstitial spaces) can be seen between the particles, which are potentially important as a means for permeability into and out of the colloidosomes.

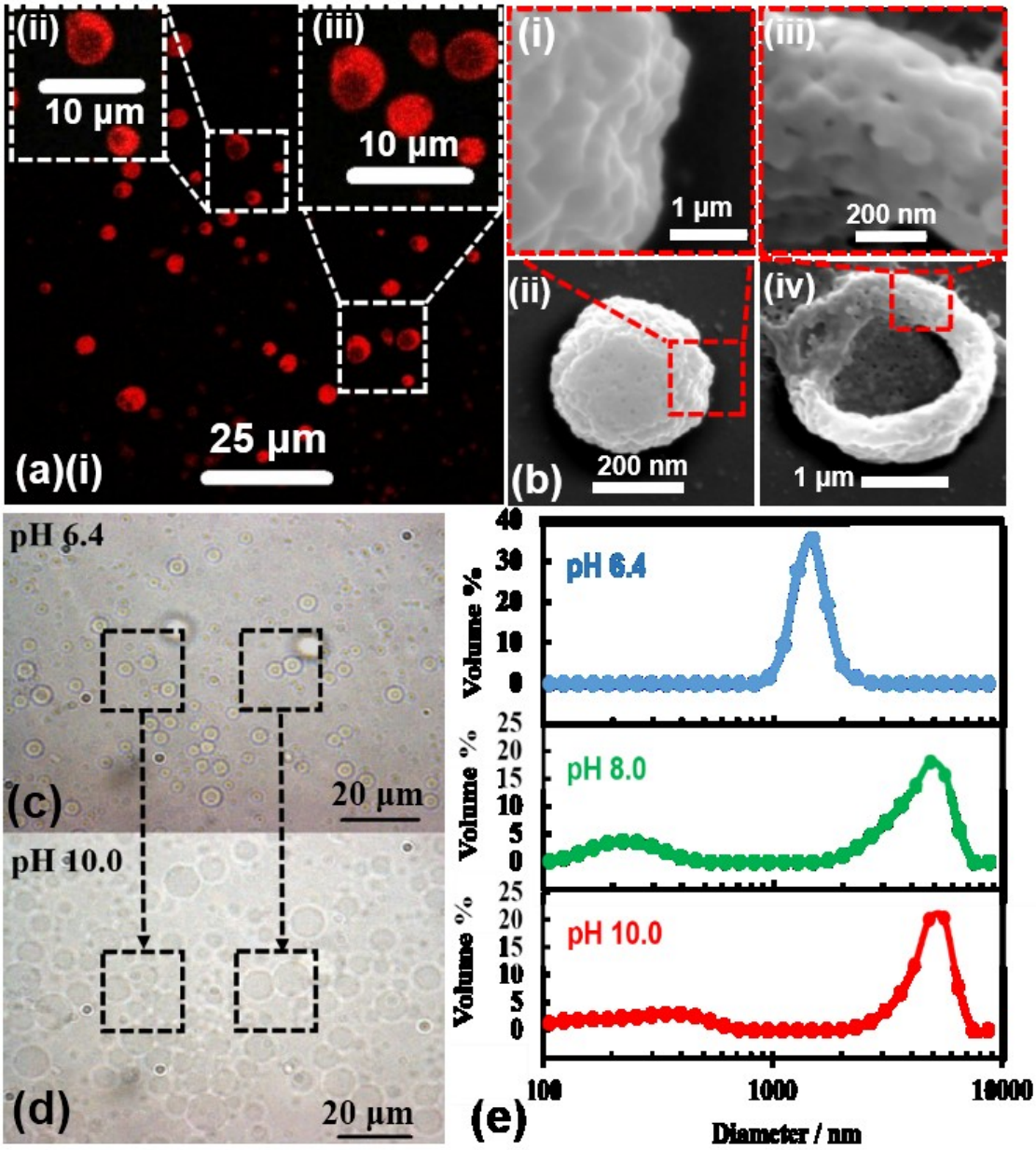

Figure 4.7 DX MG-colloidosomes prepared using the small-scale method. (a) CLSM images and (b) SEM images. The arrows in (iii) highlight small interstitial spaces between the MGs. (c) and (d) show optical micrographs for the colloidosomes at pH = 6.4 and 10.0, respectively. (e) DLS data measured at various pH values for DX MG-colloidosomes.

It was decided to study the swelling properties of DX microgel-colloidosome particles by DLS (Fig. 4.7e). The DLS data was measured for the DX MG-colloidosomes dispersions at three different pH values (Fig. 4.7e). From top to bottom (Fig. 4.7e), they were pH 6.4 (blue curve), 8.0 (green curve) and 10 (red curve). All of the strong peaks were indicated on the right for the DX MG-colloidosomes. When the pH equaled to 6.4, the diameter of the peak (blue) was 1.4 μm. With the pH increased, the green and red peaks were shifted to 4.8 μm and 5.0 μm, respectively. (Fig. 4.7e). The fast swelling of the colloidosomes to pH variation can be seen under the microscope which shows the response of the particles to a pH change (Fig. 4.7(c) and (d)). The colloidosome swelling was complete within 1 s, in which time there was an increase from ~ 6.4 to ~ 10. Furthermore, the pH-triggered swelling property of DX MG-colloidosome was probed using an optical microscope directly (Fig. 4.7 (c) and (d)). In this experiment, a drop of DX MG-colloidosome dispersion (pH 6.4) was prepared on the glass slide and covered by a piece of glass under the optical microscope (Fig. 4.7c). Some droplets of pH 10 buffer solutions were added from the edge of glass slide. Several DX MG-colloidosome were washed out by the addition buffer solution. Some of the colloidosomes had adsorbed on the glass slide which prevented their motion upon addition of the buffer solution (Fig. 4.7c). These absorbed DX MG-colloidosomes provided a good chance to directly track their diameter changes with increasing pH. Compared to the DX MG-colloidosome in Fig. 4.7c and Fig. 4.7d, the DX MG-colloidosome (Fig. 4.7d) became larger and more transparent.

4.3.6 Morphological and swelling characterisation of DX MG-colloidosomes prepared by large scale (VHS)

After having established that pH-responsive DX MG colloidosomes could be prepared using a small-scale thermal approach (above) the ability to scale up the approach to a gram scale was investigated. Compared to the small scale, the gram scale method use 60 times the amount of each original material (Table 4.1.). The morphology of the DX MG-colloidosomes was probed using several complementary microscopy techniques (Fig. 4.8 (a) to (d)). Comparison of Fig. 4.8(a) with Fig. 4.7(a) shows that the average size of gram scale DX MG colloidosomes (820 ± 40 nm) is much smaller than that that of the small scale DX MG colloidosomes (1.8 μm, CV = 21%). The diameter of gram scale DX MG colloidosomes have larger distribution range than small scale one, this result was confirmed by DLS measurement in Fig. 4.8(e) . That result is due to using the different shear mixing head during emulsion preparation. It is very interesting that the size of the DX MGs prepared by the large-scale method is much smaller than those prepared by the small-scale method. Furthermore, the large-scale DX MG colloidosomes have the smallest diameter of any microgel-based colloidosomes reported to our knowledge.

DX MG-colloidosomes morphology was also investigated at higher magnification using SEM (Fig. 4.8b to d). The spherical morphology of DX MG-colloidosomes was confirmed in Fig. 4.8(b) and (d). The DX MG-colloidosomes was very small (~800 nm ± 300 nm) and there is a broad distribution of size. This result is consistent with in CLSM images (Fig. 4.8a). The individual colloidosomes had a crumpled appearance. The highest magnification inset images in Fig. 4.8c clearly showed the presence of MG particles at the surface.

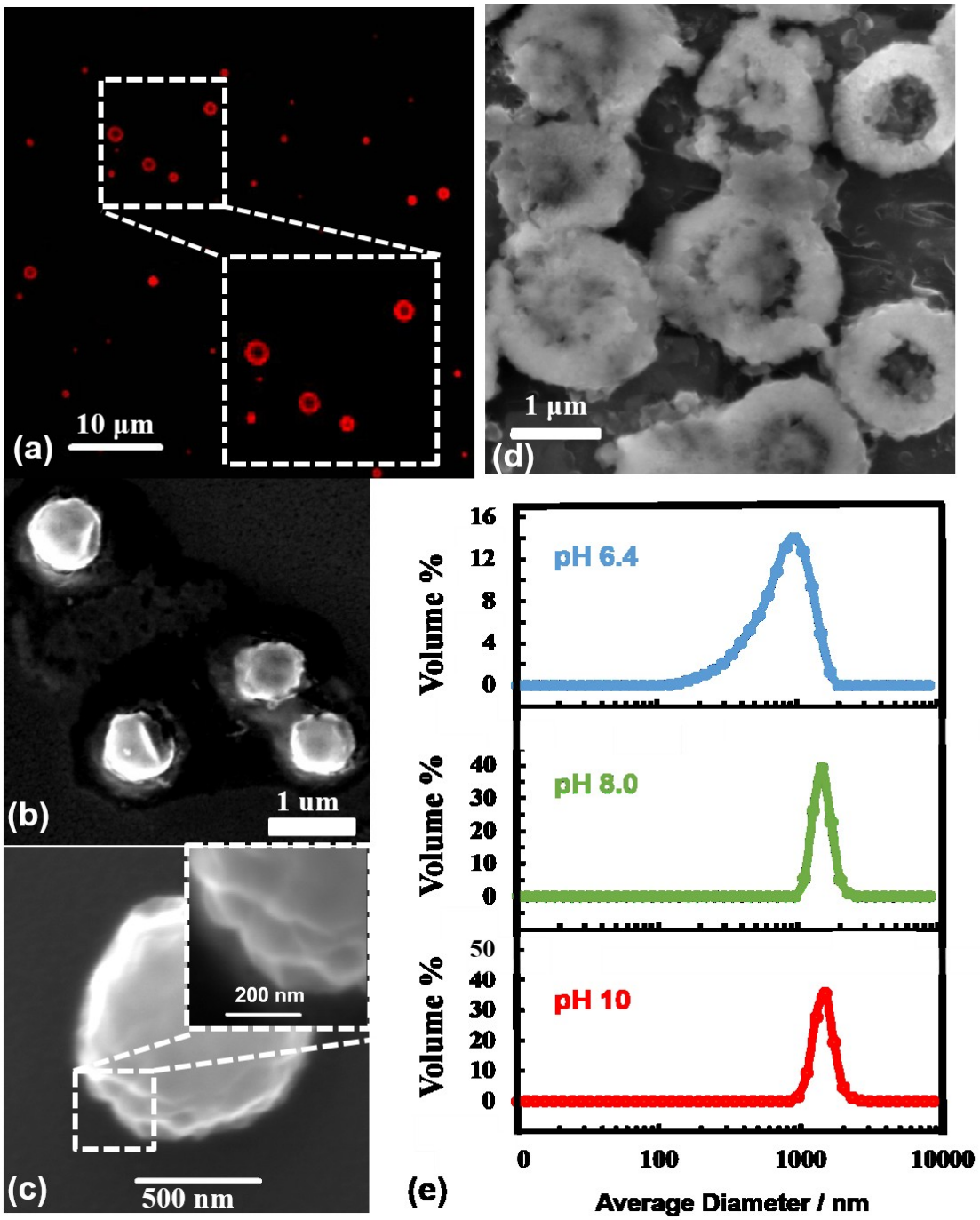

Figure 4.8 DX MG colloidosomes prepared using the large-scale method. (a) CLSM image. (b) and (c) show SEM images deposited at pH 6.4. (d) SEM image of DX MG colloidosomes deposited from the swollen state at pH 10. (e) DLS data measured at various pH values.

It was difficult to find cracked / broken colloidosomes to confirm the thickness of the shell and so we deposited colloidosomes from higher pH (Fig. 4.8d). The SEM images of swollen DX MG-colloidosomes could confirm whether the GMA-MGs successfully crosslink together. In Fig. 4.8d, the swollen DX MG colloidosomes with average diameter of about (~2000 nm ± 500 nm) were more transparent and had not dispersed when the pH was increased. It is certain that the MG particles were covalently inter-linked. This data confirms that the shells were comprised of MG particles in both Fig. 4.8(c) and (d). Due to the relatively brittle and swollen colloidosomes being under the high pressure, some cracked and broken swollen colloidosoems were found (Fig. 4.8(d)). The fact that is the colloidosomes retained significant three-dimensional morphology supports the view that the shells contained DX MGs. When deposited from the swollen state the colloidosomes were less robust and tended to collapse which showed the shells clearly.

In Fig. 4.8e, the DLS data was measured for the DX MG-colloidosomes dispersions at three different pH values. From top to bottom (Fig. 4.8e), they were pH 6.4 (blue curve), 8.0 (green curve) and 10 (red curve). The peaks in each curve were indicated in relation to the DX MG-colloidosomes. The peaks shifted to a larger value with increasing the pH (Fig. 4.8e). The GMA-MGs had shown the strong pH-triggered swelling property when the pH was higher than pK_a (6.2) (Fig. 4.1). The peak at pH 4 (blue) showed that the diameter of DX MG-colloidosomes was 700 nm, which was similar to the size measured from SEM of 0.67 ± 0.17μm (Fig. 4.8b). The major peak was shifted to 1700 nm when increasing the pH of DX MG-colloidosomes to 8 or 10. The swelling ratio ($Q = (d_{pH10}/d_{pH6.4})^3$) data could be calculated for DX MG-colloidosomes and it was about 14. This result provides strong evidence to prove the

DX MG-colloidosomes had a strong pH-triggered swelling property as well These results also show that the large-scale preparation method has provided DX MG colloidosomes with improved robustness to pH-triggered swelling. Furthermore, they were prepared at the gram scale (Table 1) which demonstrates good scalability. In the future, we can crosslink the neighbor colloidosomes after increasing the pH value to form super porous hydrogels. This hydrogel is used for better loading of drugs and tissue therapy for IVDD repair.

4.3.7 The permeability of DX MG colloidosome using largr scale (VHS) method.

One of the advantages of colloidosomes is that they potentially offer selective shell permeability because of the interstitial sites between MG particles**.** Microgel-based colloidosomes also have the advantage of potentially providing tuneable shell porosity because the microgel particle size is itself tunable. Having established a scalable method for preparing robust DX MG colloidosomes their permeability to solutes was investigated. All data obtained from this point involved DX MG colloidosomes prepared by the large-scale method.

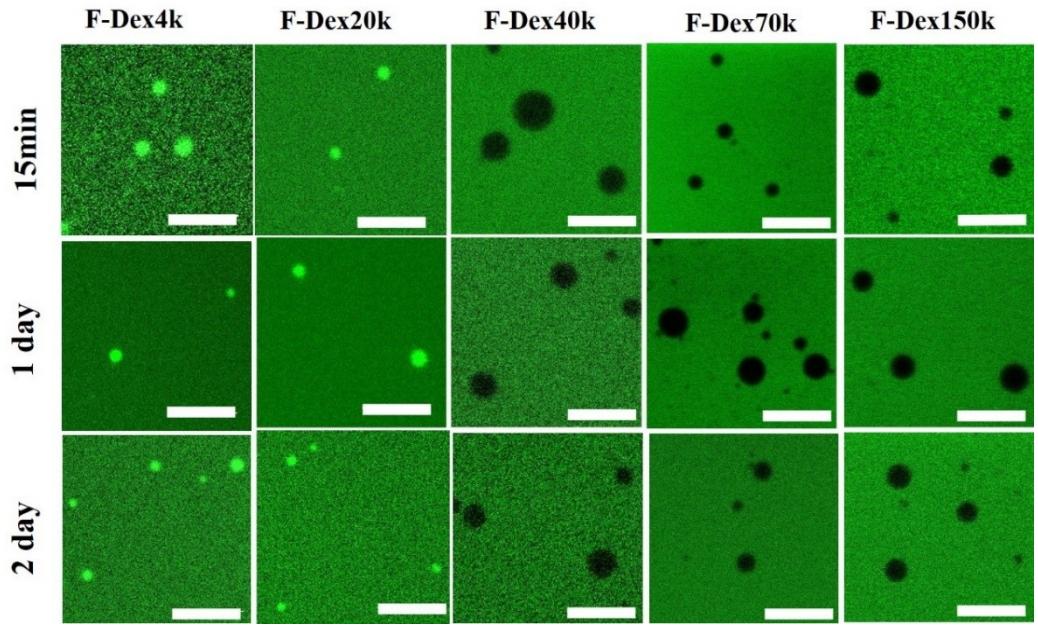

Figure 4.9 CLSM images of DX MG-colloidosomes mixed with FITC-Dextran with various molecular weights at different times. The pH was 6.2. The mixing times are shown on the left-hand side and the identities of the solutes are shown. As the dye penetrated the DX MG colloidosome interior the contrast was progressively lost. The scale bars are 5μm.

Fig. 4.9 probes the different permeabilities of the DX MG colloidosomes for FITC-labeled dextran with increasing molecular weight. The permeability was probed at pH 6.4 by mixing the colloidosomes with FITC-Dextran of different molecular weights using CLSM. It is interesting that the colloidosomes were permeable to dextran with a molecular weight less 40kDa immediately and were impermeable for dextrans with a molecular weight above 40 kDa. Thus, size-selective permeation was demonstrated at pH 6.2. The F-Dex 20k and F-Dex40 species correspond to a permeability / impermeability transition. The latter two species have hydrodynamic diameters of 6.6 and 9.0 nm, respectively[32]. Therefore, we estimate the pore size for the VHS MG-colloidosomes at pH 6.2 to be between 6.6 and 9.0 nm. The effect of pH on the permeability was also studied.

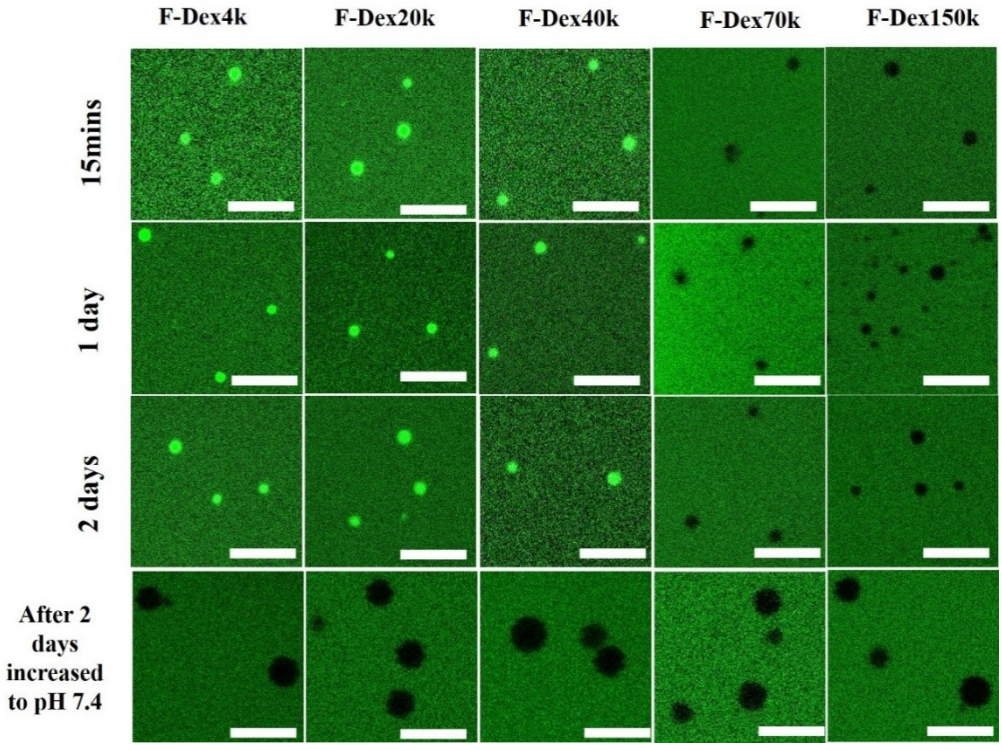

Figure 4.10 CLSM images of DX MG-colloidosomes mixed with FITC-Dextran with various molecular weights at various times. The pH was 5.5. The mixing times are shown on the left-hand side and the identities of the solutes are given above the top row. All scale bars are 5 μm.

The first of all, when pH is 5.5, The colloidosomes were collapsed and impermeable to 70 kDa and 150 kDa FITC–dextrans, while becoming completely open to the 4 kDa, 20 kDa and 40 kDa FITC–dextran (Fig. 4.10). Because the pH was below the pK_a of the MGs hydrogen bonding between the fluorescein and MG –COOH groups can be expected, which is a likely mechanism for adsorption. Interestingly, adsorption also occurred for the F-Dex4k, F-Dex20k and F-Dex40k samples (Fig. 4.10), which again is suggestive of hydrogen bonding. However, this could be reversed when the pH was subsequently increased to 7.4, which supports the hydrogen-bonded mechanism proposed above.

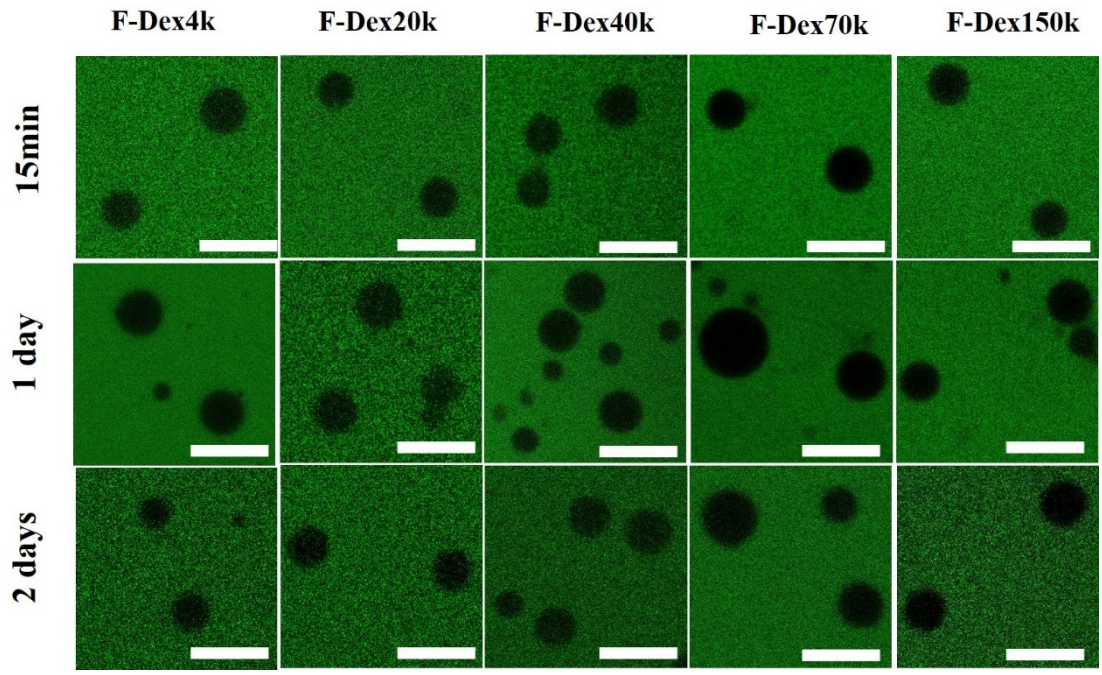

Figure 4.11 CLSM images of DX MG-colloidosomes mixed with FITC-Dextran with various molecular weights at various times. The pH was 7.4. The mixing times are shown on the left-hand side and the identities of the solutes are given above the top row. All scale bars are 5 μm.

Permeation tests were also conducted at pH 7.4 (Fig. 4.11). The colloidosomes were swollen and impermeable to Fluorescein and any molecular weight of dextran (Fig. 4.11). These results can be understood by taking into consideration the interactions between the fluorescent dextran probe and the DX MG-colloidosomes shell under the studied conditions. FITC–dextrans used as fluorescent probes are anionic because of FITC which is an anionic dye used for the dextrans' fluorescence modification[33]. The DX MG-colloidosmes were pH-sensitive and when the pH was above the pK_a of MG, the shell surface of colloidosmes would be subject to strong negative charges and that would lead to the electrostatic repulses between $–COO^-$ and FITC-dextrans. Therefore, the pores on the colloidosomes had been fully closed. According to the images showed in Fig. 4.11, the DX MG-colloisomes had been swollen at pH 7.4. It is proposed to say the FTIC-dextrans may be prevented solute prenetration the by fully inter-meshed effect of the swollen GMA-MG particles.

4.4 Conclusion

In this study, we investigated fully optimised microgel-stabilisation emulsion of EA-in-water emulsions system. We also have shown that our novel single building block assembly method is general by using more than one initiator approaches (UV and thermal) to prepare DX MG-colloidosomes. Especially, the thermal approach enables the DX MG-colloidosomes to be scaled up to the gram scale. This DX MG-colloidosoems enables control of the permeability of the colloidosome shell by changing the pH environment. The DX MG-colloidosoemes have the potential to be applied in a number of areas which include cosmetics and delivery.

Reference

1. Richtering, W.; Saunders, B. R., Gel architectures and their complexity. *Soft Matter* 2014, 10, 3695-3702.

2. Binks, B. P., Particles as surfactants—similarities and differences. *Current opinion in colloid & interface science* 2002, 7, 21-41.

3. Binks, B. P.; Clint, J. H., Solid wettability from surface energy components: relevance to Pickering emulsions. *Langmuir* 2002, 18, 1270-1273.

4. Lawrence, D. B.; Cai, T.; Hu, Z.; Marquez, M.; Dinsmore, A., Temperature-responsive semipermeable capsules composed of colloidal microgel spheres. *Langmuir* 2007, 23, 395-398.

5. Lin, Y.; Skaff, H.; Emrick, T.; Dinsmore, A.; Russell, T., Nanoparticle assembly and transport at liquid-liquid interfaces. *Science* 2003, 299, 226-229.

6. Melle, S.; Lask, M.; Fuller, G. G., Pickering emulsions with controllable stability. *Langmuir* 2005, 21, 2158-2162.

7. Pieranski, P., Two-dimensional interfacial colloidal crystals. *Physical Review Letters* 1980, 45, 569.

8. Velev, O. D.; Furusawa, K.; Nagayama, K., Assembly of Latex Particles by Using Emulsion Droplets as Templates. 1. Microstructured Hollow Spheres. *Langmuir* 1996, 12, 2374-2384.

9. Velev, O.; Nagayama, K., Assembly of latex particles by using emulsion droplets. 3. Reverse (water in oil) system. *Langmuir* 1997, 13, 1856-1859.

10. Dinsmore, A.; Hsu, M. F.; Nikolaides, M.; Marquez, M.; Bausch, A.; Weitz, D., Colloidosomes: selectively permeable capsules composed of colloidal particles. *Science* 2002, 298, 1006-1009.

11. Hsu, M. F.; Nikolaides, M. G.; Dinsmore, A. D.; Bausch, A. R.; Gordon, V. D.;

Chen, X.; Hutchinson, J. W.; Weitz, D. A.; Marquez, M., Self-assembled shells composed of colloidal particles: fabrication and characterization. *Langmuir* 2005, 21, 2963-2970.

12. Geisel, K.; Isa, L.; Richtering, W., Unraveling the 3D localization and deformation of responsive microgels at oil/water interfaces: a step forward in understanding soft emulsion stabilizers. *Langmuir* 2012, 28, 15770-15776.

13. Morse, A. J.; Madsen, J.; Growney, D. J.; Armes, S. P.; Mills, P.; Swart, R., Microgel Colloidosomes Based on pH-Responsive Poly (tert-butylaminoethyl methacrylate) Latexes. *Langmuir* 2014, 30, 12509-12519.

14. Kim, J.-W.; Fernández-Nieves, A.; Dan, N.; Utada, A. S.; Marquez, M.; Weitz, D. A., Colloidal assembly route for responsive colloidosomes with tunable permeability. *Nano letters* 2007, 7, 2876-2880.

15. Li, Z.; Ngai, T., Microgel particles at the fluid–fluid interfaces. *Nanoscale* 2013, 5, 1399-1410.

16. Berger, S.; Zhang, H.; Pich, A., Microgel‐Based Stimuli‐Responsive Capsules. *Advanced Functional Materials* 2009, 19, 554-559.

17. Richtering, W., Responsive Emulsions Stabilized by Stimuli-Sensitive Microgels: Emulsions with Special Non-Pickering Properties. *Langmuir* 2012, 28, 17218-17229.

18. Agrawal, G.; Ülpenich, A.; Zhu, X.; Möller, M.; Pich, A., Microgel-Based Adaptive Hybrid Capsules with Tunable Shell Permeability. *Chemistry of materials* 2014, 26, 5882-5891.

19. Schmidt, S.; Liu, T.; Rütten, S.; Phan, K.-H.; Möller, M.; Richtering, W., Influence of Microgel Architecture and Oil Polarity on Stabilization of Emulsions by Stimuli-Sensitive Core–Shell Poly(N-isopropylacrylamide-co-methacrylic acid)

Microgels: Mickering versus Pickering Behavior? *Langmuir* 2011, 27, 9801-9806.

20. Duan, H.; Wang, D.; Sobal, N. S.; Giersig, M.; Kurth, D. G.; Möhwald, H., Magnetic colloidosomes derived from nanoparticle interfacial self-assembly. *Nano letters* 2005, 5, 949-952.

21. Reincke, F.; Hickey, S. G.; Kegel, W. K.; Vanmaekelbergh, D., Spontaneous assembly of a monolayer of charged gold nanocrystals at the water/oil interface. *Angewandte Chemie International Edition* 2004, 43, 458-462.

22. Cayre, O. J.; Noble, P. F.; Paunov, V. N., Fabrication of novel colloidosome microcapsules with gelled aqueous cores. *Journal of Materials Chemistry* 2004, 14, 3351-3355.

23. Noble, P. F.; Cayre, O. J.; Alargova, R. G.; Velev, O. D.; Paunov, V. N., Fabrication of "hairy" colloidosomes with shells of polymeric microrods. *Journal of the American Chemical Society* 2004, 126, 8092-8093.

24. Wang, W.; Milani, A. H.; Carney, L.; Yan, J.; Cui, Z.; Thaiboonrod, S.; Saunders, B. R., Doubly crosslinked microgel-colloidosomes: a versatile method for pH-responsive capsule assembly using microgels as macro-crosslinkers. *Chemical Communications* 2015, 51, 3854-3857.

25. Mourran, A.; Wu, Y.; Gumerov, R. A.; Rudov, A. A.; Potemkin, I. I.; Pich, A.; Möller, M., When Colloidal Particles Become Polymer Coils. *Langmuir* 2016, 32, 723-730.

26. Brugger, B.; Richtering, W., Magnetic, Thermosensitive Microgels as Stimuli-Responsive Emulsifiers Allowing for Remote Control of Separability and Stability of Oil in Water-Emulsions. *Advanced Materials* 2007, 19, 2973-2978.

27. Brugger, B.; Rütten, S.; Phan, K.-H.; Möller, M.; Richtering, W., The Colloidal Suprastructure of Smart Microgels at Oil–Water Interfaces. *Angewandte*

Chemie International Edition 2009, 48, 3978-3981.

28. Brugger, B.; Rosen, B. A.; Richtering, W., Microgels as stimuli-responsive stabilizers for emulsions. *Langmuir* 2008, 24, 12202-12208.

29. Wang, W.; Milani, A. H.; Carney, L.; Yan, J.; Cui, Z.; Thaiboonrod, S.; Saunders, B. R., Doubly crosslinked microgel-colloidosomes: a versatile method for pH-responsive capsule assembly using microgels as macro-crosslinkers. *Chem. Commun.* 2015, 51, 3854-3857.

30. Fielding, L. A.; Armes, S. P., Preparation of Pickering emulsions and colloidosomes using either a glycerol-functionalised silica sol or core–shell polymer/silica nanocomposite particles. *Journal of Materials Chemistry* 2012, 22, 11235-11244.

31. Napper, D. H., Steric stabilization. *Journal of Colloid and Interface Science* 1977, 58, 390-407.

32. Bojko, A.; Andreatta, G.; Montagne, F.; Renaud, P.; Pugin, R., Fabrication of thermo-responsive nano-valve by grafting-to in melt of poly(N-isopropylacrylamide) onto nanoporous silicon nitride membranes. *J. Membr. Sci.* 2014, 468, 118-125.

33. Liu, F.; Kozlovskaya, V.; Zavgorodnya, O.; Martinez-Lopez, C.; Catledge, S.; Kharlampieva, E., Encapsulation of anticancer drug by hydrogen-bonded multilayers of tannic acid. *Soft matter* 2014, 10, 9237-9247.

Chapter 5: Highly-stretchable pH-responsive doubly crosslinked nanogels

Abstract

In this chapter, were studied by tuning the crosslinking monomers and we expected to have more stretchable hydrogels. The NGs were synthesised by emulsion polymerisation of methyl methacrylate and methacrylic acid and without any crosslinking monomer. Compared to the earlier chapters, this is a new nanogel-based approach for preparing highly stretchable -COOH-rich hydrogels. The NGs had very high MAA content (84 mol. %). The latter was vinyl functionalised and gave dispersions that could be crosslinked to form highly stretchable double crosslinked nanogels (DX NGs). The gels could be tied in knots and stretched considerably without damage. The DX NGs prepared at pH 10 could be stretched to more than 250% of its original length without the sample breaking. The compressive strain-at-break for the DX NGs prepared at pH 10 was greater than 93 % which is the highest value reported for a DX NGs system to date. The DX NGs was highly-stretchable with a stretchability of up to 520%. The results of this study provide design tools for improving DX NGs ductility and hence increasing the range of potential applications for this new class of hydrogel.

5.1 Introduction

Hydrogel is a polymer with high water content and good water absorption, which can expand in aqueous solution and form three-dimensional network structure through intertwined and cross-linked[1]. Hydrogels are attracting large interest in biomaterial applications[2-4] such as drug delivery[5], regenerative medicine[6] and soft tissue engineering[7, 8] due to their strong property resemblance with native gel matrix[9]. The swelling and mechanical properties of hydrogels are directly related to the number-density of elastically effective chains[10]. When compared to high ductility gels such as double network hydrogels[11], our previous doubly crosslinked nanogels (DX NGs) were relatively brittle[12, 13]. However, a lack of ductility is a key limitation for the DX NGs systems. In this study, we aimed to design a new nanogel (NG) system to reduce the brittleness. The use of pre-formed nanogels for DX NG gel construction is a potential advantage for biomaterial applications because it decreases the assembly required in vivo. DX NGs have been shown to have potential application as injectable gels for load bearing tissue repair[14]. Heterogeneity of elastically effective chain length is common in hydrogels which results in brittleness because stress concentrates at the shortest chains. This approach is commonly used to prepare highly stretchable, tough, gels and usually involve making the elastically effective chains a similar length[15] or introducing sacrificial crosslinks to dissipate energy[16]. Normally, the previous DX NGs consisted of inter-linked nanogels with two types of elastically effective chains; *intra*-nanogel chains and *inter*-nanogel chains. The intra-nanogel chains gave the stable network stability, but at the same time, it limited the swelling property of the nanogel particles. A nanogel is a crosslinked polymer particle with a swollen size of less than 100nm. Therefore, the previous DX NGs and DX MGs were brittle, due to most of the stress being focussed on the inter-nanogel chains. In recent research, the

highly hydrophobic crosslinker (DVB) was studied to prepare highly swellable MG particles and improve the DX MGs mechanical property[17]. In this research, we expect to build up a new nano-particle which would be substantially decrease the population of *intra*-nanogel elastically effective chains by preparing nanogels *without* added crosslinker. It was assumed that if one major population of elastically effective chains were present then DX NG stretchability would increase.

Scheme 5.1 depict the approach used in this study. The pH-triggered nanogels prepared in this study contained very high content of methacrylic acid (MAA) and did not add a crosslinker. The nanogels contained mostly MAA and a minor proportion of methyl methacrylate (MMA). They were subsequently vinyl-functionalised by reaction with glycidyl methacrylate (GMA). During the reaction, we used a relatively low temperature to avoid self-crosslinking. The nanogels then disassembled and were covalently interlinked to form DX NGs. In this study we first characterise the NGs and show that they were only weakly self-crosslinking. The morphology and mechanical properties of the new DX NGs are then investigated. The results show that the pH used for DX NG preparation had a major effect on the mechanical properties. The gels prepared at pH 7.4 and 10 were by far the toughest and most stretchable DX NGs reported to date.

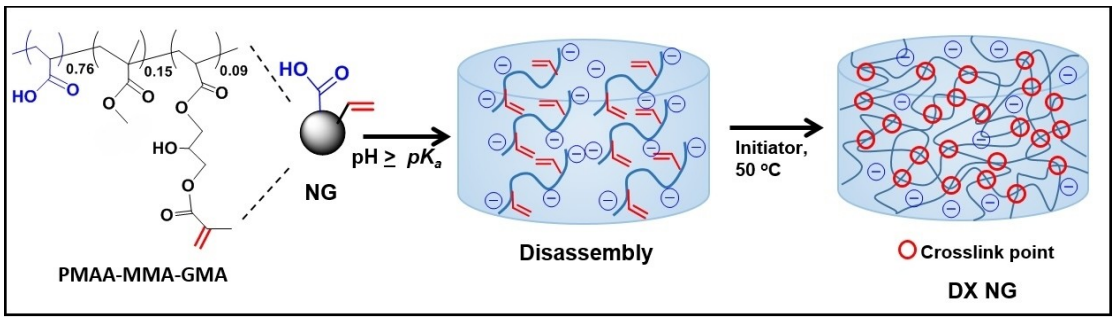

Scheme 5.1 Depiction of lightly self-crosslinked pH-triggered nanogel particles disassembly and DX NG formation.

5.2 Materials and Experimental Methods

5.2.1 Materials

Methyl methacrylate (MMA, 99%), methacrylic acid (MAA, 99%), glycidyl methacrylate (GMA, 97%) and NaOH (97%), ammonium persulfate (APS, 98%), sodium dodecyl sulphate (SDS, > 92.5%) and N,N,N′,N′-tetramethylethylenediamine (TEMED, 99%) were purchased from Sigma-Aldrich and used as received. All water was of ultrahigh purity and was distilled and de-ionised.

5.3.2 Nanogel synthesis using emulsion polymerisation

The synthesis of the self-crosslinked nanogels which contained very high MAA contents was conducted using a modified seed-feed emulsion polymerisation method. In order to minimise self-crosslinking whilst achieving particle growth with colloid stability a seed-feed method was used in the presence of TEMED. Accordingly, a mixed solution (35.0 g) containing MMA (14.0 g, 0.14 mol) and MAA (21.0 g, 0.25 mol) was prepared. A total of 5.0 g of the co-monomer solution was used for the seed formation. The latter solution was added to water (480 g) containing SDS (2.4 g, 0.008 mol) and then TEMED solution (1.0 ml of 11 wt% solution) and APS (5 g of a 11.0 wt.% solution) were added. The seed was prepared at 50 ˚C with mechanical stirring for 15 min. A total of 20.0 g of the co-monomer solution was added at a uniform rate of 0.5 ml/min over a period of 40 min and the temperature was increased to 60 ^{o}C. APS (2.75 g of a 11.0 wt% solution) was added and the remaining co-monomer solution was fed into the mixture at the same rate. The particle growth was continued for a further 1 h. The product was purified by extensive dialysis using water. The vinyl functionalisation of the nanogel (NG) was synthesised using an epoxide

ring opening reaction using GMA as described earlier[12] and is depicted in Scheme. 1. Briefly, GMA (1.25 g, 9.0 mmol.) was added to the purified precursor nanogel dispersion (100 g, 3.0 wt.%) and the reaction performed for 8.0 h at pH ~ 5.0. Unreacted GMA was removed by extensive dialysis using water.

5.3.3 Hydrogel preparation

Aqueous NaOH solution (4.0 M) was added to NG dispersion (4.0 g of 13.3 wt% dispersion) and the pH adjusted to the required pH (5.8, 7.4 or 10.0) to form a slightly viscous dispersion. DX NGs were formed by mixing APS solution (50 μL, 5.0 wt%) with the NG dispersion by stirring and subsequently heating the dispersions (10.6 wt.%) in sealed molds at 50 ^{o}C for 24 h.

5.3.4 Physical Measurements

Dynamic light scattering (DLS) measurements were conducted using a 50 mW He/Ne laser operated at 633 nm with a standard avalanche photodiode (APD) and 901 detection optics connected to a Malvern Zetasizer Nano ZS90 autocorrelator. Potentiometric titration was conducted using a Mettler Toledo DL15 titrator. The titrations were performed in the presence of aqueous NaCl (0.01 M) and the titrant was aqueous NaOH solution (0.1 M). TEM images were obtained using an FEI Tecnai Bio Twin instrument at an accelerating 100 kV voltage, and samples were supported by 300 mesh copper TEM grids. The MG dispersion concentration used was 0.001 wt,% and uranyl acetate staining was used. SEM measurements were obtained using a Philips XL30 FEG SEM instrument. Dispersions of particles were deposited on SEM stubs by evaporation at room temperature. The sample was coated

by platinum or carbon. Uniaxial compression measurements were performed using an Instron series 5569 load frame equipped with a 100 N compression testing head. Cyclic compression experiments were conducted at 10 mm/s. Gel samples for the qualitative tensile tests using a knot were prepared as described above using a cylindrical mold. Uniaxial tensile stress-strain measurements were conducted using an Instron series 5569 load frame equipped with a 10 N compression testing head at a rate of 10 mm/s. This was done using a dog-bone shaped sampled prepared using molds with a central rectangular region measuring a length of 20 mm. The width and thickness were both 4 mm. The paddle regions had a width of 17.5 mm. Gel swelling measurements were conducted using a by immersing gel samples in buffer for 24h.

5.4 Results and Discussion

5.4.1 Nanogel particle size and pH-triggered swelling

A new class non-crosslinker nanogel was prepared for this study. The SX nanogel were contained MAA (84.5 mol.%) and MMA (15.5 mol.%) (Table 5.1). In the following sections, the difference in swelling behaviour, morphology, mechanical properties of both singly crosslinked nanogels (SX NGs) and DX NGs were determined.

5.4.1.1 Potentiometric titration

The content of acid group (-COOH) and the content of GMA functionalisation of the SX NGs was determined by potentiometric titration data (Fig. 5.1). The –COOH contents were directly determined by the potentiometric titration data of SX NGs and the GMA contents were determined from the difference of MAA content in particles before and after GMA functionalisation (i.e. the mol. % of MAA consumed during GMA functionalisation). The measurements were performed in the presence of aqueous 0.01 M NaCl solution as electrolyte background.

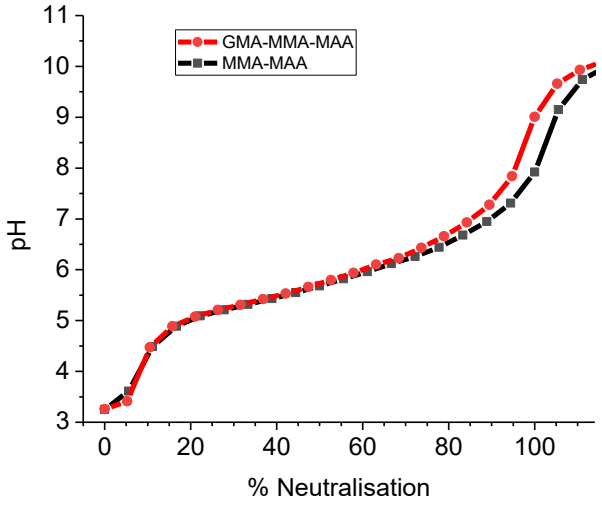

Figure 5.1 Potentiometric titration data for MMA-MAA and GMA-MMA-MAA.

The calculated values from titration data were shown in Table 5.1. The -COOH content of SX NGs (about 84.5 mol.%) and the concentrations of GMA in the SX NGs were 8.6 mol.%, which was enough to achieve the DX gelation process. The pK_a values of these NGs ranged from 5.6 to 5.8 (Table 5.1). Those pK_a values are less than physiological pH (~7.4) which means that the nanogel particles (and respective DX NGs) would be swollen in such an environment.

Table 5.1 Composition and properties of the nanogels

Nanoparticles	MAA[a]/ mol%	MMA[a]/ mol%	GMA / mol%	pK_a[b]	d_{TEM}[c] /nm [CV]	d_z/ nm (pH 4.0)
$PMAA_{85}$-MMA_{15}	84.5 ± 0.3	15.5 ± 0.3	-	5.6 ± 0.1	39.94 [78]	74.42 ± 1.35
$PMAA_{0.76}$-$MMA_{0.15}$-$GMA_{0.09}$	75.9 ± 0.2	15.5 ± 0.2	8.6	5.8 ± 0.1	32.59 [41]	66.60 ± 1.08

[a] Calculated from potentiometric titration data shown in Figure S1. [b] Apparent pK_a values were obtained from data (Figure S1). [c] Number-average diameters determined from TEM images.

5.4.1.2 DLS and zeta potential measurements

The hydrodynamic diameter (d_z) of the non-GMA-NGs and GMA-NGs over a range of pH values was determined by DLS measurements (see Fig. 5.2). The d_z values for the NGs and GMA-NGs were 74 nm and 67 nm at pH 4.0 (Table 5.1), respectively, which is in the collapsed state. The d_z values of the NGs and GMA-NGs increased strongly once the pH exceeded the pK_a and then passed through a maximum at pH 7.0 which was followed by a subsequent decrease at pH 10. The d_z values of both NGs

and GMA-NGs reached to the highest value of 6665 nm and 375 nm, respectively, at pH 7.0.

To further investigate the disassembly process pH-dependent zeta potential (ζ / mV) measurements were conducted (Fig. 5.2). The magnitude of zeta potential (ζ / mV) increased when the pH exceeded the pK_a. The latter was due to the neutralisation of -COOH to form $-COO^-$ groups. The similarity in the relative changes for d_z and zeta potential (ζ / mV) confirms that the NGs disassembled because of pH-triggered increase in electrostatic repulsion. Interestingly, both zeta potential (ζ / mV) for NGs and GMA-NGs system reached a stable value of ~ -55 mV when the pH was higher than 7.0, and even the d_z decreased. These results indicate that the polyelectrolyte composition was constant even though the particles continued to disassemble.

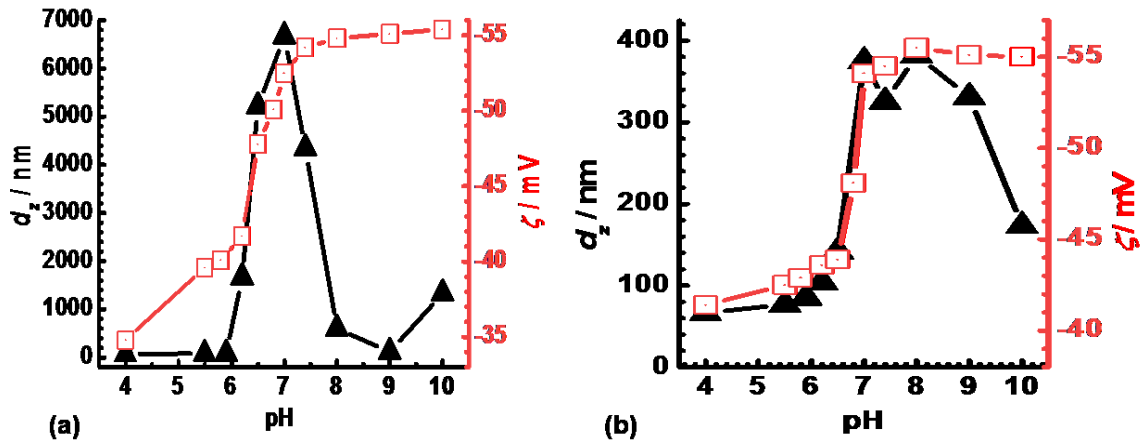

Figure 5.2 Hydrodynamic diameters and zeta potential of (a) Non-GMA nanogels particles and (b) GMA- nanogels particles at pH 4 to pH 11 measured at various values.

DLS diameter distributions (Fig. 5.3) revealed profound changes occurred for both NGs and GMA-NGs particles. As the pH increased the distributions changed from monomodal to multi-peak. For GMA-NGs (see Fig. 5.3b), at pH 7.4 there was clear evidence of species that were both smaller and larger than the initial NGs present at pH 4.0. These changes are attributed to pH-triggered swelling and disassembly of the NGs. This process led to considerable fragmentation as well as also left some larger species present where self-crosslinking and entanglements prevented complete disassembly.

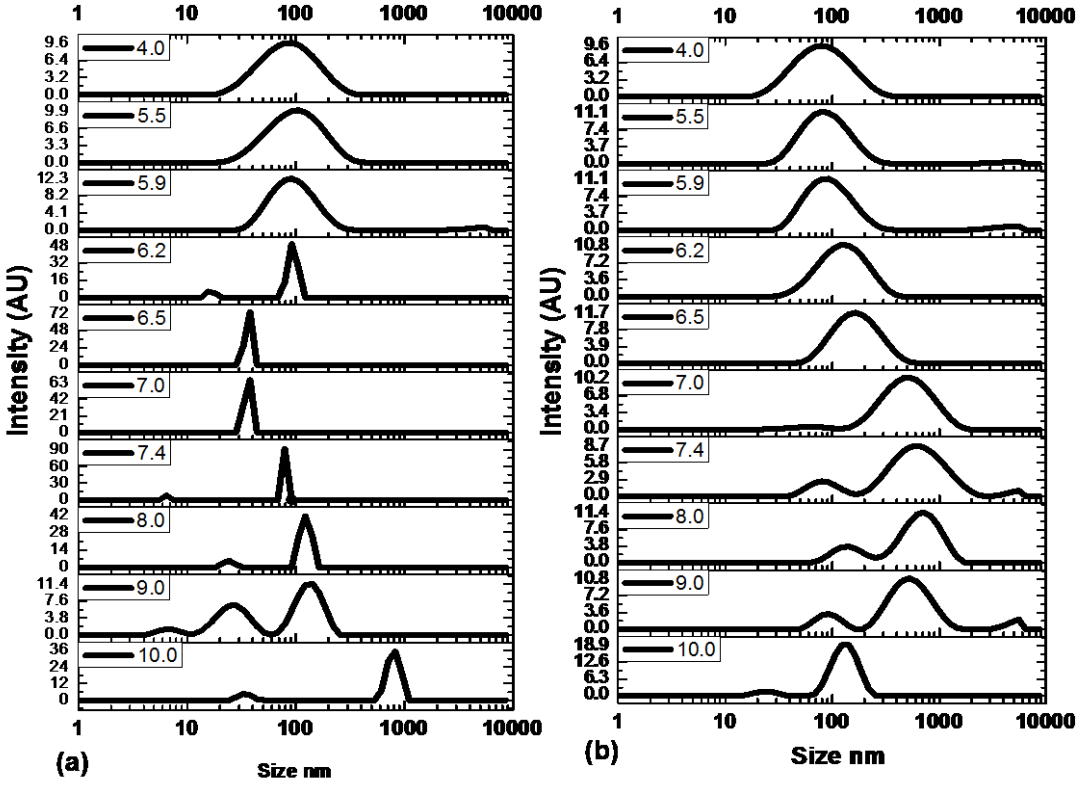

Figure 5.3 DLS size distributions for the (a) NGs and (b) GMA-NGs dispersions measured at various pH values (shown).

5.4.2 NGs and GMA-NGs morphology by TEM

The TEM images of NGs and GMA-NGs were obtained in Fig. 5.4 and Fig. 5.5 at different pH values. The particles had high polydispersity (see Fig. 5.4a and b) and the number-average diameters from TEM (d_{TEM}) at pH~5.0 of NGs and GMA-NGs were 40 nm [CV=78] and 33 nm [CV=41], respectively (Table 5.1). They were significantly different to the hydrodynamic diameter (d_z) in the collapsed state at pH 4.0 (Table 5.2). Compared to the respective hydrodynamic diameter (d_z) in the collapsed state, the d_{TEM} values are smaller and the coefficient variation is higher. This is due to the strong dependence of d_z on light scattering from the largest particles are not being totally "dry" in water as in previous reports[18].

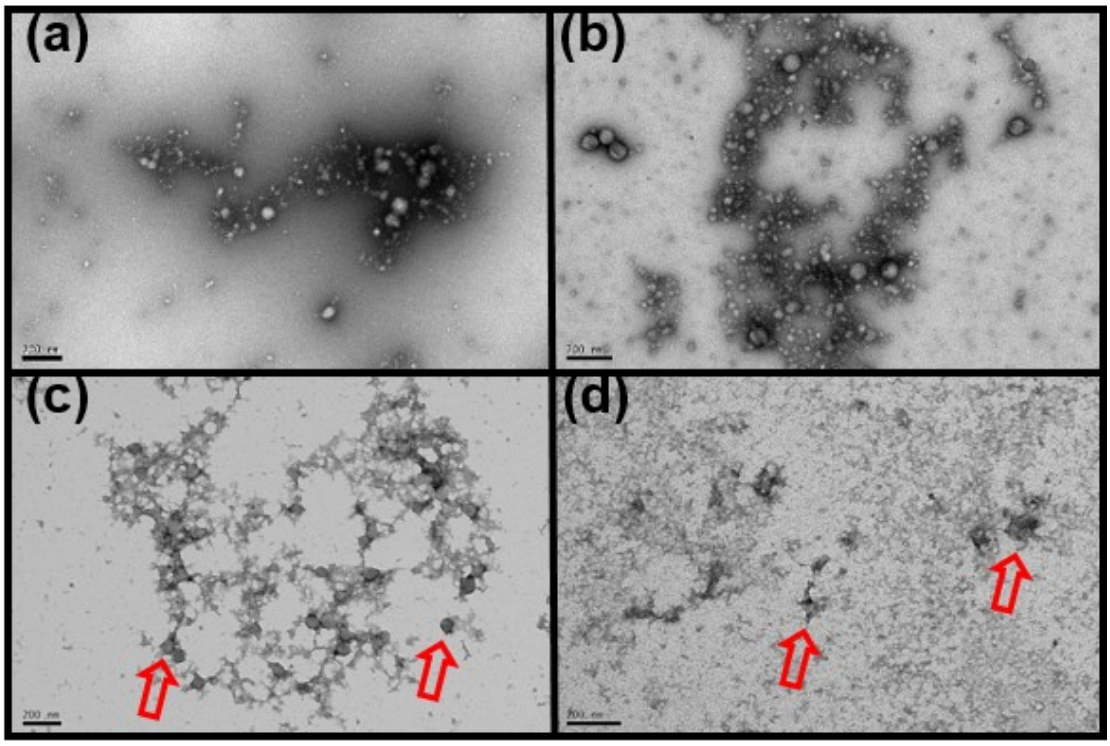

Figure 5.4 Lower magnification TEM images for (a) $PMAA_{0.85}$-$MMA_{0.15}$ at pH ~5; $PMAA_{0.76}$-$MMA_{0.15}$-$GMA_{0.09}$ nanoparticles obtained when the dispersions had pH values of (b) ~ 5, (c) 7.4 and (d) 10. The red arrows highlight nanogels that have not fully disassembled when pH > pK_a.

The reason for the large particle size polydispersity is the low temperature emulsion polymerisation method employed. Following earlier reports[19], we sought to decrease self-crosslinking with *N*,*N*,*N*′,*N*′-tetramethylethylenediamine (TEMED) and used a low temperature (60 ^{o}C) during emulsion polymerisation. It appears that particle nucleation was not short-lived as judged by the significant polydispersity evident. During the low temperature polymerisation with the TEMED, the polymer chains of the NGs would be relatively short. Furthermore, the use of a re-add addition of APS during growth may have occurred during secondary nucleation.

The TEM images showed that the NGs morphology changed dramatically when the dispersion pH was increased to 7.4 and 10.0 (Fig. 5.5(b) and (c) as well as Fig. 5.4(c) and (d)). With the increasing pH, the particles became more transparent. They did not fully disassemble, however the disassembled polymer can be found on the background (Fig. 5.4(c) and (d). These images (Fig. 5.5) showed considerable debris (yellow arrows) from disassembled NGs, which was most significant at pH 10. There was also clear evidence of occasional incompletely disassembled NGs (red arrows), which were most prevalent at pH 7.4 (Fig. 5.5). The latter was due to self-crosslinking.

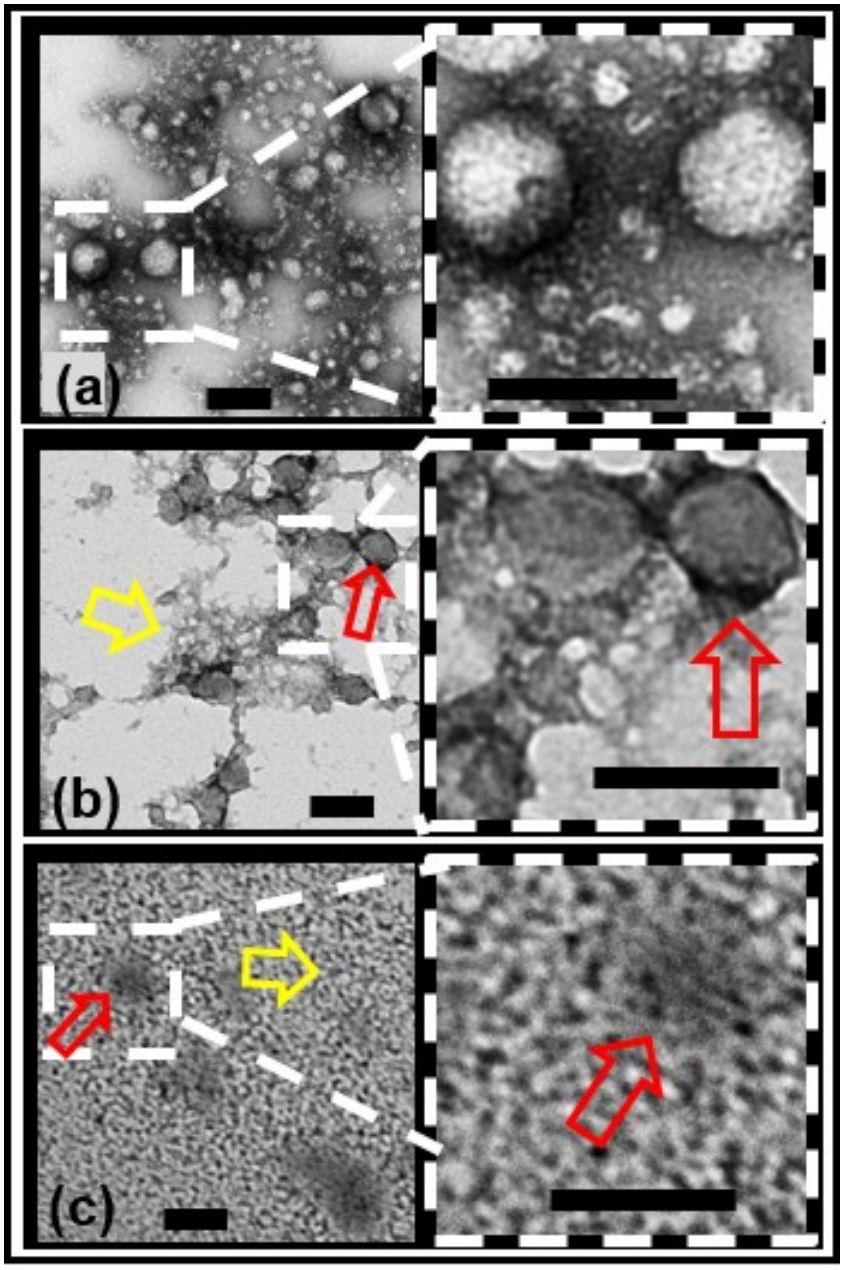

Figure 5.5 TEM of the NGs at pH ~ 5.0 (a), 7.4 (b) and 10.0 (c). Scale bars: 100 nm. The red and yellow arrows show, respectively, NGs that have not fully disassembled and disassembled polymer. Scale bars: 100nm.

5.4.3 DX GMA-NGs morphology by SEM

The morphology of DX GMA-NGs were assessed by SEM images as shown in Fig 5.6. The images of freeze-dried DX MGs showed typical hydrogel structures[20] which are highly porous. The pores were formed during the rapid ice formation. Interestingly, an obvious difference between Fig 5.6 (a) to (c) is that with the pH increasing during preparation of the DX GMA-NGs, the average pore size of DX GMA-NGs becomes larger. The following average pore sizes were determined by measuring at least100 pores at the value of pH 5.8, 7.4 and 10.0 (Fig. 5.6a – c), respectively. They were 4.0 ± 0.9, 7.2 ± 1.5 and 15.4 ± 4.5 μm, respectively. Whilst it is understood that the pores were evidently from a freeze-dried origin during ice-formation[21], useful qualitative mechanical property information can still be obtained from the SEM images. For example, in previous work for conventional DX NGs it was shown that the pore size increased as the gel modulus decreased[17]. Here, the average pore-size increased with increasing preparation pH suggesting that the gel modulus decreased. This trend is supported by the tensile data (below).

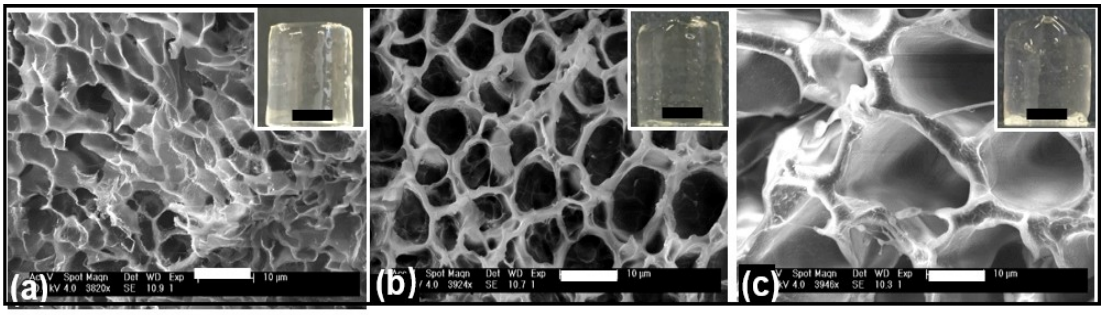

Figure 5.6 SEM images of freeze-dried gels prepared at (a) pH 5.8 (b) pH 7.4, and (b) pH 10. The insets show digital photographs of the gels. Scale bars: SEM 10 μm; Gel images 5 mm.

Such porous materials have been considered as potential materials for tissue scaffold applications[21, 22]. Moreover, the previous work gives a possible method in tuning the pore size of the freeze-dried hydrogel by selection of the crosslinking monomers[23]. Now, a new class non-crosslinker NG gave a larger pore size than that within the crosslinker and good mechanical properties.

5.4.4 FTIR spectra of freeze-dried gels.

The FTIR spectra was used to probe neutralisation of the freeze-dried gels (Fig. 2d). FTIR spectra reveal the appearance of stretching vibration of hydrogen bonded -COOH pairs at 1710 cm^{-1} and $-COO^-$ at 1544 cm^{-1}, respectively[24, 25]. The absorbance area ratio of the peak of $-COO^-$ and -COOH were calculated (see Fig. 5.7). The relative absorbance ratio for the $-COO^-$/-COOH peak increased from 0.3 (pH 5.8) through 1.5 (pH 7.4) to 4.0 (at pH 10.0) when the pH increased. Hence, the extent of neutralisation increased for the gels as the pH increased. This data showed that neutralisation was not complete at pH 7.4 even though the pH was 1.6 pH units more than the pK_a. Interesting, the similar performance occurred and was confirmed in TEM imaged (Fig. 5.4 and Fig. 5.5). The NGs particles are not fully swollen and disassembled (Fig. 5.5b). We attribute this delayed neutralisation to electrostatic repulsion between mobile OH^- (from NaOH) and the fixed $-COO^-$ groups on the gel network.

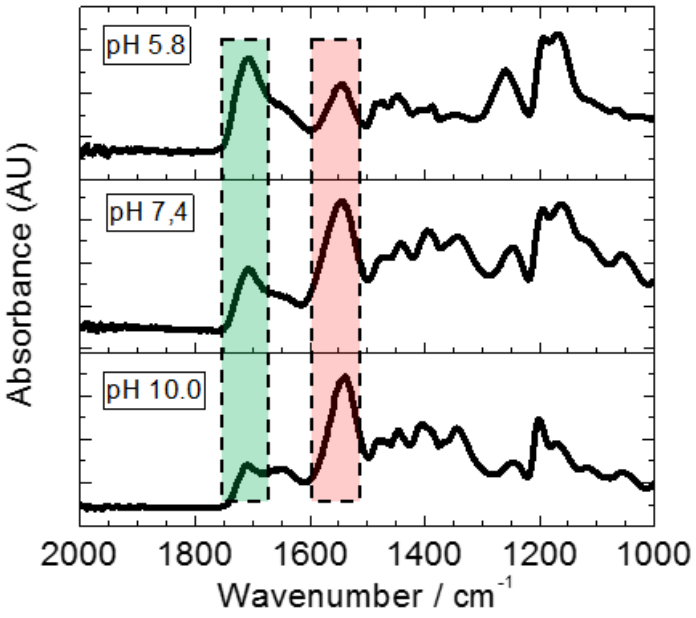

Figure 5.7 FTIR spectra of freeze-dried gels prepared at various pH values (shown).

5.4.5 Uniaxial compression of the DX NGs

Static uniaxial compression tests were performed for all DX NGs. The stress *vs.* strain data of selected representative measurements are shown in Fig. 5.8. The compression modulus (E) was calculated from the slope of the initial 10% part in the total curves before failure. The strain-at-break (ε_b) was determined when the curve started to fail and the associate stress at this point is the stress-at-break (σ_b). The previous DX NGs it was reported that they were prepared using MAA and MMA and had limited ductility when compressed[24]. In contrast, the present gels had remarkable ductility, especially those prepared at pH 10. Those gels could be strongly (and reversibly) compressed without breaking (Fig. 5.8b). Uniaxial compression data (Fig. 5.8 and Table 5.2) were obtained for the gels prepared at pH 5.8, 7.4 and 10.0. With the increasing of the preparation pH, the modulus and extension ratio-at-break ($\lambda_b = 1 - \varepsilon_b$, where ε_b is the strain-at-break) both decreased. In here, a low λ_b value equates to a high ε_b and ductility.

Table 5.2 Compression properties for the DX NG gels studied

pH	Vol. %[a]	Compression modulus (kPa)	Compression stress at break σ_b (kPa)	Compression extension ratio at break λ_b
5.8	16.9 ± 0.6	35.6 ± 0.2	133 ± 2	0.34 ± 0.02
7.4	17.2 ± 0.3	21.1 ± 0.1	215 ± 3	0.28 ± 0.01
10.0	17.8 ± 0.2	3.09 ± 0.1	> 1170 ± 5[b]	< 0.07 ± 0.01[c]

[a] Measured polymer volume fraction in the as-prepared state (Vol. %). [b] Gel did not break at maximum compression stress.

Firstly, the modulus (and λ_b) values were 35.6 (0.34), 21.1 (0.28) and 3.09 (< 0.07) kPa, respectively. Hence, the gels became more ductile as their stiffness decreased. The DX NGs at pH 10 was much more ductile than DX NGs at pH 7.4 and pH 5.8 systems. The average value of ε_b for the DX NGs at pH 10 was 93.0 % which is an outstanding improvement compared to the largest ε_b of 49.0% reported for a DX PMMA-MAA-EGD gel[26]. The E value showed the opposite behaviour and increased in the order DX NGs at pH 10 < DX NGs at pH 7.4 < DX NGs at pH 5.8. (Table 5.2). This trend follows the observation of pore size in Fig 5.7 and supports the view that the stiffer gels formed the smaller pores.

The compression data trends for stiffness (E) and ductility (ε_b) matched those observed with them from tensile test as measured by the Young's modulus (E) and tensile extension ratio-at-break ($\lambda_{b(T)}$) (see Fig. 5.9), respectively. Moreover, the stress-at-break (σ_b) for the present DX NG gel prepared at pH 10.0 was > 1170 kPa. This minimum value is by far the largest σ_b reported to date for DX NG gels. In fact, the average ε_b value of 93.0% for DX NGs is a record for DX NGs prepared using GMA functionalisation[12, 17].

Cyclic compression measurements were determined of the gels prepared at pH 5.8, pH 7.4 and 10.0 for the mechanism responsible of stiffness and ductility (Fig. 5.8b). For each system, there was a relatively low hysteresis. But there is no any residual strain for each system. If a major contribution to crosslinking was contributed by reversible or dynamic crosslinks one would expect much higher hysteresis and significant residual strain[26]. Therefore, covalent crosslinking is the main crosslinking type responsible for the mechanical properties of these gels

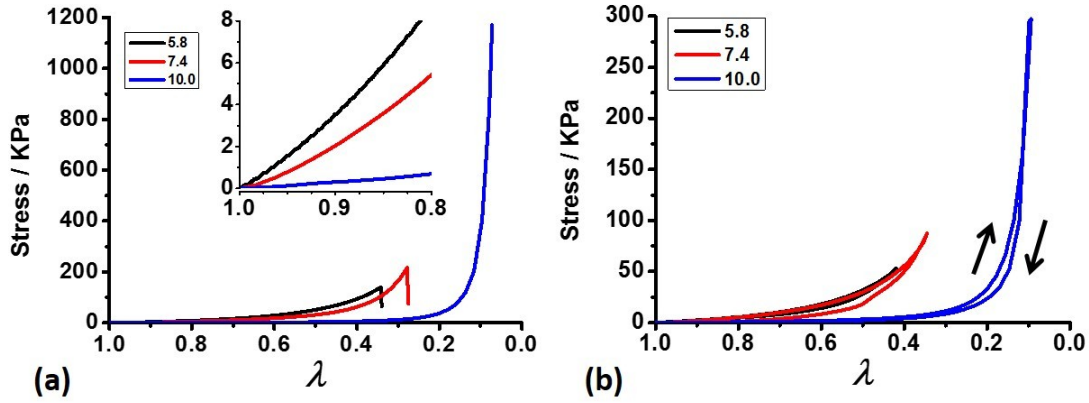

Figure 5.8 (a) Uniaxial compression stress - extension ratio data for the gels.

5.4.6 Stretchable propertied test of the DX NGs

The present DX NGs at pH 10 are not only having very impressive compressive properties but also they are remarkably stretchable. The DX NGs strings could be tied in knots and stretched considerably without damage (Fig. 5.9b). The DX NG gel prepared at pH 10 could be stretched to more than 250% of its original length without the knot or sample breaking (Fig. 5.9b).

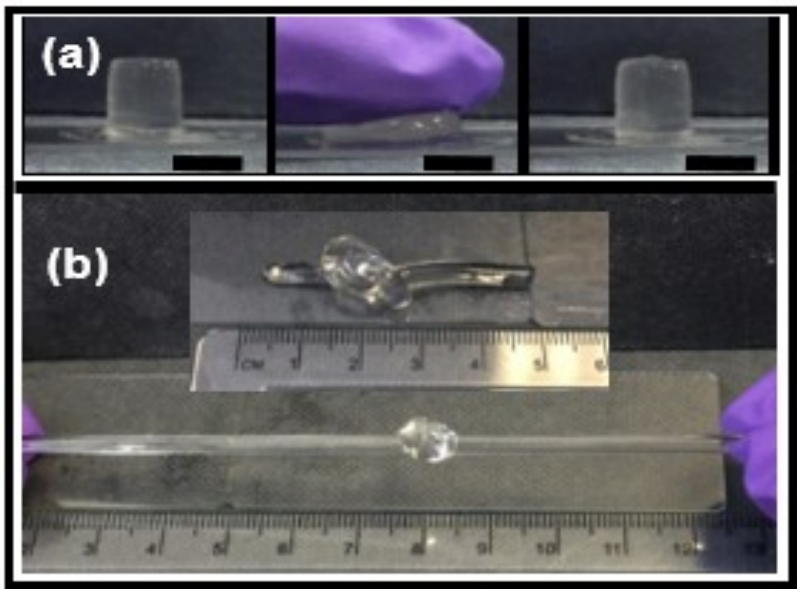

Figure 5.9 Images of DX NGs prepared at pH 10 with good ductile mechanical property (a) and stretchable property (b). The scale bars are 1 μm.

5.4.7 Tensile test of DX NGs

The tensile data were obtained for all of the gels (Fig. 5.10). These data represent the first tensile data reported for this class of gels which was first introduced in 2011[11]. The static tensile tests were performed for all DX NGs. The stress *vs.* strain data of selected representative measurements are shown in Fig. 5.10. The Young's modulus (E) was calculated from the slope of the initiate 10% part in the total curves before failure. The strain-at-break ($\varepsilon_{b(T)}$) was determined when the curve started to fail and the associate stress at this point is the stress-at-break ($\sigma_{b(T)}$). The extension ratio-at-break ($\lambda_{b(T)} = 1 + \varepsilon_{b(T)}$). First, the modulus (and $\lambda_{b(T)}$) values of the gels prepared at pH 5.0, pH 7.4 and 10.0 were 19.2 ± 0.1 (2.0), 17.4 ± 0.1 (3.4) and 2.37 ± 0.1 (5.2) kPa, respectively. The DX NGs prepared at pH 5.8, 7.4 and 10 stretched to 200, 340 and 520% of their original lengths. Hence, the gels have better stretchability as their stiffness decreased. The DX NGs at pH 10 was much more stretchable than DX NGs at pH 7.4 and pH 5.8 systems.

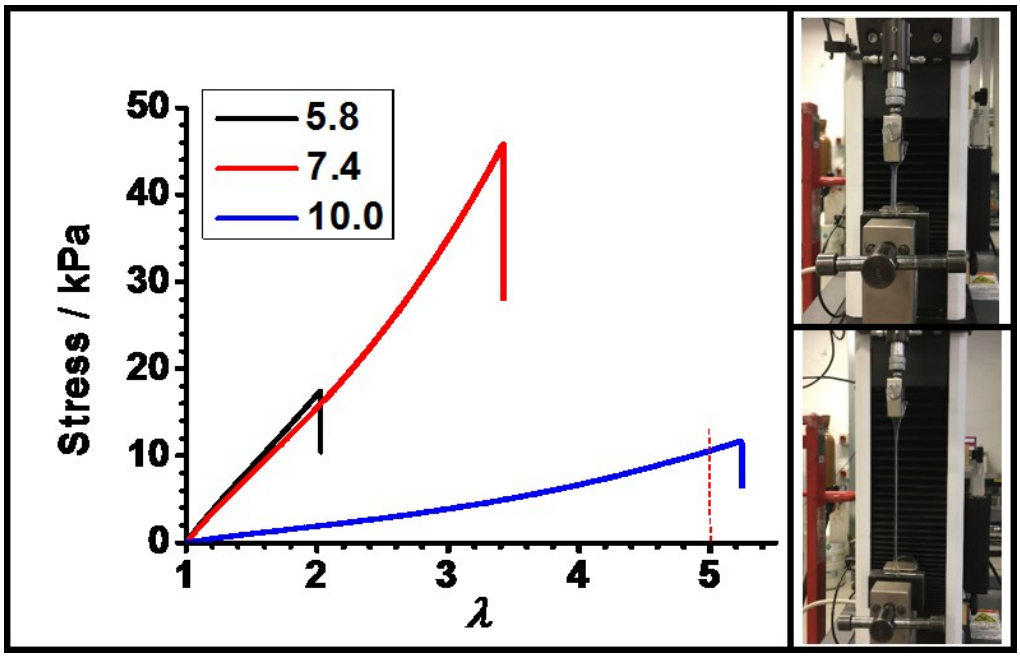

Figure 5.10 (a) Uniaxial compression stress - extension ratio data for the gels.

Interestingly, the Young's modulus of the gels prepared at pH 5.0, pH 7.4 are very similar. But the respectable $\lambda_{b(T)}$ value for the gel prepared at pH 7.4 together with its high toughness (49.4 ± 0.5 kJ/m^3, Table 5.3), which is even higher than the DX NGs at pH 10 (20.3 ± 0.3 kJ/m^3, Table 5.3) are encouraging for future biomaterial applications. Moreover, the stretchability for the gel prepared at pH 10 compares favorably to other advanced gels.[27, 28]

Table 5.3 Tensile properties for the DX NG gels studied

pH	Tensile modulus (kPa)	Tensile Stress at break $\sigma_{b(T)}$ (kPa)	Tensile extension ratio at break $\lambda_{b(T)}$	Toughness (kJ/m^3) [a]
5.8	19.2 ± 0.1	17.4 ± 0.2	2.0 ± 0.1	9.19 ± 0.2
7.4	17.4 ± 0.1	45.8 ± 0.2	3.4 ± 0.1	49.4 ± 0.5
10.0	2.37 ± 0.1	10.6 ± 0.1	5.2 ± 0.1	20.3 ± 0.3

[a] Determined from the area under the tensile stress-strain curve.

The most important question about the mechanical properties of this new gel is what the reason of their high scalability is. First of all, we need to know the relationship between the structure and the properties of the polymer hydrogel. There are approximately four factors directly affecting its mechanical properties showing the following. 1. The density of high molecular polymers. 2. The uniformity of the network structure of the hydrogel. 3. The degree of freedom of the crosslinking point. 4. The flexibility of the polymer chain. The nanogels used in this study had two key differences compared to the previous works. They are (I) Increasing in the use of MAA content. (II) Omission crosslinking monomer. Therefore, the nanogel particles can swell much stronger when the pH value increased more than pK_a. This leads to decrease density and increase the flexibility of the polymer chain of nanogel particles.

In general, the crosslinking of polymer hydrogels through monomer polymers inevitably leads to the inhomogeneity of the network structure and the inhomogeneous crosslinking point. But this new nanogels are proposed to lead to the functionalized vinyl groups on the chain can be more evenly distributed. This increases the uniformity of the network structure of the hydrogel and the distance between the crosslinking points. These may improve the ability to absorb external stress.

5.5 Conclusion

In this study a new nanogel-based approach for preparing highly stretchable -COOH-rich hydrogels has been established. Without adding crosslinker and relying on self-crosslinking very high MAA-content nanogel particle dispersions were prepared (with up to 84 mol. % MAA). The latter were vinyl functionalised and gave dispersions that could be crosslinked to form highly stretchable gels. The present DX NGs at pH 10 are not only having very impressive compressive properties but also they are remarkably stretchable. The DX NGs strings could be tied in knots and stretched considerably without damage. These NGs gave highly-stretchable pH-responsive DX NGs with a stretchability of up to 520% and compression of up to 93% without damage. This ability benefits for designing and preparing improved injectable pH-responsive DX MG systems in future and these materials may provide a promising route for fabrication soft tissue engineering or degenerative medicine application[29].

References

1. Ahmed, E. M., Hydrogel: Preparation, characterization, and applications: A review. *Journal of advanced research* 2015, 6, 105-121.

2. Richtering, W.; Saunders, B. R., Gel architectures and their complexity. *Soft Matter* 2014, 10, 3695-3702.

3. Chen, Q.; Zhu, L.; Chen, H.; Yan, H.; Huang, L.; Yang, J.; Zheng, J., A Novel Design Strategy for Fully Physically Linked Double Network Hydrogels with Tough, Fatigue Resistant, and Self‐Healing Properties. *Advanced Functional Materials* 2015, 25, 1598-1607.

4. Gladman, A. S.; Matsumoto, E. A.; Nuzzo, R. G.; Mahadevan, L.; Lewis, J. A., Biomimetic 4D printing. *Nature materials* 2016, 15, 413-418.

5. Zhang, Z.; He, Z.; Liang, R.; Ma, Y.; Huang, W.; Jiang, R.; Shi, S.; Chen, H.; Li, X., Fabrication of a micellar supramolecular hydrogel for ocular drug delivery. *Biomacromolecules* 2016, 17, 798-807.

6. Rosales, A. M.; Anseth, K. S., The design of reversible hydrogels to capture extracellular matrix dynamics. *Nature Reviews Materials* 2016, 1, 15012.

7. Xavier, J. R.; Thakur, T.; Desai, P.; Jaiswal, M. K.; Sears, N.; Cosgriff-Hernandez, E.; Kaunas, R.; Gaharwar, A. K., Bioactive nanoengineered hydrogels for bone tissue engineering: a growth-factor-free approach. *ACS nano* 2015, 9, 3109-3118.

8. Motamed, S.; Del Borgo, M.; Kulkarni, K.; Habila, N.; Zhou, K.; Perlmutter, P.; Forsythe, J.; Aguilar, M., A self-assembling β-peptide hydrogel for neural tissue engineering. *Soft Matter* 2016, 12, 2243-2246.

9. Costa, A. M.; Mano, J. F., Extremely strong and tough hydrogels as prospective candidates for tissue repair–a review. *European Polymer Journal* 2015, 72, 344-364.

10. Flory, P. J., *Principles of polymer chemistry*. Cornell University Press: 1953.

11. Gong, J. P., Why are double network hydrogels so tough? *Soft Matter* 2010, 6, 2583-2590.

12. Liu, R.; Milani, A. H.; Freemont, T. J.; Saunders, B. R., Doubly crosslinked pH-responsive microgels prepared by particle inter-penetration: swelling and mechanical properties. *Soft Matter* 2011, 7, 4696-4704.

13. Cui, Z.; Milani, A. H.; Greensmith, P. J.; Yan, J.; Adlam, D. J.; Hoyland, J. A.; Kinloch, I. A.; Freemont, A. J.; Saunders, B. R., A study of physical and covalent hydrogels containing pH-responsive microgel particles and graphene oxide. *Langmuir* 2014, 30, 13384-13393.

14. Milani, A. H.; Freemont, A. J.; Hoyland, J. A.; Adlam, D. J.; Saunders, B. R., Injectable doubly cross-linked microgels for improving the mechanical properties of degenerated intervertebral discs. *Biomacromolecules* 2012, 13, 2793-2801.

15. Apostolides, D. E.; Sakai, T.; Patrickios, C. S., Dynamic Covalent Star Poly (ethylene glycol) Model Hydrogels: A New Platform for Mechanically Robust, Multifunctional Materials. *Macromolecules* 2017, 50, 2155-2164.

16. Luo, F.; Sun, T. L.; Nakajima, T.; King, D. R.; Kurokawa, T.; Zhao, Y.; Ihsan, A. B.; Li, X.; Guo, H.; Gong, J. P., Strong and Tough Polyion-Complex Hydrogels from Oppositely Charged Polyelectrolytes: A Comparative Study with Polyampholyte Hydrogels. *Macromolecules* 2016, 49, 2750-2760.

17. Cui, Z.; Wang, W.; Obeng, M.; Chen, M.; Wu, S.; Kinloch, I.; Saunders, B. R., Using intra-microgel crosslinking to control the mechanical properties of doubly crosslinked microgels. *Soft matter* 2016, 12, 6985-6994.

18. Tadros, T. F., *Emulsion formation and stability*. John Wiley & Sons: 2013.

19. Hu, X.; Tong, Z.; Lyon, L. A., Control of poly (N-isopropylacrylamide)

microgel network structure by precipitation polymerization near the lower critical solution temperature. *Langmuir* 2011, 27, 4142-4148.

20. Lally, S.; Bird, R.; Freemont, T. J.; Saunders, B. R., Microgels containing methacrylic acid: effects of composition on pH-triggered swelling and gelation behaviours. *Colloid and Polymer Science* 2009, 287, 335-343.

21. Yao, X.; Yao, H.; Li, Y., Hierarchically aligned porous scaffold by ice-segregation-induced self-assembly and thermally triggered electrostatic self-assembly of oppositely charged thermosensitive microgels. *Journal of Materials Chemistry* 2009, 19, 6516-6520.

22. Chau, M.; De France, K. J.; Kopera, B.; Machado, V. R.; Rosenfeldt, S.; Reyes, L.; Chan, K. J.; Förster, S.; Cranston, E. D.; Hoare, T., Composite hydrogels with tunable anisotropic morphologies and mechanical properties. *Chemistry of Materials* 2016, 28, 3406-3415.

23. Román, J.; Cabañas, M. V.; Peña, J.; Vallet-Regí, M., Control of the pore architecture in three-dimensional hydroxyapatite-reinforced hydrogel scaffolds. *Science and technology of advanced materials* 2011, 12, 045003.

24. Brozoski, B. A.; Coleman, M. M.; Painter, P. C., Local structures in ionomer multiplets. A vibrational spectroscopic analysis. *Macromolecules* 1984, 17, 230-234.

25. Mandal, U. K., Ionic elastomer based on carboxylated nitrile rubber: infrared spectral analysis. *Polymer international* 2000, 49, 1653-1657.

26. Milani, A. H.; Bramhill, J.; Freemont, A. J.; Saunders, B. R., Swelling and mechanical properties of hydrogels composed of binary blends of inter-linked pH-responsive microgel particles. *Soft Matter* 2015, 11, 2586-2595.

27. Bilici, C.; Ide, S.; Okay, O., Yielding Behavior of Tough Semicrystalline Hydrogels. *Macromolecules* 2017, 50, 3647-3654.

28. Du, J.; Xu, S.; Feng, S.; Yu, L.; Wang, J.; Liu, Y., Tough dual nanocomposite hydrogels with inorganic hybrid crosslinking. *Soft Matter* 2016, 12, 1649-1654.

29. Frith, J. E.; Cameron, A. R.; Menzies, D. J.; Ghosh, P.; Whitehead, D. L.; Gronthos, S.; Zannettino, A. C.; Cooper-White, J. J., An injectable hydrogel incorporating mesenchymal precursor cells and pentosan polysulphate for intervertebral disc regeneration. *Biomaterials* 2013, 34, 9430-9440.

Chapter 6. Conclusion and future work

6.1 Conclusion

At the beginning of the project, we used a simple, one component method to make uniform spherical pH sensitive DX MG colloidosomes, which had a good morphology as was described in Chapter 3. The DX MG colloidosome had a strong swelling property triggered by its pH. It could be swollen when the pH value aligned with that of the microgel particles. The calculated volume swelling ratio (Q) for the colloidosomes was about 50. This confirms that the microgel particles peripheral chains did not interpenetrate at the oil/water interface and could be interlinked directly if the peripheral chains have vinyl groups. The DX MG colloidosome were stable and did not re-disperse when the pH increased. This work showed for the first time, construction of pH responsive DX MG colloidosomes using only microgels.

In Chapter 4, firstly, we fully investigated optimised microgel-stabilisation emulsion (mickering emulsion) of the EA-in-water emulsions system. Through the analysis and the results of the experiments, we established an optimised microgel concentration (0.6 wt.%) for the preparation of stable microgel-stabilised emulsions and colloidosomes. We also investigated the effect of the pH on the microgel, microgel-stabilisation emulsion, and established an optimized pH valueof 6.4 for preparing the microgel-stabilisation emulsion and DX MG colloidosomes. Importantly, the thermal irritated DX MG-colloidosomes have been scale up to the gram scale. This means it could potentially be used for future industrial production. In addition, the DX MG-colloidosoems enables control of the permeability of the colloidosome shell by easily changing the pH environment. The DX MG-colloidosomes could potentially be used

in a number of areas which include cosmetics and delivery.

Because of the limitation of the microgels, the DX MG colloidosomes are relatively brittle. In chapter 5, a new nanogel-based approach for preparing highly stretchable –COOH rich hydrogels was discussed. Without adding crosslinker and relying on self-crosslinking very high MAA-content nanogel particle dispersions were prepared (with up to 84 mol.% MAA). The latter were vinyl functionalised and gave dispersions that could be crosslinked to form highly stretchable gels. The present DX NGs at pH 10 not only had outstanding compressive properties but also were remarkably stretchable properties. The DX NGs could be made into many shapes and be tied in knots and stretched considerably without damage. These NGs gave highly-stretchable pH-responsive DX NGs with a stretchability and compression of up to 520% and 93% without damage, respectively. This will benefit the design and preparation of improved injectable pH-responsive DX NGs systems in future. Flexible DX NGs colloidosomes may be useful in future soft tissue engineering or for application in medicine.

6.2 Future work

In the future research, we can pay attention to study the conditions and methods for the synthesis of pH responsive DX MGs colloidosomes by different microgels. Because of the difference of functional groups, the surface activity and surface tension of different microgels will be different. Therefore, when selecting the oil phase solution of preparing the Pickering emulsion and further reaction of the colloidosomes, we may to find a rule or find a universal oil phase solution that can be applied to many kinds of pH responsive microgels. Furthermore, for the new type of nanogels in chapter 5, the biggest problem of these nanoparticles is that there was no uniform size. Rather, they were polydisperse. So in the future experiments, we hope to improve the method of synthesis, to a greater extent, and to improve the size uniformity and surface integrity of nanogels. This would then lead to new DX NG colloidosomes that may be highly deformable. In future experiments, we can consider using this degenerate and super deformed nanogels to form colloidosomes. Even this nanogel and colloidosomes can be combined to form super stretchable, degenerated and porous hydrogels.

Appendix

Published works

1. **Wang, W.**; Milani, A. H.; Carney, L.; Yan, J.; Cui, Z.; Thaiboonrod, S.; Saunders, B. R., Doubly crosslinked microgel-colloidosomes: a versatile method for pH-responsive capsule assembly using microgels as macro-crosslinkers. *Chemical communications* 2015, 51, 3854-3857.

2. **Wang, W**.; Milani, A. H.; Cui, Z.; Zhu, M.; Saunders, B. R., Pickering Emulsions Stabilized by pH-Responsive Microgels and Their Scalable Transformation to Robust Submicrometer Colloidoisomes with Selective Permeability. *Langmuir* 2017, 33, 8192-8200.

3. **Wang, W**.; Lu, D.; Zhu, M.; Saunders, J. M.; Milani, A. H.; Armes, S. P.; Saunders, B. R., Highly deformable hydrogels constructed by pH-triggered polyacid nanoparticle disassembly in aqueous dispersions. *Soft Matter* 2018

Co-author works

1. Nguyen, B. T.; **Wang, W**.; Saunders, B. R.; Benyahia, L.; Nicolai, T., pH-Responsive Water-in-Water Pickering Emulsions. *Langmuir* 2015, 31, 3605-3611.

2. Cui, Z.; **Wang, W**.; Obeng, M.; Chen, M.; Wu, S.; Kinloch, I.; Saunders, B. R., Using intra-microgel crosslinking to control the mechanical properties of doubly crosslinked microgels. *Soft matter* 2016, 12, 6985-6994.

3. Cui, Z.; Zhou, M.; Greensmith, P. J.; **Wang, W.;** Hoyland, J. A.; Kinloch, I. A.; Freemont, T.; Saunders, B. R., A study of conductive hydrogel composites of pH-responsive microgels and carbon nanotubes. *Soft matter* 2016, 12, 4142-4153.

4. Mispelon, A.; Yan, J.; Milani, A. H.; Chen, M.; **Wang, W**.; O'Brien, P.; Saunders, B. R., Effects of added thiol ligand structure on aggregation of non-aqueous ZnO dispersions and morphology of spin-coated films. *RSC Advances* 2015, 5, 18565-

18577.

5. Zhu, M.; Lu, D.; Wu, S.; Lian, Q.; **Wang, W**.; Milani, A. H.; Cui, Z.; Nguyen, N. T.; Chen, M.; Lyon, L. A.; Adlam, D. J.; Freemont, A. J.; Hoyland, J. A.; Saunders, B. R., Responsive Nanogel Probe for Ratiometric Fluorescent Sensing of pH and Strain in Hydrogels. *ACS Macro Letters* 2017, 6, 1245-1250.